INVESTIGATING MAMMALIAN UNFOLDED PROTEIN RESPONSE: THE PHYSIOLOGY AND REGULATORY MECHANISMS OF IRE1α-XBP1 SIGNALING

A Dissertation

Presented to the Faculty of the Graduate School

of Cornell University

In Partial Fulfillment of the Requirements for the Degree of

Doctor of Philosophy

by

Yin He

May 2013

INVESTIGATING MAMMALIAN UNFOLDED PROTEIN RESPONSE: THE PHYSIOLOGY AND REGULATORY MECHANISMS OF IRE1α-XBP1 SIGNALING

Yin He, Ph.D.

Cornell University 2013

The endoplasmic reticulum (ER) serves as the site of protein synthesis, folding, maturation, modification, secretion, and degradation for approximately one-third of the proteome. Disruptions in ER homeostasis activate an ER-to-nucleus signaling pathway termed the unfolded protein response (UPR). The IRE1α-XBP1 pathway is the most conserved arm of UPR and upon activation, acts to restore ER homeostasis. Significantly, IRE1α-XBP1 dysfunction has been implicated in the development and pathogenesis of protein-misfolding diseases. Although the general events underlying mammalian IRE1α-XBP1 activation and signaling have been reported, the mechanistic details remain unclear.

In addition to serving as a critical arm of UPR signaling, the IRE1α-XBP1 pathway was essential and indispensable for differentiation of pre-adipocytes into mature fat cells. Upon adipogenesis, C/EBPβ, a key initiator of the adipogenic program, was shown to bind to the proximal promoter of the *Xbp1* gene and induce its expression. XBP1, an essential UPR transcription factor, was required for the subsequent modulation of C/EBPα, an adipogenic protein critical for maintaining the differentiated state. Interestingly, adipogenic differentiation was associated with a low degree of physiological UPR required

for IRE1α activation and *Xbp1* splicing. These novel findings positioned the IRE1α-XBP1 pathway as a critical modulator of the transcriptional cascade underlying adipocyte differentiation, thus supporting the notion of UPR in metabolic dysfunction.

To further understand the activation mechanism of IRE1α, a proteomics-based mass spectrometry screen was performed to uncover novel IRE1α-interacting factors that may play a role in regulating its activation and signaling. Non-muscle myosin IIB (NMIIB), a component of the cytoskeleton machinery, was identified and shown to interact specifically with IRE1α in an ER stress-dependent manner. NMIIB was further characterized to be required for IRE1α activation and downstream signaling. Specifically, the motor activity of NMIIB and the actin cytoskeleton were essential in modulating IRE1α higher-order oligomer formation, a key activating step. Physiologically, NMIIB function was conserved as both mammalian cells and *C. elegans* lacking NMII exhibited hypersensitivity to ER stress. Collectively, the studies presented in this dissertation have contributed original and novel insight into the physiology and mechanisms underlying mammalian IRE1α-XBP1 activation and signaling.

BIOGRAPHICAL SKETCH

Yin He was born in Shanghai, China on February 4, 1985 to Shu Qin and Quang Run. She was a happy child who loved her family and playing the piano. Yin immigrated to the United States at the age of 6 and her family settled in the suburbs of northern Virginia. She attended Centreville Elementary School and the Congressional Schools of Virginia where she played basketball and learned Spanish. For high school, Yin attended The Madeira School, where she interned for the former U.S. Congressman Rick Boucher (D-VA 9th) and NASA.

Following high school, Yin enrolled at the University of Virginia where she first developed an interest and discovered her passion for the life sciences through interactions with her advisor Claire Cronmiller as well as gaining first-hand exposure to research by working in the lab of Michael Timko. Yin worked on a project identifying and mapping genes in the cowpea plant required for conferring natural resistance to an agricultural parasite associated with crop devastation in sub-Saharan Africa. This project revealed to Yin the promise, opportunities and endless possibilities that research offered. She graduated from UVA in May 2007 with a B.S. in Biology and a minor in Chemistry. In August 2007, Yin began her Ph.D. studies in the Department of Molecular Biology and Genetics at Cornell University. As Yin's interest was piqued by research focusing on understanding the molecular basis of human diseases, she joined the Qi Lab in Spring 2008 to work on mammalian ER stress response and its role in metabolism.

For my mother, with endless love and admiration

ACKNOWLEDGMENTS

I am forever grateful and indebted to a tremendous number of people who have provided unconditional support and have inspired me both as a scientist and as a person. First and foremost, I would like to thank Ling Qi for affording me the opportunity and confidence to work in his laboratory as his first graduate student. I would like to acknowledge my committee members both past and present, John Lis, Tom Brenna, Sylvia Lee, and Lee Kraus. I would also like to thank all members of the Qi Lab both past and present, particularly Zhen Xue, Liu Yang, Haibo Sha, Xiaoqing Li, and Cindy Wang. I am also grateful to Eric Alani for his guidance. I would like to recognize the National Institutes of Health (Training Grant to Y.H and R01DK082582 to L.Q.) and American Diabetes Association (1-12-CD-05 to L.Q.) for funding.

I thank Michael Timko and Claire Cronmiller at the University of Virginia for providing the initial impetus in my interest in biology and research. Michael Timko provided me with an invaluable research opportunity and my first exposure to a research lab as an undergraduate researcher. Claire Cronmiller served as a resourceful and motivational advisor, and engaged my interest in human genetics.

I would like to express gratitude to all of my supportive and thoughtful friends Divya Mehra, Malia Holland, Caitlin Muse, Wallis McMillin, Rachel Holland, and Sadie Bass. I am also extremely grateful to all of the incredible and intelligent people that I was fortunate to meet at Cornell including Rajni Singh, Emily Bielecki, Xin Luo, Anna Zenno, Alexander Beatty, Ali Awan, Archit Lal, Sarah Laue, Srich Murugesan, Anne Kurtz, Fabiana Duarte, and Vlad Oncescu.

Last but not least and most importantly, I would like to thank everyone in my family, especially my mother, Shu Qin, my step-father Thomas J. Fisher and my father Quang Run for their unwavering and unconditional love, support and encouragement.

TABLE OF CONTENTS

LIST OF FIGURES

CHAPTER 1. INTRODUCTION AND LITERATURE REVIEW

CHAPTER 2. THE IRE1α-XBP1 PATHWAY OF THE UNFOLDED PROTEIN RESPONSE IS REQUIRED FOR ADIPOGENESIS

CHAPTER 3. NON-MUSCLE MYOSIN IIB LINKS CYTOSKELETON TO IRE1α SIGNALING DURING ER STRESS

CHAPTER 4. GENERAL DISCUSSION AND FUTURE DIRECTIONS

APPENDIX A. MACROPHAGE XBP1 MODULATES ER STRESS-DEPENDENT INFLAMMATION THROUH ATF3

APPENDIX B. IRE1α UNDERGOES ER STRESS-DEPENDENT PHOSPHORYLATION AT A UNIQUE "SSPS" MOTIF

LIST OF TABLES

LIST OF ABBREVIATIONS

4-PBA: 4-Phenylbutyric acid

ACC1, 2: Acetyl-CoA carboxylase 1, 2

AIP1: ASK1-interacting protein 1

Ala/A: Alanine

AML: Acute myeloid leukemia

ASK1: Apoptosis signal-regulating kinase 1

Asp/D: Aspartic acid

ATF3, 4, 6: Activating transcription factor 3, 4, 6

b-ZIP: Basic leucine zipper domain

BAT: Brown adipose tissue

BAX2: BCL-2 associated X protein 2

BCL-2: B cell lymphoma 2

BI-1: BAX inhibitor 1

BLIMP1: B lymphocyte induced maturation protein

C/EBP: CCAAT/enhancer-binding protein

ChIP: Chromatin immunoprecipitation

CHOP: C/EBPβ homologous protein

CIP: Calf intestinal phosphatase

CRE: cAMP-responsive element

CREB: cAMP-response element binding protein

DGAT2: Diacylglycerol acetyltransferase

DNAJ3/P58IPK: DnaJ homolog subfamily C member 3

DTT: Dithiothreitol

DXM: Dexamethasone

EDEM: ER degradation enhancing alpha-mannosidase like 1

eIF2α: Eukaryotic initiation factor 2 alpha

ER: Endoplasmic reticulum

ERAD: ER-associated degradation

ERDJ4: ER resident DnaJ B9 family member

ERSE: ER stress response element

GADD34: Growth arrest and DNA damage-inducible protein 34

GAPDH: Glyceraldehyde 3-phosphate dehydrogenase

GEF: Guanine nucleotide exchange factor

GO: Gene Ontology

GRP78/BiP: Glucose regulated protein 78

HA: Hemagglutinin

HRD1: ERAD-associated E3 ubiquitin protein ligase

HSP90: Heat shock protein 90

IBD: Inflammatory bowel disease

IBMX: 3-isobutyl-1-methylxanthine

IFN-α: Interferon alpha

IFN-β: Interferon beta

Ig: Immunoglobulin

IGF-1: Insulin-like growth factor 1

IgG: Immunoglobulin G

IL-1, 2, 4, 6, 12: Interleukin 1, 2, 4, 6, 12

Ins: Insulin

IP: Immunoprecipitation

IRE1/ERN1: Inositol-requiring enzyme 1; ER to nucleus signaling 1

IRF4: Interferon regulatory factor 4

IRS-1: Insulin receptor substrate 1

JNK: c-Jun N-terminal kinase

kDa: kilodalton

L32: 60S ribosomal protein

LPS: Lipopolysaccharide

MEF: Mouse embryonic fibroblast

MHC: Major histocompatibility complex

MLC: Myosin light chain

MLCK: Myosin light chain kinase

MS/MS: Tandem mass spectrometry

NF-κB: Nuclear factor kappa-light-chain-enhancer of activated B cells

NMHCII: Non-muscle myosin heavy chain II

NMIIA, B, C: Non-muscle myosin IIA, B, C

P58IPK: DnaJ homolog subfamily C member 3

PAX5/BSAP: Paired box gene 5; B cell lineage-specific activator protein

PERK: PKR-like ER kinase

PI3K: Phosphoinositide 3-kinase

PP1C: Protein phosphatase 1C

PPAR: Peroxisome proliferator-activated receptor

PRDM16: PR domain containing 16

PTP-1B: Protein-tyrosine phosphatase 1B

qPCR/Q-PCR: Quantitative polymerase chain reaction

RACK1: Receptor for activated C kinase 1

RIDD: Regulated IRE1α-dependent decay

RNase: Endoribonuclease

RLC: Myosin regulatory light chain

RT-PCR: Reverse transcription polymerase chain reaction

SEL1L: Suppressor or lin-12-like protein 1

Ser/S: Serine

shRNA: Short hairpin RNA

SOD2: Superoxide dismutase

TEM: Transmission electron microscopy

Tg: Thapsigargin

TLR2, 4: Toll-like receptor 2, 4

Tm: Tunicamycin

TNFα: Tumor necrosis factor α

TRAF2: TNFR-associated factor 2

TUDCA: Tauroursodeoxycholic acid

uORF: Upstream open reading frame

UPR: Unfolded protein response

UPRE: Unfolded protein response element

USP14: Ubiquitin specific protease 14

UTR: Untranslated region

WAT: White adipose tissue

XBP1/HAC1: X-box binding protein 1; u (unspliced); s (spliced)

CHAPTER 1*

INTRODUCTION AND LITERATURE REVIEW

1.1 CONFORMATIONAL DISEASES AND PROTEOSTASIS

Conformational disorders are a set of clinically and pathologically-related diseases that arise from protein misfolding or proteins adopting non-native conformational states (Carrell and Lomas, 1997). Accumulation of misfolded or unfolded proteins can disrupt the cell's normal function and physiology through a loss- or gain-of-function mechanism. Loss-of-function occurs when the aberrant conformer of a protein undergoes mislocalization, engages in abnormal interactions or is targeted for degradation by the ubiquitin-proteasome system. On the other hand, a misfolded protein acquiring a new, but toxic function such as forming destructive amyloid fibrils or other insoluble aggregates in the cell, serves as the basis for gain-of-function disorders. Currently, conformational diseases encompass broad pathologies including prion encephalopathies, cystic fibrosis, neurodegenerative disorders (Alzheimer's, Parkinson's, Huntington's), α1-antitrypsin deficiency, type 2 diabetes, amyloidosis, specific types of cancer, and others.

Recently, a new paradigm in the field of protein folding has been introduced and termed proteostasis, a phrase coined from the words protein and homeostasis (Balch et al., 2008; Powers et al., 2009). Proteostasis represents the delicate balance within a cell between protein synthesis and folding with its

* Sections 1.6-1.7 of this chapter have been adapted from **He, Y**., Sun, S., Sha, H., Liu, Z., Yang, L., Xue, Z., Chen, H., and Qi, L. *Gene Expression* **15**, 13-25 (2010) and is reprinted here with modifications with permission.

degradation. The proteostasis network is comprised of pathways that regulate all aspects of protein maturation from protein synthesis, folding, and modification to trafficking and degradation. The proteostasis network is highly flexible, adaptable and cell-type specific. However, there does exist an inherent maximal capacity that can be influenced by factors including aging, metabolic or environmental-induced stress and overexpression of misfolding-prone proteins. Hence, the overall proteostasis network determines the folding energetics of a protein and influences the balance between folding, unfolding, aggregation and degradation (Powers et al., 2009).

Small chemical compounds have been identified that can modulate, increase and shift the proteostasis network towards a more favorable energetic landscape for misfolding-prone proteins. These fall into two categories: pharmacologic chaperones and proteostasis regulators (Balch et al., 2008). Pharmacologic chaperones can benefit loss-of-function diseases by acting in a similar fashion as endogenous chaperones. They bind to and stabilize proteins while also concomitantly preventing degradation and aggregation (Balch et al., 2008; Fan et al., 1999). Mutant proteins that have been shown to be stabilized by pharmacologic chaperones include G protein-coupled receptors, cystic fibrosis transmembrane conductance regulator (CFTR) and neurotransmitter receptors (Conn et al., 2007; Loo et al., 2008; Millar and Harkness, 2008; Yoo et al., 2008). On the other hand, proteostasis regulators act by enhancing the capacity of the proteostasis network and can benefit gain-of-function diseases (Hammarström et al., 2003; Powers et al., 2009). Collectively, pharmacologic chaperones and proteostasis regulators have been proposed as an effective therapeutic

intervention to shift, expand and modulate the capacity of the proteostasis network and stabilize misfolding-prone proteins.

1.2 ENDOPLASMIC RETICULUM (ER) STRESS

The ER is a eukaryotic organelle comprised of a vast and complex network of interconnected tubules and cisternae. Structurally, the ER can be characterized and visualized by microscopy as smooth or rough ER. Rough ER is appropriately named as it contains ribosomes on the cytosolic surface, thus creating a "rough" appearance, and serves as the site of protein translation in the cell; smooth ER lacks ribosomes. In addition to protein synthesis, the ER functions in a number of essential physiological processes including lipid and carbohydrate metabolism, detoxification, and productive protein folding, modification, transport, and secretion for approximately one-third of the proteome that encodes secretory or transmembrane proteins. Hence, establishing and maintaining homeostasis within the dynamic ER luminal environment is critical for normal cellular physiology and function.

ER homeostasis can be viewed as a delicate balance between the folding capacity of the ER (i.e. chaperones and components of the degradation machinery) and the protein load (i.e. newly synthesized proteins that require folding, modification, and transport). Many physiological and pathological conditions such as expression of misfolded proteins, viral infections, disruptions in calcium homeostasis, and glucose deprivation can disrupt ER homeostasis and lead to the harmful accumulation of misfolded proteins and ER stress (Ron and Walter, 2007). As unresolved and persistent ER stress can ultimately engage

apoptosis pathways, responding appropriately and quickly to ER stress and restoring ER homeostasis are vital and essential.

1.3 UNFOLDED PROTEIN RESPONSE (UPR)

In response to ER stress, organisms have developed an evolutionarily conserved ER-to-nucleus signaling pathway termed the unfolded protein response (UPR). Together, UPR and ER-associated degradation (ERAD) maintain ER homeostasis and quality control. In 1988, Kozutsumi and colleagues observed the induction of a group of ER chaperones, glucose-regulated proteins (GRPs), in response to disrupted protein folding (Kozutsumi et al., 1988). This led them to propose the presence of an active regulatory mechanism in the ER to maintain ER homeostasis (Kozutsumi et al., 1988). To date, metazoan UPR consists of three primary ER transmembrane proteins that serve as sensors of the internal ER environment and initiate signaling pathways that act in parallel to coordinate and alleviate ER stress: inositol-requiring enzyme 1α (IRE1α), PKR-like ER kinase (PERK) and activating transcription factor 6 (ATF6) (Ron and Walter, 2007; Walter and Ron, 2011). Of the three, the IRE1α pathway is the most conserved and represents the only UPR branch in yeast (Ron and Hubbard, 2008). In response to perturbations in ER homeostasis, UPR sensors become engaged and initiate downstream signaling cascades that act to transcriptionally induce chaperones and components of ER-associated degradation (ERAD), attenuate global protein synthesis and in the face of persistent ER stress, activate apoptosis (Ron and Walter, 2007; Schröder and Kaufman, 2005; Walter and Ron, 2011). ER stress and UPR activation have been implicated in the development

and pathogenesis of various disorders including metabolic dysfunction (type 2 diabetes, obesity), cardiovascular complications, cancer, neurodegenerative diseases, and conformational disorders (Schröder and Kaufman, 2005). Therefore, a comprehensive and thorough mechanistic understanding of UPR activation, signaling and regulation is of both basic and clinical relevance, and is essential for the development of potential therapeutics targeting these health-related complications.

1.4 ATF6 PATHWAY

ATF6 activation upon ER stress is mediated by a series of unique proteolytic cleavages at the Golgi apparatus and differs from that of PERK and IRE1α activation (Fig. 1.1). Mammalian ATF6 exists in two isoforms, ATF6α (Hai et al., 1989; Haze et al., 1999) and ATF6β (Haze et al., 2001; Khanna and Campbell, 1996; Min et al., 1995), with both isoforms being reported to induce the expression of pro-survival genes (Haze et al., 2001; Yamamoto et al., 2007). Upon ER stress, ATF6, a 90 kilodalton (kDa) ER transmembrane protein with a large luminal domain, translocates by budding to the Golgi apparatus, where it undergoes regulated proteolytic cleavage by two proteases (site 1 and site 2 proteases) that sequentially remove the luminal domain and transmembrane linker (Chen et al., 2002; Haze et al., 1999; Shen and Prywes, 2004; Ye et al., 2000). The cleavage events release the N-terminal cytosolic-exposed region of ATF6. The 50 kDa active ATF6(N) enters the nucleus and functions as a basic region leucine zipper (b-ZIP) transcription factor to induce the expression of canonical UPR target genes including chaperones and ERAD components containing an ER

stress response element (ERSE) in their promoters such as BiP/GRP78, protein disulfide isomerase (PDI) and ER degradation-enhancing alpha-mannosidase-like protein 1 (EDEM1) (Kokame et al., 2001; Wang et al., 2000; Yoshida et al., 1998; 2000). Of the three UPR pathways, ATF6 activation, signaling and regulation is the least well understood. Particularly, how ER stress activates ATF6 is unknown. A study proposed that similar to IRE1α and PERK activation, dissociation of the ER chaperone BiP/GRP78 from ATF6 upon ER stress induced its activation (Shen et al., 2002). However, the underlying details are unclear.

ATF6 signaling is primarily believed to be pro-survival and cyto-protective through its transcriptional regulation of chaperones and degradation machinery. In addition, ATF6 has been reported to induce XBP1 expression, suggesting cross-talk and integration among the UPR pathways (Yoshida et al., 2001). Recently, a number of ATF6 homologs were identified and although one of these factors, CREBH, was regulated by ER stress, the output of CREBH activation was not transcriptional induction of classical UPR genes but rather, inflammatory mediators (Ron and Walter, 2007; Zhang et al., 2006). This raised the intriguing possibility of the role of ATF6 and its homologs in physiology. Hence, the development and optimization of reagents to study ATF6 are critical in the future and will greatly expand our understanding of this pathway, its physiology and its contribution to UPR and cell fate determination.

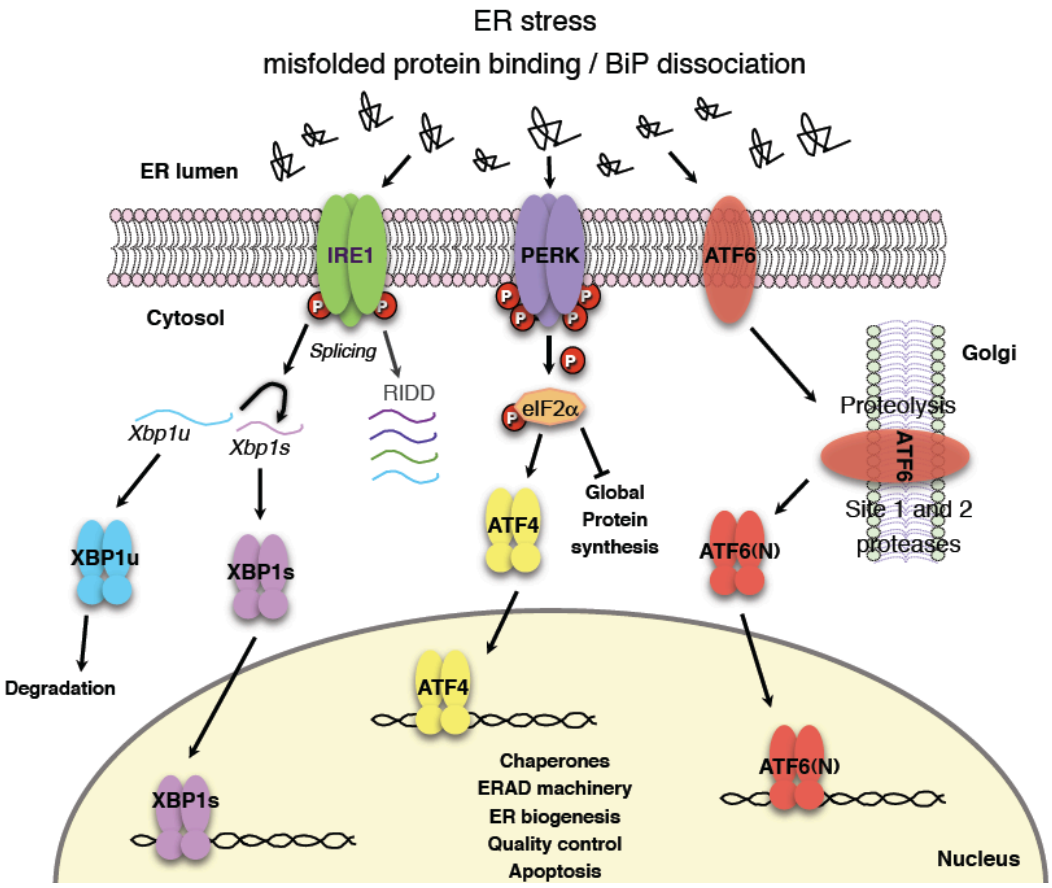

Figure 1.1. Metazoan Unfolded Protein Response (UPR).

ER homeostasis is sensitively monitored by three transmembrane sensors, inositol-requiring enzyme 1 (IRE1), PKR-like ER kinase (PERK) and activating transcription factor 6 (ATF6). Upon ER stress, the three sensors become activated either through dissociation of the ER chaperone BiP/GRP78 or direct binding of misfolded proteins (for IRE1 and PERK). ATF6 translocates to the Golgi where it undergoes two sequential proteolytic cleavages to release an N-terminal 50 kDa fragment that enters the nucleus and functions as a b-ZIP transcription factor. PERK undergoes dimerization/oligomerization, trans-autophosphorylation and phosphorylates Ser51 of eukaryotic initiation factor 2α (eIF2α) to attenuate global protein synthesis. PERK also selectively induces the expression of several proteins including activating transcription factor 4 (ATF4), which can activate CHOP, a pro-apoptosis factor. Similar to PERK, IRE1α activation occurs by dimerization/oligomerization and trans-autophosphorylation. Activation of the RNase domain of IRE1α splices the *Xbp1u* mRNA to generate XBP1s, a b-ZIP transcription factor. IRE1α RNase activity also participates in regulated IRE1-dependent mRNA decay (RIDD). Collectively, UPR sensor activation serves to restore ER homeostasis and promote quality control. However, persistent and unresolved ER stress activates apoptosis.

1.5 PERK PATHWAY

PERK is a type 1 ER transmembrane protein containing an ER luminal domain that monitors ER conditions and a cytosolic kinase domain. Under basal conditions, PERK is bound by the ER chaperone BiP/GRP78. BiP dissociation upon ER stress allows for PERK activation through dimerization / oligomerization and trans-autophosphorylation (Kebache et al., 2004). PERK kinase activity also acts on the serine 51 residue of eukaryotic initiation factor 2α (eIF2α) to attenuate global protein synthesis and decrease the protein load entering the ER (Harding et al., 1999; Raven and Koromilas, 2008; Shi et al., 1998). Hence, eIF2α phosphorylation is commonly used as a marker for detecting ER stress. However, as PERK belongs to a family of eIF2α kinases that respond to various cellular stresses including amino acid and heme deprivation (Harding et al., 1999; Shi et al., 1998; 1999), interpretation of UPR activation based solely on eIF2α phosphorylation status requires caution.

Apart from a global decrease in protein synthesis, a select group of transcripts containing an upstream open reading frame (uORF) in their 5′ untranslated regions (UTR) are up-regulated by PERK activation including the transcription factor, activating transcription factor 4 (ATF4) (Harding et al., 2003; Schröder and Kaufman, 2005). ATF4 subsequently induces the expression of transcription factor C/EBP homologous protein (CHOP), an apoptosis factor, and growth arrest and DNA damage-inducible 34 (GADD34), a regulatory subunit of protein phosphatase 1C (PP1C) that attenuates PERK signaling by dephosphorylating eIF2α (McCullough et al., 2001; Novoa et al., 2001; Ron and

Habener, 1992). Activation of the PERK pathway has typically been associated with apoptosis upon persistent and unresolved ER stress.

1.6 IRE1α-XBP1 PATHWAY

Although IRE1α-XBP1 is the most evolutionarily conserved UPR pathway, its physiological role and regulatory mechanisms are unclear. Metazoans have two isoforms of IRE1, the constitutively-expressed IRE1α and the gut-specific IRE1β (Kaufman et al., 2002). IRE1α protein encodes an ER luminal and a transmembrane domain followed by two functional cytosolic domains conferring kinase and RNase activity (Fig. 1.2) Current literature proposes two mechanistic models of IRE1α activation in response to misfolded or unfolded proteins. One model suggests that in an inactive state, monomeric IRE1α is constitutively bound to the ER chaperone, BiP/GRP78 (Bertolotti et al., 2000; Kimata et al., 2003). Accumulation of misfolded proteins requiring chaperone activity titrates BiP away from IRE1α, allowing IRE1α monomers to dimerize and undergo activation. Alternatively, IRE1α binds misfolded proteins directly through its N-terminal MHC-like ER luminal domain, promoting its dimerization (Credle et al., 2005). The two models are not mutually exclusive and in fact, may work together sequentially through BiP dissociation first followed by misfolded protein binding (Kimata et al., 2007). As these models were established in yeast, they may have different implications for mammalian IRE1α. Indeed, even under basal non-stress conditions, mammalian IRE1α mutants unable to bind BiP can still be activated, and in vitro assays did not detect a direct interaction between IRE1α

and unfolded proteins (Oikawa et al., 2009). Furthermore, a crystal structure of mammalian IRE1α luminal domain suggested that unlike yeast IRE1p, the MHC-like groove of mammalian IRE1α may not be able to bind misfolded proteins directly (Zhou et al., 2006).

Although the precise mechanistic details underlying IRE1α activation remain unclear, the general consensus in the field is that upon activation, the luminal domains of IRE1α monomers dimerize first followed by dimerization of the cytosolic domains and trans-autophosphorylation of neighboring IRE1α monomers, which further reinforce IRE1α clustering into foci or higher-order oligomers (Fig. 1.4). This model is supported by the crystal structure of the cytosolic domain of IRE1p in yeast (Korennykh et al., 2009; Lee et al., 2008b), which revealed higher-order oligomer formation (Korennykh et al., 2009). Supporting oligomerization, foci formation of mammalian IRE1α was also detected and visualized (Li et al., 2010). However, whether oligomer formation is required for activation of the RNase domain of IRE1α is debatable as studies have suggested that IRE1α dimerization is sufficient for enzymatic activity (Bertolotti et al., 2000).

Collectively, IRE1α dimerization/oligomerization activates the cytosolic RNase domain of IRE1α to splice 26 nucleotides from the mRNA encoding X-box binding protein 1 (*Xbp1u*, unspliced), resulting in a frameshift and the generation of XBP1s (spliced) (Fig. 1.3, Calfon et al., 2002; Lee et al., 2002; Yoshida et al., 2006). In contrast to XBP1u, XBP1s protein is more stable and contains a transactivation domain, which allows it to translocate to the nucleus and

function as a potent b-ZIP transcription factor (Fig. 1.1, Lee et al., 2003b). XBP1s induces classical UPR target genes such as chaperones, ERAD components and ER expansion, but also exhibits tissue-specificity as the targets of XBP1 are critical mediators of B cell development, myogenesis, adipogenesis and lipogenesis (Fig. 1.4, Acosta-Alvear et al., 2007; Lee et al., 2003a). In addition to splicing *Xbp1* mRNA, IRE1α has been implicated to participate in regulated IRE1α-dependent decay (RIDD) or the rapid turnover of mRNAs encoding secretory and trans-membrane proteins through the action of its RNase domain (Han et al., 2009; Hollien and Weissman, 2006; Hollien et al., 2009; So et al., 2012). More recently, IRE1α RNase activity was implicated in microRNA degradation (Upton et al., 2012). However, the physiological implications of these events are currently unclear. Collectively, these two outputs of IRE1α signaling, *Xbp1* splicing and RIDD processing, function primarily to alleviate ER stress and restore ER homeostasis.

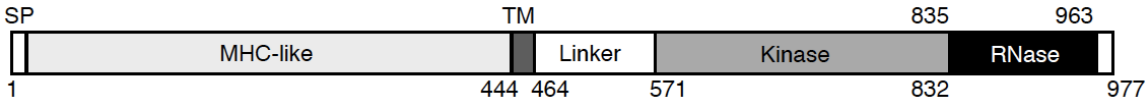

Figure 1.2. Schematic of human IRE1α protein.

Human IRE1α protein is drawn to scale according to UniProt domain predictions. This 977-amino acid type 1 ER transmembrane protein contains a N-terminal signal peptide (SP) to direct its localization to the ER. The MHC-like luminal domain senses the internal ER environment and may be involved in direct binding of misfolded proteins although the validity of this occurrence for metazoan IRE1α is unclear. Following the transmembrane (TM) region is a short linker domain and two functional cytosolic domains conferring kinase and RNase activities involved in IRE1α phosphorylation and *Xbp1u*/RIDD mRNA splicing, respectively.

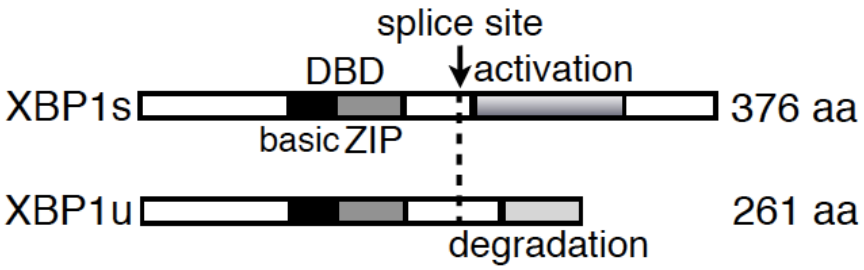

Figure 1.3. Mouse XBP1 protein.
Diagram depicting both the spliced (XBP1s) and unspliced (XBP1u) forms of mouse XBP1 protein. The cytosolic RNase domain of activated IRE1α splices 26 nucleotides from the mRNA of *Xbp1u* to generate *Xbp1s*. Unlike yeast *Hac1* (homolog of *Xbp1*) in which *Hac1u* is not translated, both metazoan *Xbp1u* and *Xbp1s* are translated. The splicing event causes a frameshift and as a result, XBP1s protein has a different C-terminal domain containing a transactivation domain that is absent from XBP1u. Both forms encode a DNA binding domain and a basic leucine zipper domain, thus characterizing XBP1 as a b-ZIP transcription factor that binds to CRE-like sequences. Although XBP1u is translated, it has been proposed to contain a C-terminal degradation domain, thus rendering it unstable and susceptible to degradation.

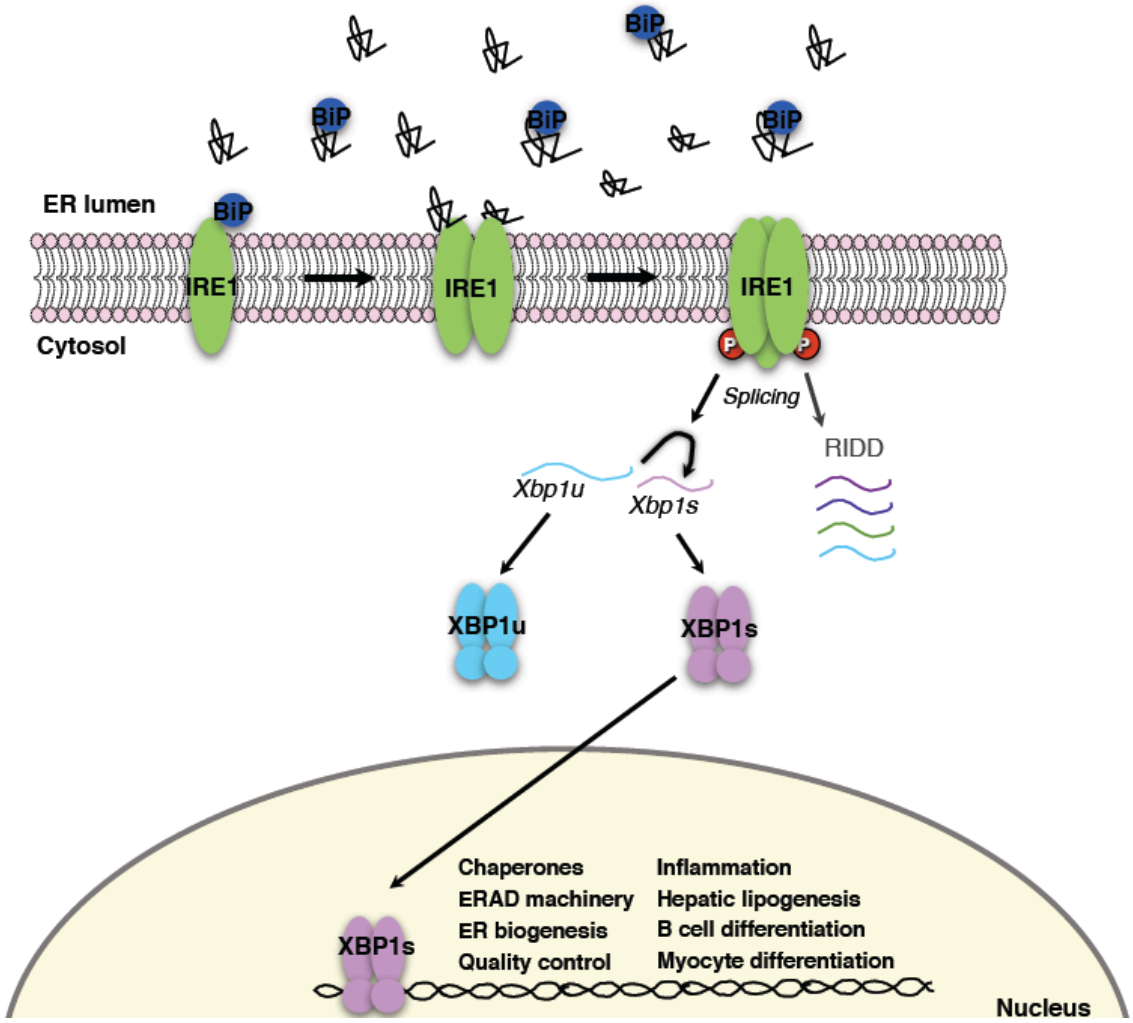

Figure 1.4. Metazoan IRE1α-XBP1 pathway.

BiP dissociation and/or binding of misfolded proteins activate IRE1α protein at the ER membrane. Following dimerization, trans-autophosphorylation and further clustering into oligomers, the RNase domain of IRE1α splices 26 nucleotides from *Xbp1u* mRNA to generate a b-ZIP transcription factor XBP1s. In addition to inducing canonical UPR target genes involved in quality control and ER homeostasis, XBP1 also regulates genes in physiological processes including inflammation, hepatic lipogenesis, and B cell and myocyte differentiation. IRE1α also splices other ER targeted mRNAs in a process known as regulated IRE1α-dependent decay (RIDD). The role and requirement of the IRE1α-XBP1 pathway in other cellular processes as well as identification of regulatory factors modulating this pathway are discussed in this dissertation.

1.6.1 Biology and function of the IRE1α-XBP1 pathway

The human XBP1 gene was discovered and characterized in 1990 as a b-ZIP transcription factor present in B cells that interacted specifically with the conserved X2 boxes located in the promoters of MHC class II genes (Liou et al., 1990). XBP1 formed a stable functional heterodimer with c-fos that was critical for the expression of XBP1 target genes (Ono et al., 1991). Further analysis of the XBP1 promoter revealed multiple regulatory *cis* elements including a motif identical to the X2 sites bound by XBP1 (Ponath et al., 1993; Reimold et al., 1996). In situ hybridization studies revealed ubiquitous expression of XBP1 in adult tissues as well as in fetal exocrine glands and osteoblasts (Clauss et al., 1993). Importantly, mice with germline XBP1 deletion died in utero from severe liver or heart hypoplasia, and apoptosis (Masaki et al., 1999; Reimold et al., 2000).

In 1993, two laboratories independently reported that communication between the ER and nucleus, termed UPR, was mediated by an ER transmembrane kinase ERN1/IRE1 (Cox et al., 1993; Mori et al., 1993). Subsequent work in yeast demonstrated that in addition to a kinase domain, IRE1 possessed RNase activity and *Hac1* was the substrate (Cox and Walter, 1996). IRE1 activation led to splicing of the mRNA of *Hac1u* (un-induced) to generate *Hac1i* (induced) (Sidrauski and Walter, 1997). *Hac1i* mRNA encoded a potent transcription factor responsible for the up-regulation of many genes involved in protein folding, degradation and trafficking (Travers et al., 2000). XBP1 was later identified as the mammalian homolog of HAC1 (Calfon et al., 2002; Lee et al., 2002; Yoshida et al., 2001).

From an evolutionary perspective, the presence of eukaryotic genes with

overlapping reading frames such as *Xbp1u* and *Xbp1s* presents an intriguing but puzzling question. Using comparative approaches, the *Xbp1u* coding sequence (CDS) was observed to be strongly conserved and both the unspliced and spliced CDS had similar non-synonymous substitution rates, providing evidence for a functional role for XBP1u (Nekrutenko and He, 2006). In the current model, XBP1u negatively regulates XBP1s transcriptional activity and hence UPR signaling (Lee et al., 2003b; Yoshida et al., 2006). However, this model was challenged by the observation that overexpression of stabilized XBP1u increased the expression of XBP1s targets (Tirosh et al., 2006), implying a much more complex role of XBP1u in UPR signaling. Indeed, a recent study showed that XBP1u recruited its own mRNA to the ER membrane for efficient IRE1α-mediated splicing (Yanagitani et al., 2009). Thus, although the precise role of XBP1u remains elusive, it does appear to serve a biphasic role in UPR initiation and resolution.

1.6.2 Transcriptional regulation of XBP1 expression

In addition to the well-characterized *Xbp1* mRNA splicing event by IRE1α, accumulating evidence suggested that transcriptional regulation of *Xbp1* gene expression may also play an important role with profound pathological and therapeutic implications. Indeed, several recent studies have shown that the *Xbp1* proximal promoter serves as a target for various tissue-specific and developmentally regulated transcription factors, contributing to the temporal- and spatial-specific expression of XBP1.

As the role of XBP1 in plasma cell differentiation was unraveled, studies

demonstrated that *Xbp1* mRNA was induced by interleukin (IL)-6 in human multiple myeloma cells (Wen et al., 1999) and IL-4 in primary B cells (Iwakoshi et al., 2003). B lymphocyte induced maturation protein (BLIMP1) and interferon regulatory factor 4 (IRF4) are two major transcription factors critical for *Xbp1* expression and plasma cell differentiation. Microarray studies placed BLIMP1 upstream of XBP1 but as BLIMP1 was a transcriptional repressor, mechanistic questions arose as to how BLIMP1 could induce *Xbp1* expression (Shaffer et al., 2002; 2004). It was revealed that BLIMP1 repressed paired box gene 5/B cell lineage-specific activator protein (BSAP/PAX5), a known repressor of *Xbp1* in B cells (Reimold et al., 1996; Shaffer et al., 2002). IRF4 is an interferon (IFN)-regulatory family member that is expressed in B cells committed to the plasma cell lineage and required for plasmacytoid differentiation (Klein et al., 2006). XBP1s induction was ablated in IRF4-deficient cells, but BLIMP1 expression was unaffected, suggesting that IRF4 acted upstream of XBP1 in a non-redundant manner. Furthermore, other adaptive immune responses such as effector $CD8^+$ T cell differentiation and macrophage activation up-regulated *Xbp1* expression through IL-2 (Kamimura and Bevan, 2008) and the ligand for Toll-like receptor 4-(TLR4), lipopolysaccharide (LPS) (Martinon et al., 2010; Roach et al., 2007).

Various other factors contributing to the regulation of *Xbp1* gene expression are emerging as well. Two myogenic transcription factors, MyoD and myogenin, were shown to directly regulate *Xbp1* expression (Blais et al., 2005). In addition, *Xbp1* gene expression was regulated by ATF6 as well as itself, resulting in a positive feedback loop during UPR activation (Yoshida et al., 2001). Indeed, a human polymorphism in the proximal promoter of *Xbp1* (-116C-G) that disrupted the putative binding site for XBP1s correlated with an increased risk

for bipolar disorder (Kakiuchi et al., 2003). Furthermore, parathyroid hormone played a role in regulating *Xbp1* expression during osteoblast differentiation (Zambelli et al., 2005). Finally, a recent study identified XBP1 as a highly-enriched white adipose gene that was repressed by PR domain containing 16 (PRDM16), a brown fat-specific transcriptional activator (Kajimura et al., 2008; Seale et al., 2008).

Thus, although IRE1α-mediated splicing of *Xbp1* mRNA is the most well characterized regulatory mechanism for this transcription factor, its mRNA expression is also tightly controlled by various factors in a highly dynamic manner. As UPR may be constitutively active even under basal conditions (Acosta-Alvear et al., 2007; Shen et al., 2005; Yang et al., 2010), regulation through either induction or repression of *Xbp1* expression may serve to fine-tune ER homeostasis. Indeed, a similar situation was identified in yeast and termed "super-UPR" (Leber et al., 2004). Further characterization of novel XBP1 regulators at the transcriptional level may provide insight into the role of "super-UPR" and as well as into the design and development of therapeutic strategies targeting human ER-associated disorders.

1.6.3 XBP1-mediated transcriptional events

XBP1 was initially reported to bind to cAMP-responsive elements (CRE) sites in the promoters of MHC class II genes (Clauss et al., 1996). Further studies were performed validating that XBP1 did indeed preferentially bind to CRE-like elements in which the core "ACGT" was highly conserved (Clauss et al., 1996). To identify transcriptional networks regulated by XBP1, ChIP-on-chip arrays

showed that XBP1 was constitutively bound to a subset of genes involved in ER homeostasis including folding, trafficking and ERAD (Acosta-Alvear et al., 2007), confirming the presence of a low level of basal or constitutive UPR (Shen et al., 2005). In most genes, XBP1 binding occurred within 200 bp of transcriptional start sites (TSS) (Acosta-Alvear et al., 2007). In support of previous reports (Clauss et al., 1996), high-throughput studies showed that XBP1 did indeed bind to the core "ACGT" element under physiological conditions, but XBP1 targets were also enriched in additional distinct motifs including UPR element (UPRE) and a CCACG box (Acosta-Alvear et al., 2007).

As XBP1 is involved in various facets of biology, it is not surprising that its targets are also extremely diverse (Acosta-Alvear et al., 2007). Canonical XBP1 targets in UPR signaling have been shown to include ER chaperones and components of ERAD including EDEM1, ERDJ4 and P58IPK. Additional tissue-specific XBP1 targets that have been identified include IL-6 in plasma cells, lipogenic genes in hepatocytes, pro-inflammatory cytokines in macrophages and MIST1 in myocytes (Fig. 1.4). XBP1 was also enriched on the promoters of genes involved in a number of UPR-unrelated processes including glycolysis, gluconeogenesis, lipid metabolism, and DNA replication and repair (Acosta-Alvear et al., 2007). The biological relevance of these bindings requires further investigations.

1.7 ROLE OF IRE1α-XBP1 IN PHYSIOLOGY

As a b-ZIP transcription factor, XBP1 can exert direct influence over the expression of genes critical not only for classical UPR signaling, but also for

many other physiological processes ranging from immunity to metabolism. This section highlights and addresses recent reports on the relevance and importance of the IRE1α-XBP1 pathway in multiple pathophysiological conditions such as pathogen defense and immunity, obesity and type 2 diabetes, cancer, neurodegeneration, and aging.

1.7.1 IRE1α-XBP1 in adaptive immunity

XBP1 is required for plasma cell differentiation (Reimold et al., 2001), but does not influence the decision of B cells to commit to the memory lineage (Todd et al., 2008; 2009). XBP1-deficient B cells exhibited normal proliferation and activation, but expressed decreased levels of J chain, a component required for Ig assembly. Consequently, these animals were more susceptible to infections, but restoration of XBP1s expression rescued Ig production (Reimold et al., 2001). Furthermore, *Xbp1* mRNA splicing was attenuated in mice lacking Ig heavy chains, suggesting that IRE1α activity and UPR were modulated and induced by Ig synthesis and production (Iwakoshi et al., 2003; Zhang et al., 2005). XBP1-mediated ER expansion was required for adoption of a "professional secretory cell" phenotype characteristic of plasma cells (Shaffer et al., 2004). In addition, XBP1s induced IL-6 expression in splenic B cells (Iwakoshi et al., 2003). Thus, XBP1 in professional secretory cells may have evolved additional functions allowing these cells to respond to "physiological" UPR (Shaffer et al., 2004).

In contrast to previous reports (Gass et al., 2002; 2008; Iwakoshi et al., 2003; Zhang et al., 2005), a more recent study reported that *Xbp1* induction was independent of differentiation as B cells lacking IgM still maintained *Xbp1*

activation. This discovery suggested that *Xbp1* activation may be required for normal plasma cell differentiation rather than as a consequence of massive Ig synthesis and secretion (Hu et al., 2009). Furthermore, a study showed that while XBP1 was required for IgM synthesis and secretion, glycoprotein degradation was unaffected by loss of XBP1 (Tirosh et al., 2005). Hence, the timing and mechanism of UPR and XBP1 activation during plasma cell differentiation remain an interesting and open question.

1.7.2 IRE1α-XBP1 in innate immunity

The IRE1α-XBP1 signaling pathway of UPR is critical for the development and survival of another immune population, dendritic cells (DCs). Loss of XBP1 in DCs reduced IFN-α production upon stimulation with CpG, an agonist of TLR2, and rendered cells prone to ER stress-induced or differentiation-associated cell death (Iwakoshi et al., 2007). Indeed, both conventional and plasmacytoid DCs in XBP1- deficient animals exhibited decreased survival at basal levels and in response to TLR signaling. Conversely, forced expression of XBP1s enhanced DC development (Iwakoshi et al., 2007).

Most recently, XBP1 was shown to have a critical role in regulating the expression of key pro-inflammatory cytokines in macrophages (Martinon et al., 2010). TLR2/4 signaling specifically activated the IRE1α-XBP1 branch, which in turn increased the expression and secretion of IL-6, tumor necrosis factor α (TNFα), and interferon β (IFN-β) without inducing canonical UPR genes. Mice with a macrophage-specific deficiency of XBP1 exhibited increased bacterial

burden post-infection (Martinon et al., 2010). The function of XBP1 in innate immunity seemed to be highly conserved as similar observations were made in worms; XBP1-deficient worms were hypersensitive to pathogen infection during development (Richardson et al., 2010). Therefore, XBP1 plays a critical and protective role in both innate and adaptive immunity. This is not surprising given that the RNase domain of both isoforms of IRE1 shares unique homology with RNase L (Tirasophon et al., 2000), a critical component of the antiviral system that cleaves single-stranded RNA (Stark et al., 1998).

1.7.3 IRE1α-XBP1 in inflammatory bowel disease (IBD)

In line with the role of the IRE1α-XBP1 pathway in immunity, XBP1 has been implicated in inflammatory bowel disease (IBD), a common chronic human disorder. Mice with specific *Xbp1* deletion in intestinal epithelial cells were more susceptible to developing spontaneous small intestinal enteritis (Kaser et al., 2008). Patients with Crohn's disease and ulcerative colitis, two forms of IBD, exhibited decreased XBP1s levels. In addition, several genome-wide linkage studies hinted at an association between IBD and a region of the genome physically close to the *Xbp1* gene (Barmada et al., 2004; Hampe et al., 1999; Vermeire et al., 2004) and the IRE1β gene (Brant et al., 1998; Hugot et al., 1996). Moreover, deep sequencing identified novel rare single nucleotide polymorphisms in the *Xbp1* gene that along with other environmental and genetic risk factors, might confer susceptibility to IBD (Kaser et al., 2008). Further supporting a key role of XBP1 in IBD, loss of IRE1β, the isoform expressed predominantly in the gastrointestinal tract, resulted in hypersensitivity to

dextran sodium sulfate (DSS)-induced colitis in mice (Bertolotti et al., 2001). It is quite interesting that IRE1α expression alone in intestinal epithelial cells failed to protect IRE1β$^{-/-}$ animals from induced colitis. Thus, these studies pointed to a non-redundant and unique role of the IRE1β-XBP1 pathway in the pathogenesis of IBD.

1.7.4 IRE1α-XBP1 in metabolism

ER stress, particularly the IRE1α-XBP1 branch, has been implicated in obesity-induced insulin resistance and type 2 diabetes (Ozcan et al., 2009; 2004; 2006; Sha et al., 2011; Zhang et al., 2008). Initial reports demonstrated a link between IRE1α activation and c-Jun N-terminal kinase (JNK)-dependent inhibitory phosphorylation of insulin receptor substrate 1 (IRS-1) at serine 307 (Ser307) (Ozcan et al., 2004; Urano et al., 2000). In line with the role of IRE1α activation in attenuating insulin signaling, XBP1s overexpression in mouse embryonic fibroblasts (MEFs) suppressed ER-stress-induced JNK activation and IRS-1 phosphorylation on Ser307, whereas XBP1$^{+/-}$ tissues showed opposite effects (Ozcan et al., 2004). Furthermore, XBP1$^{+/-}$ mice exhibited increased ER stress and more severe insulin resistance upon high fat-diet (HFD)-induced obesity accompanied with elevated p-Ser307 on IRS1 (Ozcan et al., 2004). Conversely, reduction of ER stress through the administration of chemical/pharmacologic chaperones such as 4-phenylbutyric acid (PBA) and tauroursodeoxycholic acid (TUDCA) attenuated phosphorylation of IRS1 at Ser307 and improved the insulin sensitivity of obese animals (Ozcan et al., 2006).

More recently, it was shown that compromised insulin signaling during obesity might decrease the levels of functional nuclear XBP1s in the liver of obese mice (Park et al., 2010). The interaction between the heterodimer p85α and p85β, the regulatory subunits of phosphoinositide 3-kinase (PI3K) and XBP1 was disrupted in obese animals, leading to defects in the nuclear entry of XBP1s and elevated ER stress. Overexpression of p85α or β in the liver improved glucose tolerance in obese animals (Park et al., 2010). Hence, ER stress has been proposed to be a critical link between obesity with insulin resistance (Hotamisligil, 2010).

Several studies, however, have suggested that this model may not be all-inclusive. First, liver specific XBP1-null mice failed to exhibit overt changes in ER ultrastructure or activation of the other two UPR braches PERK and ATF6 (Lee et al., 2008a). This is in line with another report showing that *Xbp1* expression and the active form of ATF6 were reduced in the hepatocytes of obese mice, indicative of decreased ER stress (Wang et al., 2009b). Furthermore, ER stress was not detectable in white adipose tissues (WAT) upon 12 weeks HFD in XBP1-splicing reporter mice (Yoshiuchi et al., 2008), questioning the notion that ER stress in adipose tissues played a causal role in obesity-associated insulin resistance. Moreover, a recent study demonstrated that phosphorylation of IRS1 at Ser307 was not critical for the development of insulin resistance, but rather promoted insulin sensitivity in mice (Copps et al., 2010). The IRS1 Ser307Ala knock-in mice exhibited increased insulin resistance upon HFD-induced obesity. Finally, liver-specific disruption of p85α improved systemic glucose tolerance and insulin sensitivity in both lean and obese mice while overexpression of p85α in the liver had the opposite effects (Taniguchi et al., 2007; 2006). Hence, the role

of ER stress and the IRE1α-XBP1 pathway in obesity and diabetes warrants further studies.

XBP1 has also been implicated in hepatic lipid metabolism and adipocyte differentiation (Fig. 1.4). Using hepatocyte-specific conditional XBP1 knockout mice, it was shown that XBP1-deficient hepatocytes exhibited reduced *de novo* lipid biosynthesis (Lee et al., 2008a). XBP1 played an unexpected role in regulating hepatic lipogenesis by directly binding to the promoters of key lipogenic factors including diacylglycerol acetyltransferase 2 (DGAT2), stearoyl-CoA reductase 1 (SCD1) and acetyl-CoA carboxylase (ACC2) (Lee et al., 2008a). In addition, we showed that XBP1-deficient pre-adipocytes and MEF cells showed dramatic defects in adipogenesis (Chapter 2, Sha et al., 2009). During this developmental process, a key early adipogenic factor C/EBPβ induced *Xbp1* expression; subsequently, XBP1s interacted with the promoter of *Cebpα*, a master regulator of adipogenesis, and activated its expression (Sha et al., 2009). Thus, XBP1 played a critical regulatory role during adipogenesis by integrating into the transcriptional cascade underlying adipogenic differentiation. This finding was consistent with reports of an absence of fat depot in $XBP1^{-/-}$ neonates rescued with hepatic XBP1s overexpression (Lee et al., 2005).

1.7.5 IRE1α-XBP1 in cancer

Genome-wide profiling along with association studies demonstrated that XBP1 expression was induced in a variety of cancers including lymphoid malignancies such as multiple myeloma and acute myeloid leukemia (Davies et al., 2003; Juric et al., 2007; Leleu et al., 2009; Munshi et al., 2004) as well as breast

cancers (Doane et al., 2006; Gomez et al., 2007; Lacroix and Leclercq, 2004). Moreover, multiple myeloma cells with overexpression of superoxide dismutase (SOD2), an enzyme that eliminates free superoxide radicals, exhibited decreased proliferation correlated with decreased *Xbp1* expression (Hurt et al., 2007). In support of a direct role for XBP1 in tumorigenesis, the loss of XBP1 was shown to severely inhibit tumor growth (Romero-Ramirez et al., 2004). Indeed, transformed cells with XBP1 deficiency were more sensitized to hypoxia and underwent apoptosis, implicating XBP1 as a survival factor (Romero-Ramirez et al., 2004). In addition, mice with ectopic expression of XBP1s in B cells exhibited enhanced B cell proliferative potential along with development of multiple myeloma that recapitulated the human disease (Carrasco et al., 2007). Finally, it was shown that XBP1 was activated in primary mammary tumors with its expression correlating with enhanced tumor growth (Spiotto et al., 2010).

Thus, the role of XBP1 as a survival factor deems it a very attractive therapeutic target. However, UPR can also initiate apoptosis in the face of persistent ER stress. A study demonstrated that acute myeloid leukemia patients with UPR activation actually merited better prognosis as indicated by lower relapse rates coupled with a better overall and disease-free survival (Schardt et al., 2009). Therefore, to fully understand the involvement of XBP1 in cancer development and progression, future studies that can carefully monitor UPR activation and delineate the respective roles of all three UPR branches are required.

1.7.6 IRE1α-XBP1 in neurodegeneration and aging

The role of IRE1α-XBP1 in neurodegeneration remains controversial and appears to be disease-specific. Toxic intracellular protein aggregates, one of the primary underlying causes of neurodegenerative pathologies, can induce ER stress and activate UPR (Lindholm et al., 2006). Indeed, cellular and animal models of Huntington's (Nishitoh et al., 2008; 2002) and Parkinson's (Holtz and O'Malley, 2003) diseases are reportedly associated with activation of the IRE1α-XBP1 pathway. However, it remains unclear whether UPR activation in these models represents a direct cause of the diseases or a secondary effect associated with tissue damage.

XBP1 occupancy was observed on the promoters of genes linked to neurodegenerative pathologies including Alzheimer's disease (Acosta-Alvear et al., 2007), although the relevance of these events remains speculative. Ectopic expression of XBP1s played a protective role in cells against chemical-induced cell death and significantly attenuated the degeneration of dopaminergic neurons in a mouse model of Parkinson's disease (Sado et al., 2009). In contrast, SOD1 transgenic mice with XBP1 deficiency specifically in the nervous system were more resistant to the development of familial amyotrophic lateral sclerosis (ALS) (Hetz et al., 2009). These animals exhibited increased macroautophagy concomitant with reduced accumulation of mutant SOD1, supporting an intimate link between UPR and autophagy. In contrast, XBP1 did not appear to influence prion pathogenesis as loss of XBP1 had no effect on prion aggregation, neuronal survival or overall animal survival (Hetz et al., 2008). Consistently, many UPR markers were unaffected in the brains of prion-infected XBP1-

deficient mice when compared to the wild-type cohort (Hetz et al., 2008).

Recent studies have implicated the IRE1-XBP1 pathway in aging in worms (Chen et al., 2009; Henis-Korenblit et al., 2010). First, loss of hypoxia inducible factor 1 (HIF1) extended lifespan in part through the activation of the IRE1 pathway. Defects in IRE1 signaling significantly reduced the lifespan of the long-lived *hif1* loss-of-function mutant (Chen et al., 2009). This effect appeared to be IRE1-specific as a PERK deletion mutant had no effect. A similar observation was recently reported in insulin/IGF-1 pathway mutant worms (Henis-Korenblit et al., 2010). Loss of IRE1 or XBP1 shortened the lifespan of long-lived *daf-2* mutants to a much lesser extent than in wild-type worms, suggesting that the effect of XBP1 on lifespan may depend on one of these factors in the insulin/IGF-1 pathway. Nonetheless, IRE1 activity and *Xbp1s* mRNA were unexpectedly very low in the *daf-2* mutant, indicative of improved overall ER homeostasis. Mechanistically, it was proposed that XBP1 might regulate the expression of a conserved Zinc-finger protein *dox-1* (downstream of XBP1) in a DAF-16/FOXO dependent manner. The effect of IRE1-XBP1 in the aging process of higher organisms merits further studies.

	Effect on IRE1α signaling	Reference
BAX/BAK	+	Scorrano, L. et al (2003) *Science*
AIP1	+	Luo, D. et al. (2008) *JBC*
HSP72	+	Gupta, S. et al. (2010) *PLoS Biol*
JIK	+	Yoneda, T. et al. (2001) *JBC*
TRAF2	+	Urano, F. et al (2000) *Science*
NCK	-	Nguyen, D.T. et al. (2004) *MBC*
HSP90	-	Marcu, M.G. et al. (2002) *Nat Cell Biol*
JAB1	-	Oono, K. et al. (2004) *Neurochem Int*
PP2A	-	Qiu, Y. et al. (2010) *Sci Signal*
RACK1	-	Qiu, Y. et al. (2010) *Sci Signal*
BI-1	-	Lee, G.H. et al. (2007) *JBC*

Figure 1.5. IRE1α interacting factors constitute the IRE1α interactome.
List of current factors that have been reported to interact with and regulate IRE1α activation and signaling. Factors highlighted in green and marked with "+" indicate an up-regulation/activation of IRE1α signaling whereas those highlighted in red and marked with "-" indicate a down-regulation/inhibition of IRE1α signaling.

1.8 REGULATING IRE1α-XBP1 SIGNALING

Given the importance and clinical relevance of the IRE1α-XBP1 signaling pathway to human health, a comprehensive understanding of the underlying regulatory mechanisms is essential and will be informative for the development of intervention strategies. Recently, reports demonstrating the dynamic assembly and formation of various protein complexes containing IRE1α in a tissue- or cell-specific manner has proposed the concept of a "UPRosome" or IRE1α interactome that plays a key role in regulating both the activation and kinetics of mammalian IRE1α activation, signaling and downstream cellular responses (Hetz et al., 2011; Hetz and Glimcher, 2009; Woehlbier and Hetz, 2011).

IRE1α signaling is highly and tightly regulated by a set of co-factors including both activators and inhibitors (Fig. 1.5). These include apoptosis-related proteins such as members of the apoptosis-associated BCL-2 family that localize to the ER membrane. BAX and BAK are pro-apoptotic factors that specifically activate IRE1α signaling through an interaction between the cytosolic domain of IRE1α and the BH domain of BAX/BAK (Hetz et al., 2006). Additionally, other members of the BCL-2 family containing only a BH3 domain such as BIM and PUMA activated the IRE1α pathway in the presence of BAK (Klee et al., 2009). BAX inhibitor-1 (Bl-1) is an ER protein that interacted with IRE1α and a deficiency in Bl-1 enhanced IRE1α activation and signaling (Lisbona et al., 2009). Interestingly, Bl-1 function was highly conserved, but appeared to be specific to multi-cellular organisms as yeast lacking a Bl-1 homolog displayed normal HAC1 (XBP1 homolog) expression (Lisbona et al., 2009). Furthermore,

the cytosolic domain of IRE1α interacted with TNFR-associated factor 2 (TRAF2) to activate downstream targets apoptosis signal-regulating kinase 1 (ASK1) and c-Jun-N terminal kinase (JNK), ultimately leading to activation of apoptosis in cells unable to restore ER homeostasis (Kanda and Miura, 2004; Mauro et al., 2006; Nishitoh et al., 2002; Urano et al., 2000). Another pro-apoptotic factor ASK1-interacting protein 1 (AIP1) enhanced IRE1α activation and signaling specifically with no effect on the PERK pathway (Luo et al., 2008). AIP1 interacted with IRE1α in an ER stress-dependent manner and promoted IRE1α dimerization (Luo et al., 2008). Lastly, caspase-12 cleavage and activation was also reported to be correlated with the TRAF2-IRE1α pathway (Yoneda et al., 2001). All together, these co-factors interact with IRE1α to inhibit or promote its activation and signaling, providing an additional layer of regulation and fine-tuning.

Given the role of IRE1α and XBP1 in immunity, IRE1α signaling has also been reported to integrate with inflammatory pathways including that of NF-κB, p38 and ERK potentially through interactions with the adaptor protein Nck and IKK or TRAF2 (Hu et al., 2006; Nguyên et al., 2004). However, the exact mechanistic details and biological implications and significance remain unknown.

In response to ER stress, both the UPR and ERAD networks are activated and coordinately function together to restore ER homeostasis. However, knowledge regarding the relationship and regulation between UPR and ERAD by ER stress and their inter-dependency remain in its infancy. Under basal non-

stress conditions, inactive IRE1α interacted with the ubiquitin specific protease 14 (USP14); this interaction disappeared with ER stress and IRE1α activation, suggesting that USP14 was a negative modulator (Nagai et al., 2009). Intriguingly, the same study showed that inactive IRE1α was found to be in a complex containing critical ERAD regulators, Derlin-1, Derlin-3, Sel1, and Hrd1 (Nagai et al., 2009). However, the functional consequences of these findings require additional studies.

IRE1α activation is highly correlated with its phosphorylation. Not surprisingly, IRE1α signaling was reported to be modulated by an ER localized phosphatase, protein-tyrosine phosphatase 1B (PTP-1B). This regulation was specific to IRE1α as PERK signaling was unaffected by a PTP-1B deficiency (Gu et al., 2004). The physiological relevance of PTP-1B was supported by studies of UPR in a diabetes mouse model. However, whether PTP-1B can interact with IRE1α in a temporal manner remains to be established. Speculatively, PTP-1B would function during the later stages of ER stress to dephosphorylate and inactivate IRE1α. Other studies have attempted to study the later stages of IRE1α signaling to determine how this protein is inactivated. In addition to PTP-1B, the ubiquitous cytosolic chaperone protein HSP90 may also negatively regulate IRE1α activation and signaling by modulating IRE1α protein stability. HSP90 inhibition by chemical drugs disrupted the interaction with the cytosolic segment of IRE1α and promoted proteasome-mediated IRE1α degradation (Marcu et al., 2002). As HSP90 has reported roles in regulating the stability of other proteins and protein complexes, this finding suggests that HSP90 may function to

stabilize the IRE1α protein and permit formation of the IRE1α interactome.

Emergence of the IRE1α interactome has conceptualized and revolutionized the way in which IRE1α activation and signaling is viewed. Prior to these discoveries, IRE1α activation was perceived simplistically as the progressive arrangement of IRE1α monomers into dimers concomitant with trans-autophosphorylation of adjacent IRE1α monomers. The identification of dynamic and tissue-specific formation of regulatory complexes demonstrated that IRE1α signaling occurs by precise and tightly-controlled mechanisms to enhance or dampen IRE1α signal propagation. However, these discoveries inevitably raise additional questions that warrant future studies aiming to comprehensively identify all components of the IRE1α interactome as well as delineate their functional and physiological roles in IRE1α activation and signaling.

Several yeast studies have reported novel compounds that can engage IRE1 activation in novel ways and shed light on IRE1 activation that may be relevant to mammalian IRE1α. First, the use of an ATP-competitive drug 1NM-PP1 demonstrated that a conformational change induced by the binding of 1NM-PP1 in the kinase active site of IRE1 was sufficient to induce downstream effector events (Papa et al., 2003). Impaired IRE1 kinase activity was irrelevant to downstream functions as long as the active site was occupied, in this case by 1NM-PP1 (Papa et al., 2003). This finding has critical implications for understanding metazoan IRE1α activation and drug development as 1NM-PP1 can dissociate IRE1 RNase and kinase activities, allowing for independent

characterizations of both domains. More recently, a study identified a novel ligand binding site located at the interface of the kinase and RNase domains of yeast IRE1 (Wiseman et al., 2010). This site was bound by the quercetin flavonol, which greatly enhanced IRE1 RNase activity (Wiseman et al., 2010), thus resulting in the identification of another compound that can disconnect IRE1 kinase and RNase activities to allow for precise mechanistic characterizations of IRE1 activation. Additionally, whether an endogenous compound exists that structurally resembles and behaves similarly to quercetin is an intriguing question.

1.9 TEMPORAL REGULATION OF UPR SIGNALING

The dynamics and kinetics of UPR signaling greatly influence cell fate determination. Although UPR commences as an adaptive response to restore ER homeostasis, the three UPR sensors are kinetically and temporally regulated upon ER stress and can be characterized by four stages of response (Woehlbier and Hetz, 2011). During the initial or acute phase of ER stress, PERK activation and phosphorylation of eIF2α contribute to a global decrease in protein synthesis (Harding et al., 1999; Novoa et al., 2003). This is coupled with IRE1α-mediated mRNA decay (RIDD) to attenuate protein flux and load into the ER (Han et al., 2009; Hollien and Weissman, 2006; Hollien et al., 2009). The second wave of response is transcriptional and is mediated by all three pathways to collectively increase ER capacity and quality control. The main contributors are the transcription factors XBP1, ATF4 and ATF6 that induce the expression of chaperones, degradation machinery, and enzymes for ER expansion and lipid

synthesis (Yamamoto et al., 2007). The first two phases are adaptive and attempt to restore ER homeostasis. However, if ER stress remains unresolved, IRE1α signaling becomes dampened whereas PERK activation remains sustained and is believed to induce apoptosis through CHOP, a downstream target of ATF4. This transition stage highlights a shift from adaptation and pro-survival to pro-apoptotic (Woehlbier and Hetz, 2011). The last stage of chronic ER stress involves further reinforcement of apoptosis through transcriptional induction of genes related to the BCL2 pro-apoptosis protein family and integrating with the canonical mitochondria-mediated apoptotic network (Woehlbier and Hetz, 2011). The four stages of UPR signaling highlight and emphasize the double-edged sword property of UPR and should be a key consideration in drug and therapeutic development. Whereas acute and early activation of UPR may be cyto-protective, prolonged and persistent ER stress engages the pro-apoptosis pathways.

Though ER stress-modulated cell fate determination by IRE1α and PERK has been well-studied, knowledge of the role of ATF6 is greatly lacking. Speculatively, as ATF6 needs to translocate to the Golgi network and undergo proteolysis before becoming an active UPR transcription factor, the temporal dynamics of ATF6 activation will be different than that of IRE1α and PERK. Also, as ATF6 transcriptional targets include genes functioning in folding and ERAD, this pathway likely promotes pro-survival. However, how ATF6 integrates with the IRE1α and PERK pathways to regulate cellular survival and apoptosis is an intriguing question. Furthermore, a key remaining enigma in the field is how these ER signaling pathways are inactivated. As IRE1α and PERK both undergo

extensive phosphorylation correlated with their activation status, the presence and action of phosphatases have been proposed to down-regulate these sensors. Notably, although IRE1α and PERK signaling are typified in the literature as pro-survival and pro-apoptosis respectively (Lin et al., 2009), this delineation is not so straightforward as IRE1α signaling has also been reported to promote apoptosis through an interaction with apoptosis-related factors including BAX and BAK as well as autophagy through JNK activation (Hetz and Glimcher, 2009). Hence, further investigations are warranted to tease out the relationship and dependency of these three signaling pathways on cell fate determination as well as the physiological and in vivo significance of these findings.

1.10 RESEARCH AIM AND DISSERTATION ORGANIZATION

In summary, UPR activation and signaling has been implicated in a variety of human diseases and a complete understanding of how these pathways are regulated is critical in the development of therapeutics. Of the three major metazoan UPR pathways, the IRE1α-XBP1 is the most evolutionarily conserved. However, a comprehensive and mechanistic examination of how IRE1α-XBP1 signaling is regulated as well as its function in different tissues remains incomplete. Hence, the *overarching aim* of this dissertation is to elucidate the regulatory mechanisms and understand the physiological relevance of IRE1α-XBP1 activation and signaling by utilizing complementary biochemical, cellular, and genomics and proteomics-based assays.

An introduction and relevant literature review on protein homeostasis, ER

stress and IRE1α activation and signaling are presented in Chapter 1. Chapter 2 focuses on the critical and indispensable role of IRE1α-XBP1 signaling in a cellular differentiation process in fat cells termed adipogenesis in which XBP1 induces the expression of a key adipogenic factor, C/EBPα. Chapter 3 reports the identification and characterization of a novel cytoskeleton-associated factor, NMIIB, that regulates a key activation step of IRE1α signaling, namely oligomerization and foci formation. Lastly in Chapter 4, I review the implications, contribution and significance of my dissertation research by proposing a new model for the activation of the mammalian IRE1α-XBP1 pathway as well as discuss how these studies may advance our knowledge of UPR signaling and their potential to identify new targets for drug intervention in treating conformational diseases.

The appendices in this dissertation are organized by independent projects and provide exciting and promising new insight into IRE1α activation and its physiological role. However, as most of these findings are preliminary, they have been excluded from the main chapters. Appendix A describes a novel role of XBP1 in macrophages in mediating the expression of key inflammatory mediators in response to canonical ER stress. This modulation may occur through a physical interaction with ATF3, a factor known to influence and integrate signaling pathways associated with immunity. Appendix B identifies a new "SSPS" motif located on the cytosolic linker region of IRE1α that is extensively phosphorylated upon ER stress and may be required for IRE1α trans-autophosphorylation. Appendix C lists additional putative IRE1α-interacting

factors identified through a proteomics-based tandem mass spectrometry collaboration and postulates how they may function to modulate IRE1α activation and integrate into UPR signaling.

CHAPTER 2*

THE IRE1α-XBP1 PATHWAY OF THE UNFOLDED PROTEIN RESPONSE IS REQUIRED FOR ADIPOGENESIS

2.1 ABSTRACT

Signaling cascades during adipogenesis culminate in the expression of two essential adipogenic factors, PPARγ and C/EBPα. Here we demonstrate that the IRE1α-XBP1 pathway, the most conserved branch of the unfolded protein response (UPR), is indispensable for adipogenesis. Indeed, XBP1-deficient mouse embryonic fibroblasts and 3T3-L1 cells with XBP1 or IRE1α knockdown exhibit profound defects in adipogenesis. Intriguingly, C/EBPβ, a key early adipogenic factor, induces *Xbp1* expression by directly binding to its proximal promoter region. Subsequently, XBP1 binds to the promoter of *Cebpa* and activates its gene expression. The posttranscriptional splicing of *Xbp1* mRNA by IRE1α is required as only the spliced form of XBP1 (XBP1s) rescues the adipogenic defect exhibited by XBP1-deficient cells. Taken together, our data show that the IRE1α-XBP1 pathway plays a key role in adipocyte differentiation by acting as a critical regulator of the morphological and functional transformations during adipogenesis.

---

* This chapter has been published as Sha, H.Ω, **He, Y**.Ω, Chen, H., Wang, C., Zenno, A., Shi, H., Yang, X., Zhang, X., and Qi, L. *Cell Metabolism* **9**, 556-564 (2009) and is reprinted here with permission. Ω Co-first authors.

2.2 INTRODUCTION

Excess adipose tissue mass plays a central role in obesity-related complications such as cancer, cardiovascular diseases, insulin resistance and type 2 diabetes. A comprehensive understanding of the molecular mechanisms underlying adipocyte formation and development is of both fundamental and clinical relevance. Cellular models, such as 3T3-L1 and mouse embryonic fibroblasts (MEFs), are invaluable in studying adipocyte differentiation or adipogenesis (Farmer, 2006). During adipogenesis, two transcription factors, CCAAT/enhancer-binding protein β (C/EBPβ) and C/EBPδ, are induced very early and play a crucial role in initiating the differentiation program by activating the expression of peroxisome proliferator-activated receptor γ (PPARγ) and C/EBPα, two key adipogenic transcription factors that positively regulate each other to promote and maintain the differentiated state (Farmer, 2006; Tontonoz and Spiegelman, 2008). Ectopic expression of either PPARγ or C/EBPα induces non-adipogenic fibroblasts to differentiate into adipocytes. Cells or adipose tissues with disruption in either gene exhibit severe defects in adipocyte differentiation or fat depot formation (Farmer, 2006; Tontonoz and Spiegelman, 2008).

Under the regulation of this complex transcriptional circuit, pre-adipocytes undergo dramatic transformations that ultimately lead to terminal adipogenic differentiation. However, it remains unclear how cells adapt to such dramatic morphological changes. Given their endocrine capacity and unique cellular structure, it has recently been hypothesized that adipocytes may display elevated UPR in an attempt to alleviate stress in the endoplasmic reticulum (ER)

caused by increased protein and lipid biosynthesis (Gregor and Hotamisligil, 2007). In yeast, upon ER stress, ER-resident transmembrane protein IRE1α oligomerizes and undergoes trans-autophosphorylation, leading to activation of its cytosolic endoribonuclease domain (Cox et al., 1993; Mori et al., 1993; Ron and Walter, 2007). Although phosphorylation of IRE1α has been used widely as an activation marker in experiments using ER stress inducers such as DTT or thapsigargin (Tg), recent studies in yeast suggest that the kinase activity may not be required for the endoribonuclease activity of IRE1α (Korennykh et al., 2009; Papa et al., 2003). However, the mechanism by which mammalian IRE1α is activated under physiological stress conditions remains largely unexplored.

Once activated, mammalian IRE1α splices 26 nucleotides from the *Xbp1* mRNA, leading to a frameshift and the generation of an active b-ZIP transcription factor, XBP1s, that contains a C-terminal transactivation domain absent from the unspliced form XBP1u. XBP1s subsequently translocates to the nucleus and activates the transcription of genes involved in protein folding and degradation to restore ER homeostasis (Ron and Walter, 2007). Studies in animal models have revealed that the IRE1α-XBP1 pathway is essential for the development and function of the liver and heart as well as professional secretory cells such as pancreatic exocrine and plasma cells (Lee et al., 2005; Masaki et al., 1999; Reimold et al., 2000; 2001; Zhang et al., 2005). Recently, XBP1 has been shown to regulate hepatic lipogenesis via a UPR-independent manner (Lee et al., 2008a). However, its role in other cell types remains unclear.

Interestingly, XBP1 is highly expressed in embryonic adipose depot (Clauss et al., 1993) and white adipose cells (Kajimura et al., 2008). Moreover,

XBP1$^{-/-}$ neonates rescued with hepatic XBP1s overexpression have no fat depot (Lee et al., 2005). These findings prompted us to hypothesize that XBP1 plays a role in adipocyte development. Indeed, our data demonstrate that XBP1 controls adipogenesis in part by transactivating the expression of a key adipogenic factor C/EBPα. In addition, our results suggest that adipogenic differentiation is associated with a low degree of UPR that is responsible for IRE1α activation and the subsequent splicing of *Xbp1* mRNA. Intriguingly, IRE1α activity peaks during early adipogenesis and does not involve its hyperphosphorylation.

2.3 MATERIALS AND METHODS

Cells

3T3-L1 pre-adipocytess, XBP1$^{-/-}$ and wild-type control MEFs (gifts from Laurie Glimcher, Harvard Medical School), HEK293T and phoenix cells were maintained in DMEM supplemented with 10% FBS (Hyclone) and 1% penicillin/streptomycin (Cellgro). Tg and Tm (EMD Calbiochem) were used at a final concentration of 300 nM and 2.5 μg/ml, respectively dissolved in DMSO.

Generation of the pSuper/U6/retro vector

The pSuper/U6/retro vector was constructed by subcloning the 350 bp EcoRI-BamHI fragment including the U6 promoter and multiple cloning sites from the pBS/U6 vector to the pSuper/retro vector (EcoRI-BglII), replacing the H1 promoter.

Retroviral transduction and stable cell line generation

Phoenix cells were transfected with the plasmids encoding the gene of interest in pSuper or pBabe vectors and VSVG at 2:1 ratio for 16 h and then replaced with fresh culture media. Following 48 h culture, media containing retroviruses were harvested and used to transduce target cells in the presence of 5 μg/ml polybrene (Sigma) for 24 h. Stable cell lines were selected in the presence of 2 μg/ml puromycin (Sigma) or 500 μg/ml G418 (EMD Calbiochem) and then used for differentiation. Typically, puromycin-resistant cell lines developed in 6 days whereas G418 resistant cell lines were generated in 12 days. In rescue experiments, 3T3-L1 cells transduced with two retroviruses were selected with both puromycin and G418. To minimize the batch-to-batch difference, we only compared cells made from the same batch of cells.

shRNA knockdown

Two vectors were used in this study: pSuper/retro (H1 promoter, a gift from Lee Kraus, Cornell University) and pSuper/U6/retro (U6 promoter, described in Generation of the pSuper/U6/retro vector). XBP1i and IRE1αi were driven by the U6 promoter while C/EBPβi was driven by the H1 promoter. Control RNAi were against the firefly luciferase or the GFP gene. Target sequences are shown in Table 2.1.

Table 2.1. shRNA target sequences.
List of shRNA targeting sequences designed using Dharmacon. XBP1i#4 targets the 3' UTR and thus, has no effect on exogenously-transfected XBP1 cDNAs – the basis of the rescue experiments. All shRNAs are mouse-specific unless otherwise indicated.

Promoter-shRNA	Target sequences	Positions (mRNA), Specificity and Reference
H1-XBP1i #1 (control)	TCTTAAAGGTGGTAGTATA	nt. 1370-1388
H1-XBP1i #2 (control)	GGATTCATGAATGGCCCTT	nt. 1558-1576
U6-XBP1i #4	GGATTCATGAATGGCCCTTA	nt. 1558-1577 at 3' UTR (Lee et al., 2003)
U6-XBP1i #5	GGTCTGCTGAGTCCGCAGCA	nt. 463-483, against human and mouse
U6-IRE1αi #2 (control)	GGCTCCATCAAGTGGACTTT	nt. 274-293
U6-IRE1αi #4	GGAAGAGCAAGCTGAACTAC	nt. 1169-1188
H1-C/EBPβi	AGATGTTCCTGCGGGGTTG	nt. 1284-1302 at 3' UTR (Chen et al., 2005)
H1-Firefly luciferase	GCTATGGGCTGAATACAAA	(Reynolds et al., 2004)
H1-GFP	GAAGCTGACCCTGAAGTTCATC	

Mice and tissues

Wildtype and *ob*/*ob* mice on C57BL/6 background were purchased from the Jackson Laboratory. The epididymal WAT, BAT and liver were harvested from (a) wildtype mice fed with either 60% HFD (Research Diets Inc.) or 10% chow diet for over 13 weeks; (b) *ob*/*ob* mice at the age of 12-26 week old. Tissues were harvested immediately following cervical dislocation, snap-frozen in liquid nitrogen and stored at -80^{0}C (Qi et al., 2009). All animal procedures were approved by the Cornell IACUC.

Plasmids and viruses

XBP1u and XBP1s cDNAs, cloned from the mouse WAT cDNA library using pfu polymerase (Stratagene), were subcloned into pcDNA3/Flag or 3x HA vectors. Retroviral encoding XBP1u and Flag-XBP1s were cloned by shuttling XBP1 cDNA into the pBabe-puro vector. For retroviral transduction in the 3T3-L1 experiments, cDNAs encoding the mouse C/EBPβ and rat C/EBPα were cloned into the pBabe-puro vector using standard PCR reactions. Promoter regions of mouse *Xbp1* (-689 to +37 bp), *Edem* (-336 to +15 bp) and *Cebpa* (-320 to +45 bp) were cloned via PCR of tail genomic DNA of C57BL/6 mice and ligated into the pGL3-basic luciferase reporter construct (Promega). Constructs generated by PCR were sequenced by the Cornell DNA sequencing facility.

Adipogenesis

(a) 3T3-L1: Two days post-confluency (d0), cells were treated for 48 h with 0.25 mM IBMX, 1 μM DXM (EMD Calbiochem) and 1 μg/ml insulin (Sigma). Afterwards, cells were fed every 48 h with 1 μg/ml insulin in culture media until d8 post confluence. (b) MEF: Cells were differentiated as 3T3-L1 with the following modifications: when the cells became confluent (d0), they were treated with 0.25 mM IBMX, 5 μM DXM, 10 μg/ml insulin and 5 μM troglitazone (EMD Calbiochem) for the first 48 h. Subsequently, cells were maintained in 1 μg/ml insulin and 5 μM troglitazone to induce terminal differentiation.

Oil Red-O staining

Cells were fixed with 10% formaldehyde in PBS for 15 min at room temperature and stained with freshly-prepared Oil Red-O working solution for 30 min followed by three washes with water. Plates were scanned using an Epson scanner. Oil Red-O working solution was prepared by mixing 6 ml of 0.5% Oil Red-O (Sigma) in isopropanol with 4 ml of ddH_2O followed by filtration through a Whatman #1 filter paper (Millipore).

Western blot

Western blot was performed using 15-30 μg of total cell lysates or 10 μg of nuclear extracts. Antibodies used in this study: C/EBPβ (mouse, 1:1000, Biolegend); GRP78 (goat, 1:1,000), C/EBPα (rabbit, 1:2,000), PPARg (mouse, 1:400), XBP1 (rabbit, 1:1,000), and HSP90 (rabbit, 1:5,000) from Santa Cruz; IRE1α (rabbit, 1:1,000, Cell Signaling); GAPDH (rabbit, 1:10,000, Novus Biologicals). Secondary antibodies, goat anti-rabbit IgG, anti-mouse IgG (Biorad), and donkey anti-goat IgG HRP (Jackson ImmunoResearch), were used at 1:10,000. The p-Ser724 IRE1α antibody from Novus Biologicals did not work in our hands.

Nuclear-cytosolic fractionation

Cells in a 6-cm dish were resuspended in 200 μl ice-cold hypotonic buffer (10 mM HEPES pH 7.9, 10 mM KCl, 0.1 mM EDTA, 0.1 mM EGTA, and 1 mM DTT) and allowed to swell on ice for 15 min followed by addition of 10% of NP-40 to a final concentration of 0.6%. Lysates were vortexed vigorously for 15 s prior to

centrifugation at top speed for 1 min. Supernatant was transferred to a fresh tube as the cytosolic fraction. Pellets were resuspended in 50 μl ice-cold high-salt buffer (20 mM HEPES pH 7.9, 0.4 M NaCl, 1 mM EDTA, 1 mM EGTA, and 1 mM DTT) and vortexed vigorously for 15 sec every 5 min for a total of 20 min. Extracts were spun at 4°C for 5 min and the supernatant (nuclear fractions) was collected.

Phos-tag gels

Phos-tag gel was carried out the same way as regular Western blots, except that: (a) 5% SDS-PAGE containing 50 μM Phos-tag (NARD Institute) and 50 μM $MnCl_2$ (Sigma) were used; (b) gels were soaked in 1 mM EDTA for 10 min prior to transfer onto a PVDF membrane.

Calf intestine phosphatase (CIP) treatment

50 μg whole cell lysates (normally with starting concentrations around 5 μg/μl) were mixed with 8 μl 10x NEB buffer 3 and 5 μl CIP (10 U/μl, NEB) in a 80 μl reaction (fill to the volume with PBS) at 37°C for 60 min. The reaction was stopped by addition of 20 μl 5x SDS sample buffer followed by boiling for 5 min. 15 μg of lysates were loaded onto a 5% gel followed by Western blot analysis of IRE1α.

RNA extraction and Q-PCR

Total RNA was extracted using Trizol per supplier's protocol (Molecular Research Center) and reverse transcribed using Superscript III kit (Invitrogen).

cDNA were analyzed using the Power SYBR Green PCR kit on the ABI PRISM 7900HT Q-PCR machine (Applied Biosystems) or the SYBR Green PCR system (gifts from Jeff Pleiss, Cornell University) on the iQ5 or Cfx384 Q-PCR machine (Bio-Rad). All Q-PCR data were normalized to ribosomal *l32* gene.

RT-PCR for *Xbp1* splicing

PCR primers were designed to encompass the splicing sequences of mouse *Xbp1* (Table 2.2). PCR products, amplified with annealing temperature at 58^0C for 30 cycles, were separated by electrophoresis on a 2.5% agarose gel (Invitrogen). Quantitation of percent of splicing, defined as the ratio of *Xbp1*s level to total *Xbp1* (*Xbp1u +Xbp1s*) levels, was carried out using the NIH ImageJ software.

Quick-change mutagenesis

Mutagenesis was carried out by PCR amplification using pfu (Stratagene) followed by digestion by DpnI (NEB) to get rid of the templates. Primer sequences are listed in Table 2.2. Mutations at specific positions were subsequently sequenced and confirmed.

Luciferase reporter assay

After overnight transfection, cells were lysed in extraction buffer (Gly-Gly buffer, 1% Triton X-100, and 1 mM DTT). 50 μl of lysates were transferred to a 96-well plate containing 50 μl of assay mix (Gly-Gly buffer, 16 mM K_2HPO_4, 2 mM DTT and 2.5 mM ATP). 100 μl of 0.4 mM luciferin mix was added to each well through injector and readings were collected using the Synergy 2 plate reader (Biotek).

Luciferase activity was normalized to activity from co-transfected Rous sarcoma virus-β-galactosidase expression plasmid.

Table 2.2. Primer sequences.
Primer position, where noted, is relative to the transcription start site (TSS).

	Gene	Forward	Reverse
RT-PCR	Xbp1	AGTTAAGAACACGCTTGGCAAT	AAGATGTTCTGGGGAGGTGAC
	L32	GAGCAACAAGAAAACCAAGCA	TGCACACAAGCCATCTACTCA
Q-PCR	Chop	ATATCTCATCCCCAGGAAACG	TCTTCCTTGCTCTTCCTCCTC
	Cebpb	CAAGCTGAGCGACGAGTACA	AGCTGCTCCACCTTCTTCTG
	Xbp1	ACATCTTCCCATGGACTCTG	TAGGTCCTTCTGGGTAGACC
	Cebpa	TGAGCCGTGAACTGGACACG	CAGCCTAGAGATCCAGCGAC
	Erdj4	CTTAGGTGTGCCAAAGTCTGC	GGCATCCGAGAGTGTTTCATA
	Edem	GGGACCAAGAGGAAAAGTTTG	GAGGTGAGCAGGTCAAATCAA
	P58ipk	GTGGCATCCAGATAATTTCCAG	GAGTTCCAACTTCTGTGGAAGG
	Grp94	CTCAGAAGACGCAGAAGACTCA	AAAACTTCACATTCCCTCTCCA
	Erol1	CGGACCAAGTTATGAGTTCCA	TCAGAGAGATTCTGCCCTTCA
	Pparg1	TGAAAGAAGCGGTGAACCACTG	TGGCATCTCTGTGTCAACCATG
	Pparg2	TGCTGTTATGGGTGAAACTCT	CGCTTGATGTCAAAGGAATGC
	Grp78	TGTGGTACCCACCAAGAAGTC	TTCAGCTGTCACTCGGAGAAT
	Sel1l	TGGGTTTTCTCTCTCTCCTCTG	CCTTTGTTCCGGTTACTTCTTG
	Herp	AACCAGGACCCCAACAATAAC	CTGGAAGAAGAGAGGCAAAGAA
	Ire1a	CTGTGGTCAAGATGGACTGG	GAAGCGGGAAGTGAAGTAGC
	Atf4	CGAGATGAGCTTCCTGAACAGC	GGAAAAGGCATCCTCCTTGC
Mutagenesis	ΔC/EBPb on XBP1 -689	GCAATCATCTCAACTCATTTTGTGAAAAATT TCCCAGGTGTGTGTG	CACACACACCTGGGAAATTTTCACAAAATG AGTTGAGATGATTGC
	XBP1mut on C/EBPa -320	CCACGGACCAAAAGTGTGCGGGGGCG	CGCCCCCGCACACTTTTGGTCCGTGG
	ΔXBP1 on C/EBPa -320	CACGGACCGTGTGCGGGGGCGACAG	CTGTCGCCCCCGCACACGGTCCGTG
ChIP	Xbp1 -580 ~ -425	CTATGTAGCCCAGGCTGCTC	GCTTAGGGTTAGCGGACACA
	Cebpa -335 ~ -82	TCCCTAGTGTTGGCTGGAAG	CAGTAGGATGGTGCCTGCTG
	Cebpa -324 ~ -93	GGCTGGAAGTGGGTGACTTA	GTGCCTGCTGGGTCTTAGAG
	Cebpa -946 ~ -775	CGCTCTCCTTAGGGTCCTTT	TGTTTTTCATTGCGTCTCCA
	Xbp1 3' UTR	GGCATCTCAAACCTGCTTTC	AGCTGGGGGAAAAGTTCATT

Chromatin immunoprecipitation (ChIP)

3T3-L1 cells were cross-linked by 1% formaldehyde at room temperature for 20 min. Glycine was added for 5 min to a final concentration of 0.125 M. Cells were resuspended in buffer containing 25 mM HEPES, 1.5 mM $MgCl_2$, 10 mM KCl, 0.5% NP-40, 1 mM DTT, and protease inhibitors. Nuclei were collected by centrifugation and pellet was resuspended in 50 mM HEPES, 140 mM NaCl, 1 mM EDTA, 1% Triton X-100, 0.1% DOC, 0.1% SDS, and protease inhibitors. Samples were sonicated on ice to an average length of 600 bp. Chromatin was pre-cleared with protein A agarose (Invitrogen) at 4°C for 30 min, then incubated with 2 μg of antibody: IgG (Santa Cruz, sc-2027), XBP1 (sc-7160x), C/EBPβ (Biolegend, 6062). 50 μl of a 30% salmon-sperm-DNA-saturated protein A agarose (Invitrogen) was added to recover immune complexes for 2 hr. Immunoprecipitates were washed and eluted. Cross-links were reversed and samples were incubated in 0.5 mM EDTA, 1 mM Tris (pH 6.5), and 10 μg/ml proteinase K (Invitrogen) at 45°C for 1 hr. Samples were purified using Qiagen PCR Purification Kit (Qiagen), and assayed by Q-PCR. Primer sequence and positions are in Table 2.2. Annealing temperature for the PCR (Tm) is 58°C. Each ChIP experiment was conducted at least twice with independent chromatin preparations from different samples to ensure reproducibility.

Electron microscopy (TEM)

The TEM study of the ER morphology in differentiating 3T3-L1 cells was carried out with the assistance of the Cornell Imaging Core Facility. 3T3-L1 adipocytes (d5) were fixed in 2% glutaldehyde in 0.1 M cacodylate pH 7.4, for 0.5 hr at room

temperature and 1 hr at 4°C. After washing in cacodylate buffer, cells were postfixed for 1 hr in 1% osmium tetroxide in the same buffer at room temperature and washed again. After dehydration in a graded series of ethanol, cells were embedded in Epon/Araldite epoxy resin (Electron Microscopy Sciences) and all samples were polymerized at 60°C for 24 hr. Ultrathin sections were cut on a ultramicrotome (Reichert Om U2), collected on formvar- and carboncoated copper 200 hex grids, stained with 2% uranyl acetate and lead citrate, and viewed on a transmission electron microscope (Tecnai 12BioTWIN; FEI Company). Pictures were taken as a blind study where the photographer was not involved in the project. Two repeats of the experiment were carried out and 3 representative pictures were shown.

Statistical analysis

Results are expressed as mean ± s.e.m. Comparisons between groups were made by unpaired two-tailed Student's *t*-test. $P<0.05$ was considered as statistically significant. All experiments were repeated at least three times and representative data are shown.

2.4 RESULTS

2.4.1 XBP1 is indispensable for adipogenesis

In 3T3-L1 differentiating adipocytes, *Xbp1* mRNA increased significantly at day 2 (d2) and peaked around d4 (Fig. 2.1A). Consistently, XBP1s protein also peaked at d4 (Fig. 2.1B); this pattern strikingly resembles the induction of PPARγ and C/EBPα. To examine the role of XBP1 during adipogenesis, we transduced 3T3-L1 cells with control retroviruses (CONi) or with retroviruses encoding short hairpin RNAs against XBP1 (XBP1i). Lines #4 and #5 exhibited over 80 and 60% knockdown efficiency, respectively, as tested by immunoblots of cells treated with Tg (Fig. 2.1C top) and Q-PCR analysis of differentiating XBP1i cells (Fig. 2.1A). When these cells were cultured under adipogenic conditions, XBP1i-expressing cells demonstrated greatly attenuated differentiation, indicating an impaired adipogenic program (Fig. 2.1C bottom). Similar observations were obtained in $XBP1^{-/-}$ MEFs (Fig. 2.1D). Arguing against a non-specific effect provoked by short interference RNAs, 3T3-L1 cells expressing XBP1i that failed to effectively knockdown XBP1 (#1-2) exhibited no defects in adipogenesis (Fig. 2.2B). Taken together, XBP1 is essential for adipogenesis.

Figure 2.1. XBP1 is essential for adipocyte differentiation.

(A) Q-PCR analysis showing total *Xbp1* mRNA levels in 3T3-L1 CONi and XBP1i #4 during differentiation. Data normalized to d0 time point of 3T3-L1 CONi cells. Data are means ± SEM. *$p<0.05$ using unpaired two-tailed Student's t test comparing CONi to XBP1i at the same time point. **(B)** Immunoblots showing the levels of XBP1s and key adipogenic markers (C/EBPβ, C/EBPα and PPARγ) during adipogenesis. 3T3-L1 pre-adipocytes treated with 300 nM Tg for 4 hr was loaded as a control. XBP1u (30 kDa) protein was not detectable. HSP90 and CREB, loading controls. **(C)** Top: Immunoblots of XBP1s protein in wild-type MEFs stably expressing CONi, XBP1i #4, #5, or both treated with 300 nM Tg for 4 hr. CREB, a loading control. Bottom: Macroscopic pictures of Oil Red-O staining of 3T3-L1 cells expressing CONi and XBP1i #4 and #5 differentiated for 8 days (d8). **(D)** Left: Macroscopic pictures of Oil Red-O staining of wild-type (WT) and $XBP1^{-/-}$ MEFs differentiated for 24 days (d24). Right: Immunoblots of XBP1s protein in MEFs treated with 300 nM Tg for 4 hr.

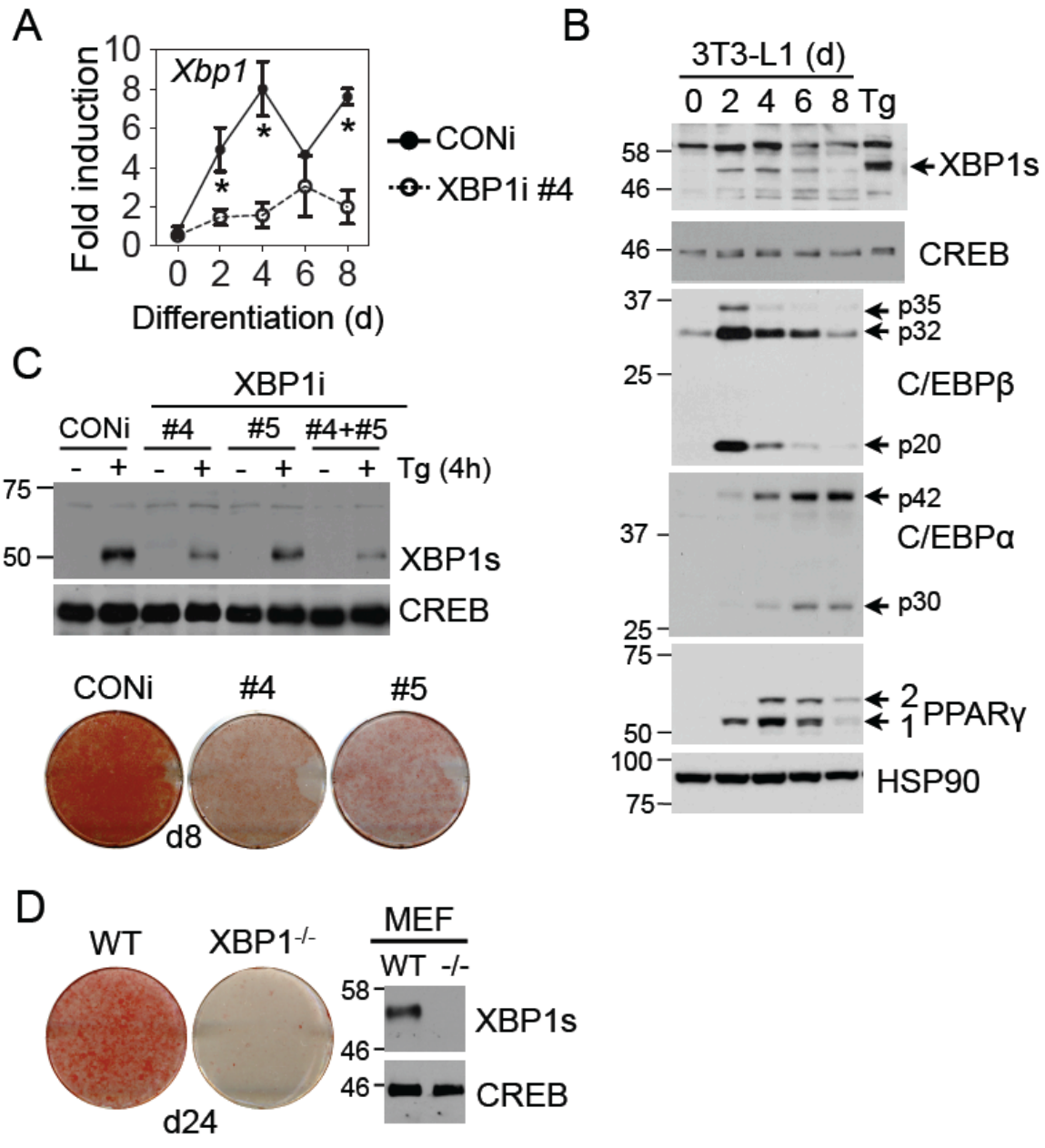
A
Xbp1
Fold induction
10
8
6
4
2
0
0 2 4 6 8
Differentiation (d)
CONi
XBP1i #4
B
3T3-L1 (d)
0 2 4 6 8 Tg
58
46
XBP1s
46
CREB
37
25
p35
p32
C/EBPβ
p20
37
25
p42
C/EBPα
p30
75
50
2
1
PPARγ
100
75
HSP90
C
XBP1i
CONi
#4
#5
#4+#5
- + - + - + - + Tg (4h)
75
50
XBP1s
CREB
CONi
#4
#5
d8
D
WT
XBP1-/-
d24
MEF
WT -/-
58
46
XBP1s
46
CREB

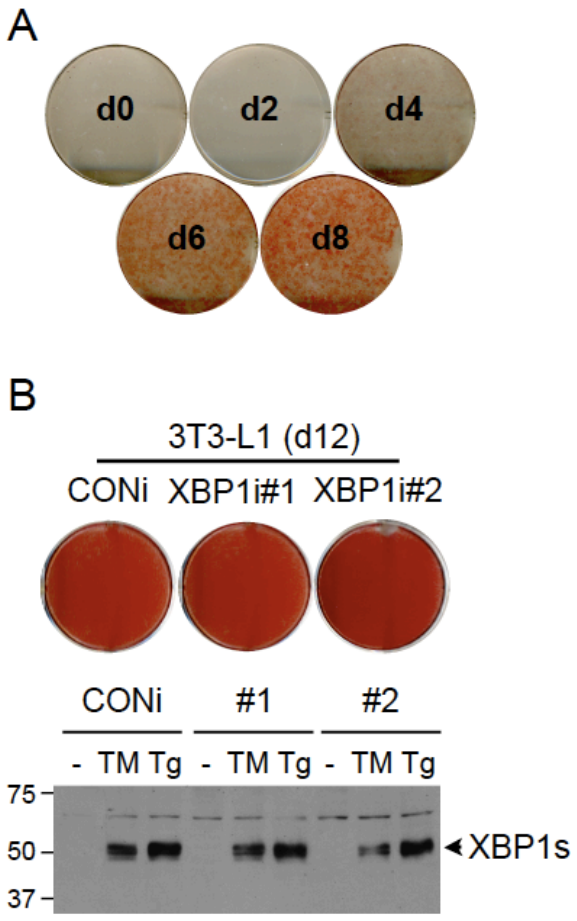

Figure 2.2. Two constructs that fail to deplete XBP1 have no effect on 3T3-L1 adipogenesis.

(A) Macroscopic pictures of Oil Red-O staining of differentiating 3T3-L1 cells. Two-days after confluence (d0), cells were induced to differentiate for 2 days (d2) followed by terminal differentiation for the next 6 days (d4, d6, d8). Cells were fixed and stained with Oil Red-O. **(B)** Top, macroscopic pictures of Oil Red-O staining of differentiated 3T3-L1 cells (d12) expressing CONi or XBP1i #1-2 (two negative controls). Bottom, immunoblot of XBP1 in cells stably expressing CONi or XBP1i #1-2 treated with 2.5 μg/ml TM or 300 nM Tg for 4 hr.

2.4.2 C/EBPβ induces Xbp1 expression

In light of a significant induction of *Xbp1* mRNA during early differentiation, we next examined the mechanism underlying the transcriptional regulation of *Xbp1*. We first tested which component(s) of the adipogenic-inducing regimen was responsible for regulating *Xbp1* induction. Only isobutylmethylxanthine (IBMX) or all three components of the regimen (IBMX, dexamethasone (DXM) and insulin) increased *Xbp1* gene expression (Fig. 2.3A), suggesting that *Xbp1* transcription is responsive to changes in cellular cAMP levels as IBMX is a phosphodiesterase inhibitor.

The ability of cAMP signals to activate C/EBPβ during adipogenesis (Cao et al., 1991; Farmer, 2006) prompted us to test whether C/EBPβ regulates *Xbp1* expression. Indeed, total *Xbp1* mRNA increased nearly 10-fold with a peak at 8 hr postinduction within the first 24 hr; this upregulation occurred subsequently to that of the *Cebpb* gene, which peaked at 2 hr postinduction (Fig. 2.3B). Consistently, XBP1s protein levels also peaked at 8 hr postinduction (Fig. 2.3C).

Supporting the scenario that C/EBPβ directly regulates *Xbp1* expression, recent genome-wide analysis identified putative C/EBP binding sites on the *Xbp1* promoter (Lefterova et al., 2008). Indeed, sequence analysis of mammalian *Xbp1* proximal promoter revealed the presence of a highly conserved C/EBP binding element (Osada et al., 1996) centered at -482 bp relative to transcription start site (Fig. 2.4A). Chromatin immunoprecipitation (ChIP) experiments showed enrichment of C/EBPβ proteins on the *Xbp1* proximal promoter at 8 hr postinduction and on d4 (Fig. 2.3D). Further confirming the specificity of the

C/EBPβ antisera, no signal was detected at the 3′ UTR region of *Xbp1* (not shown). In addition, overexpression of C/EBPβ in HEK293T cells activated a *Xbp1* promoter (-689 to +37 bp)-luciferase reporter (Fig. 2.3E). This activation was significantly attenuated over 50% by deleting the putative binding element (Figs. 2.3E and 2.4B).

To further confirm the effect of C/EBPβ on *Xbp1* induction, we generated 3T3-L1 cells stably expressing C/EBPβ shRNA with over 80% knockdown efficacy (Figs. 2.3F-G). Loss of C/EBPβ significantly blocked differentiation as expected (Fig. 2.4C). Indeed, *Xbp1* mRNA levels were reduced by nearly 60% in differentiating C/EBPβi 3T3-L1 cells compared to CONi cells at 8 h postinduction (Fig. 2.3G). Taken together, our data strongly suggest that the *Xbp1* gene is a bona fide direct target of C/EBPβ during adipogenesis.

Figure 2.3. C/EBPβ induces *Xbp1* expression.

(A) Q-PCR analysis of *Xbp1* mRNA in 3T3-L1 cells (d0) treated with various stimuli as indicated for 8 hr. Data normalized to the mock-treated sample (CON). **(B)** Q-PCR analysis showing the expression patterns of *Xbp1* and *Cebpb* mRNA within the first 24 hr postinduction in differentiating 3T3-L1 cells. **(C)** Immunoblot showing the expression patterns of XBP1s, CHOP10 and C/EBPβ proteins in differentiating 3T3-L1 cells. HSP90, a loading control. **(D)** ChIP analysis showing the recovery of *Xbp1* promoter from immunoprecipitates of C/EBPβ or control IgG prepared from differentiated 3T3-L1 cells at d0, 8 hr postinduction and d4. The amount of *Xbp1* promoter (-580 to -425 bp) recovered was quantitated using Q-PCR. Data normalized to the IgG controls at each point. **(E)** Luciferase assay showing effects of C/EBPβ on wild-type (WT) or mutated *Xbp1* reporter activity (-689 to +37 bp) in HEK293T cells transiently transfected with control GFP (CON) or C/EBPβ. ΔC/EBP, deletion of the C/EBP binding site (Fig. 2.4B). **(F, G)** Knockdown of C/EBPβ reduces *Xbp1* level. Western blot **(F)** showing the protein level of C/EBPβ in 3T3-L1 stably expressing CONi or C/EBPβi. Q-PCR analysis **(G)** of *Cebpb* and *Xbp1* mRNA levels at 4 hr or 8 hr postinduction. Data are represented as mean ± SEM. *$p<0.05$ using unpaired two-tailed Student's t test comparing either the samples included by the brackets or that particular sample to the rest samples.

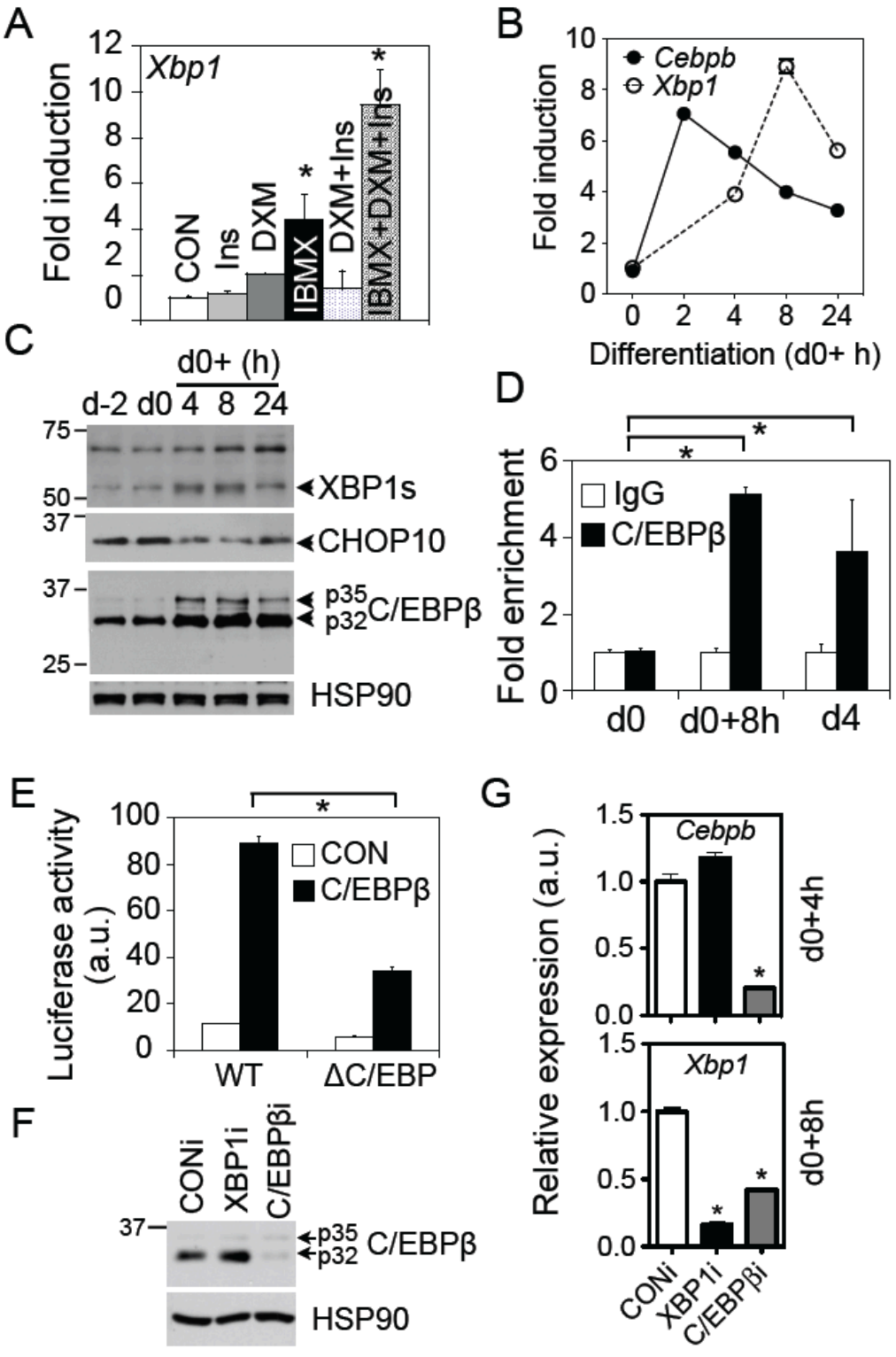
A
Xbp1
Fold induction
CON
Ins
DXM
IBMX
DXM+Ins
IBMX+DXM+Ins
B
Cebpb
Xbp1
Fold induction
Differentiation (d0+ h)
C
d0+ (h)
d-2 d0 4 8 24
XBP1s
CHOP10
p35
p32 C/EBPβ
HSP90
D
Fold enrichment
IgG
C/EBPβ
d0
d0+8h
d4
E
Luciferase activity (a.u.)
CON
C/EBPβ
WT
ΔC/EBP
F
CONi
XBP1i
C/EBPβi
p35
p32 C/EBPβ
HSP90
G
Relative expression (a.u.)
Cebpb
Xbp1
d0+4h
d0+8h
CONi
XBP1i
C/EBPβi

A

C/EBP binding site: ATT$^{G}_{T}$C..AA

	Mouse	-487 TTTTCTAAAG	-477
Xbp1	Human	-561 ATTTCTTAAA	-551
	Rat	-504 ATTTCCTAAA	-494

B

Mutagenesis of *Xbp1* promoter

	C/EBP binding site (~ -482)
Wildtype (WT)	tcaTTTTCTTAAGact
Mutant (Δ)	tcaact (ΔCEBP)

C

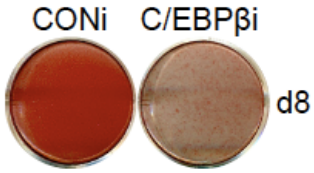

Figure 2.4. C/EBPβ binding site on *Xbp1* promoter is required for *Xbp1* induction during adipogenesis.

(A) Putative C/EBPβ binding elements on the XBP1 proximal promoter from human, mouse and rat. Consensus sites are highlighted in bold. **(B)** Mutagenesis of C/EBPβ binding element. All 10 bases of the C/EBPβ binding element were deleted (ΔCEBP). **(C)** Macroscopic image of differentiated 3T3-L1 expressing CONi or C/EBPβi at day 8.

2.4.3 Adipogenesis is associated with a low measure of UPR

IRE1α is the predominant form of IRE1 in adipocytes (not shown) and throughout adipogenesis, its mRNA expression level did not vary significantly (Fig. 2.6A). During UPR, IRE1α splices *Xbp1* mRNA to generate XBP1s, a potent transcription factor (Ron and Walter, 2007). Phosphorylation of IRE1α and *Xbp1* mRNA splicing are two common markers of UPR activation that can be assessed by the mobility shift of IRE1α protein on an SDS-PAGE gel and by the ratio of the spliced *Xbp1s* mRNA to total *Xbp1* mRNA using RT-PCR analysis, respectively.

To increase the resolution of the phosphorylated forms of a protein on a SDS-PAGE, we incorporated Phos-tag and Mn^{2+} in regular SDS-PAGE gels (Kinoshita et al., 2006). Dramatically, in HEK293T cells, nearly 100% of IRE1a proteins were hyperphosphorylated upon a 1.5 h-treatment with Tg and only ~30% after 13 h (Fig. 2.5A). Interestingly, in all the conditions and samples tested, IRE1α exhibited one predominant band shift which was reversible by phosphatase (CIP) treatment (Fig. 2.5B), suggesting that trans-autophosphorylation of mammalian IRE1α may not be as extensive as predicted for the yeast counterpart (Korennykh et al., 2009).

Surprisingly, we failed to observe a mobility shift of IRE1α at any time-point during differentiation (Fig. 2.5B). Arguing against the possibility that IRE1α in 3T3-L1 cells can not be phosphorylated, Tg treatment for as little as 20 min induced a dramatic mobility shift of nearly 100% of IRE1α proteins (Fig. 2.5A). Consistently, the majority of IRE1α in both white and brown adipose tissues (WAT and BAT) of wild-type lean animals at 23-27 weeks of age were not

phosphorylated (Figs. 2.5C and 2.6B). In contrast, IRE1α phosphorylation was readily detectable in the liver from the same set of mice (Fig. 2.6B).

Next, we quantitated the percent of *Xbp1* splicing using RT-PCR as a direct measure of IRE1α RNase activity. Unexpectedly, *Xbp1* mRNA splicing peaked at d0 (mean ± SEM; 55.9 ± 4.9%) and reached nadir at d4 (15.1 ± 2.4%) (Figs. 2.5D and 2.6C). Supporting the physiological relevance of our cell model, the level of *Xbp1* mRNA splicing on d8 of 3T3-L1 adipocytes was very similar to that of adipose tissues from wild-type lean mice (23.1 ± 4.1% vs. 18.3 ± 1.3%, Fig. 2.5E). As a positive control, *Xbp1* mRNA splicing reached approximately 50% in pancreas of lean wild-type animals [(Iwawaki et al., 2004) and not shown]. Given that d0 adipocytes and pancreas exhibit similar levels of *Xbp1* mRNA splicing, we conclude that physiological UPR is activated during early adipogenesis.

Obesity is postulated to cause ER stress or UPR in adipose tissues. However, the nature and the extent of UPR in adipose tissues of obese animals remain unclear. To this end, we examined IRE1α phosphorylation and *Xbp1* splicing in mice that were either genetically- or dietary- induced to become obese (*ob*/*ob* and HFD). Unexpectedly, ~15% of IRE1α proteins were phosphorylated in WAT of these animals (Fig. 2.5C and not shown). Correspondingly, the splicing of *Xbp1* in WAT was increased from 18.3 ±1.3% in lean mice to 33.9 ± 6.8% in obese animals (Figs. 2.5E and 2.6D). Thus, our data supports the notion that a low measure of UPR is associated with obesity.

During differentiation, XBP1s protein levels were inversely correlated with *Xbp1s* mRNA levels (Figs. 2.1B vs. 2.5D and 2.3C vs. 2.6C). We reasoned that XBP1 may function to maintain UPR in adipocytes at a low level via feedback

inhibition on UPR and IRE1α activity. To directly test this possibility, we measured *Xbp1* mRNA splicing in XBP1-deficient cells and wild-type cells. Indeed, *Xbp1* mRNA splicing was increased over two-fold in XBP1i vs. CONi adipocytes on d8 (48.6 ± 1.1% vs. 21.9 ± 3.3%, Fig. 2.5F). Similar observations were obtained in XBP1$^{-/-}$ differentiating MEF adipocytes (26.1 ± 3.9% vs. 14.6 ± 1.8%, Fig. 2.5F). Surprisingly, the majority of IRE1α was not hyper-phosphorylated in XBP1-deficient adipocytes (Fig. 2.6E).

As UPR is intimately linked to ER morphology and function (Ron and Walter, 2007), we examined the fine structure of the ER using transmission electron microscopy (TEM). Unlike the packed ER cisternae characteristic of professional secretory cells (Harding et al., 2001; Lee et al., 2005), the ER of adipocytes (d5) have few loosely dispersed cisternae with discernible ribosomes (Fig. 2.5G) as shown previously (Novikoff et al., 1980). By contrast, most of the ER in the XBP1i cells were fragmented and somewhat dilated compared to those in control adipocytes (Figs. 2.5G and 2.6I). Thus, our data suggest that XBP1 functions to maintain ER homeostasis in adipocytes; hence loss of XBP1 in adipocytes disrupts ER function and activates IRE1α.

To determine if the IRE1α-mediated splicing event is critical for differentiation, we transduced 3T3-L1 XBP1i cells with retroviruses encoding the pBabe vector, XBP1u or XBP1s (Fig. 2.6F). Only ectopic expression of XBP1s almost completely rescued the differentiation defect of 3T3-L1 XBP1i cells (Fig. 2.5H). Further supporting the role of XBP1s in adipogenesis, XBP1s protein levels were much higher than XBP1u in differentiated 3T3-L1 cells at d6 (Fig. 2.6G). Thus, *Xbp1* mRNA splicing by IRE1α RNase activity is required for adipogenesis.

To directly test the consequences of IRE1α deficiency in adipogenesis, we generated 3T3-L1 cells stably expressing IRE1α shRNA (IRE1αi). One shRNA (#4) reduced IRE1α protein levels to less than 10% of controls (Fig. 2.5I). Supporting a key role of IRE1α in mediating *Xbp1* splicing, knockdown of IRE1α significantly reduced *Xbp1* splicing (54.4 ± 2.2% CONi, 41.7 ± 6.7% XBP1i vs. 24.3 ± 3.6% IRE1αi, Fig. 2.5J) and XBP1s production in cells treated with Tg for 3 h (Fig. 2.5I). Cells stably expressing IRE1αi#4 failed to undergo differentiation to a similar degree as XBP1i or C/EBPβi cells (Fig. 2.5K); cells expressing shRNA (#2) with no knockdown effect exhibited normal differentiation (Fig. 2.6H). Thus, our data indicate that adipogenic conversion is associated with UPR and the IRE1α-XBP1 branch is indispensable for adipogenesis.

Figure 2.5. Adipogenesis is associated with a low level of physiological UPR.

(A) Western blot showing mobility shift of IRE1α using Phos-tag or regular SDS-PAGE gels in (left) HEK293T and (right) 3T3-L1 cells treated with 300 nM Tg for indicated period. "p" and "0", hyper- and non-phosphorylated IRE1α, respectively. Solid and dotted lines on the left-hand side indicate Phos-tag and regular gels, respectively. **(B)** Immunoblot showing separation of p-IRE1α from IRE1α using regular and Phos-tag gels with or without CIP treatment (1 hr) in differentiating 3T3-L1 adipocytes. Two positive controls: Tg1, HEK293T cells treated with 300 nM Tg for 1.5 hr; Tg 2, 3T3-L1 cells treated with 300 nM Tg for 4 hr. HSP90, a loading control. **(C)** Western blot showing mobility shift of IRE1α in white adipose tissues (WAT) collected from wild-type lean and ob/ob animals using Phos-tag with or without CIP treatment. The age of the mice (in weeks) shown. **(D-F)** RT-PCR analysis of *Xbp1* splicing (*Xbp1u* and *s*) in **(D)** differentiating 3T3-L1 adipocytes, **(E)** WAT of wild-type lean (wt) and obese animals, and **(F)** differentiating 3T3-L1 and MEFs with XBP1 deficiency at d8 and d9, respectively. Samples treated with Tg for 2 hr or 5 hr were used as controls. L32, a loading control. **(G)** Electron microscopic images of differentiated 3T3-L1 CONi or XBP1i adipocytes at d5. Each image taken from a different cell. Arrows, ER; m, mitochondrion; N, nucleus; L, lipid droplets. Scale bar shown at the right corner of each panel. **(H)** Macroscopic images of differentiation of 3T3-L1 expressing CONi and XBP1i plus pBabe-vector, XBP1s or XBP1u. Oil Red-O staining was carried out on d6. **(I-K)** Knockdown of IRE1α reduces *Xbp1* splicing and attenuates differentiation. Western blot analysis **(I)** showing the IRE1α and XBP1s protein levels in XBP1i and IRE1αi #4 3T3-L1 cells. Nuclear-extracts were used for blots showing the levels of XBP1s in cells treated with 300 nM Tg for 3 hr. HSP90 and CREB, loading controls. **(J)** RT-PCR analysis of *Xbp1* splicing (*Xbp1u* and *s*) in 3T3-L1 cells treated with Tg for 3 hr and quantitated as above. **(K)** Macroscopic images of differentiation of 3T3-L1 expressing CONi, XBP1i, C/EBPβi, or IRE1αi #4. Oil Red-O staining was carried out on d10. For RT-PCR analysis of *Xbp1* splicing, quantification was done using the NIH ImageJ software where band densities were calculated and subtracted from the background. Data are represented as mean ± SEM of data from at least three experiments. $^*p < 0.05$ using unpaired two-tailed Student's t test comparing the samples included by the brackets.

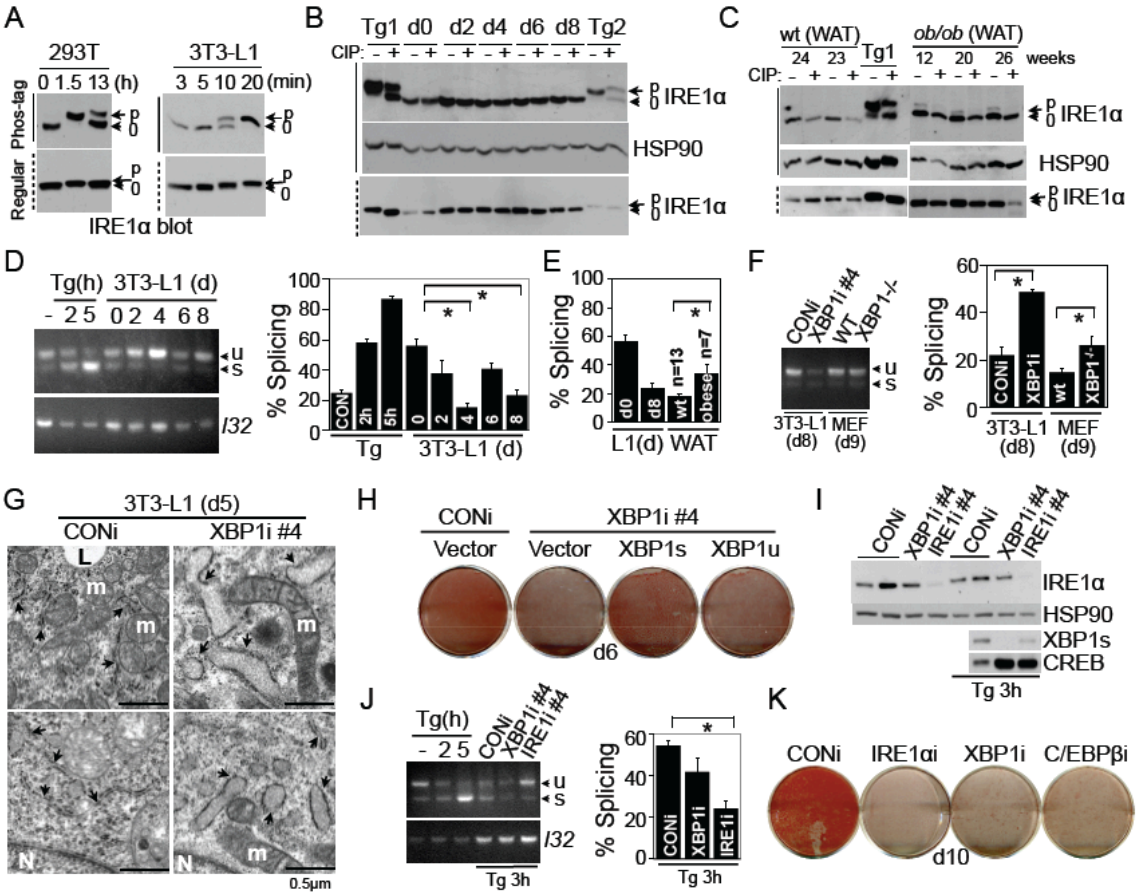
A
293T
0 1.5 13 (h)
3T3-L1
3 5 10 20 (min)
Phos-tag
Regular
IRE1α blot
B
Tg1 d0 d2 d4 d6 d8 Tg2
CIP:
IRE1α
HSP90
C
wt (WAT)
ob/ob (WAT)
24 23 Tg1
12 20 26 weeks
D
Tg(h) 3T3-L1 (d)
- 2 5 0 2 4 6 8
u
s
I32
% Splicing
Tg
3T3-L1 (d)
E
L1(d) WAT
n=13
n=7
F
CONi
XBP1i #4
WT
XBP1-/-
3T3-L1 (d8)
MEF (d9)
G
3T3-L1 (d5)
CONi
XBP1i #4
L
m
N
0.5μm
H
Vector
XBP1s
XBP1u
d6
I
IRE1α
HSP90
XBP1s
CREB
Tg 3h
J
IRE1i #4
K
IRE1αi
XBP1i
C/EBPβi
d10

Figure 2.6. Basal UPR occurs during adipocyte differentiation.

(A) Q-PCR analysis of *Ire1a* mRNA during 3T3-L1 adipogenic differentiation. Data normalized to d0. **(B)** Immunoblot showing separation of p-IRE1α from IRE1α of samples prepared from brown adipose tissues (BAT) and liver using Phos-tag gels. Tissues were collected from wild-type lean male mice at age of 27 weeks. **(C)** RT-PCR analysis of *Xbp1* splicing in samples collected during 3T3-L1 differentiation as indicated. Quantification of percent of splicing was done using NIH ImageJ software where band densities were calculated and subtracted from the background. Samples treated with Tg for 2 or 5 hr were used as controls. L32, a loading control. *$p<0.05$ using unpaired two-tailed Student's t test comparing the sample indicated by the brackets. **(D)** RT-PCR analysis of *Xbp1* splicing in WAT from wild-type lean mice (wt) and obese animals (HFD and ob/ob). The age of the animals and the length of HFD feeding indicated. **(E)** Immunoblot showing separation of p-IRE1α from IRE1α of 3T3-L1 XBP1i cells collected at different time points during differentiation using Phos-tag gels. **(F)** Western blot analysis showing the protein levels of XBP1 in the rescue experiment shown in Figure 2.5H. 3T3-L1 cells stably expressing CONi or XBP1i expressing pBabe vector (-), FKBP-XBP1u (u) or Flag-XBP1s (s) were treated with 300 nM Tg for 3 hr prior to the nuclear extraction and Western blot analysis. The FKBP tag has no effect on the stability of XBP1u protein with or without the ligand Shield-1. The bands representing Flag-XBP1s, FKBP-XBP1u, endogenous XBP1s are indicated. CREB, a loading control. **(G)** Immunoblot showing XBP1 protein levels in differentiating 3T3-L1 cells (d6) with or without 10 nM proteasome inhibitor MG132 for 1 hr. Note that XBP1u is only visible when cells were treated with MG132. **(H)** Top, Macroscopic pictures of Oil Red-O staining of differentiated 3T3-L1 cells (d8) expressing CONi or IRE1αi #2 (a negative control). Bottom, Immunoblot showing the IRE1α protein levels in lysates from 3T3-L1 CONi or IRE1αi #2 cells. **(I)** Additional electron microscopic images of the differentiated 3T3-L1 CONi or XBP1i cells. Arrows, ER; M, mitochondrion. Scale bar at the right corner of each image.

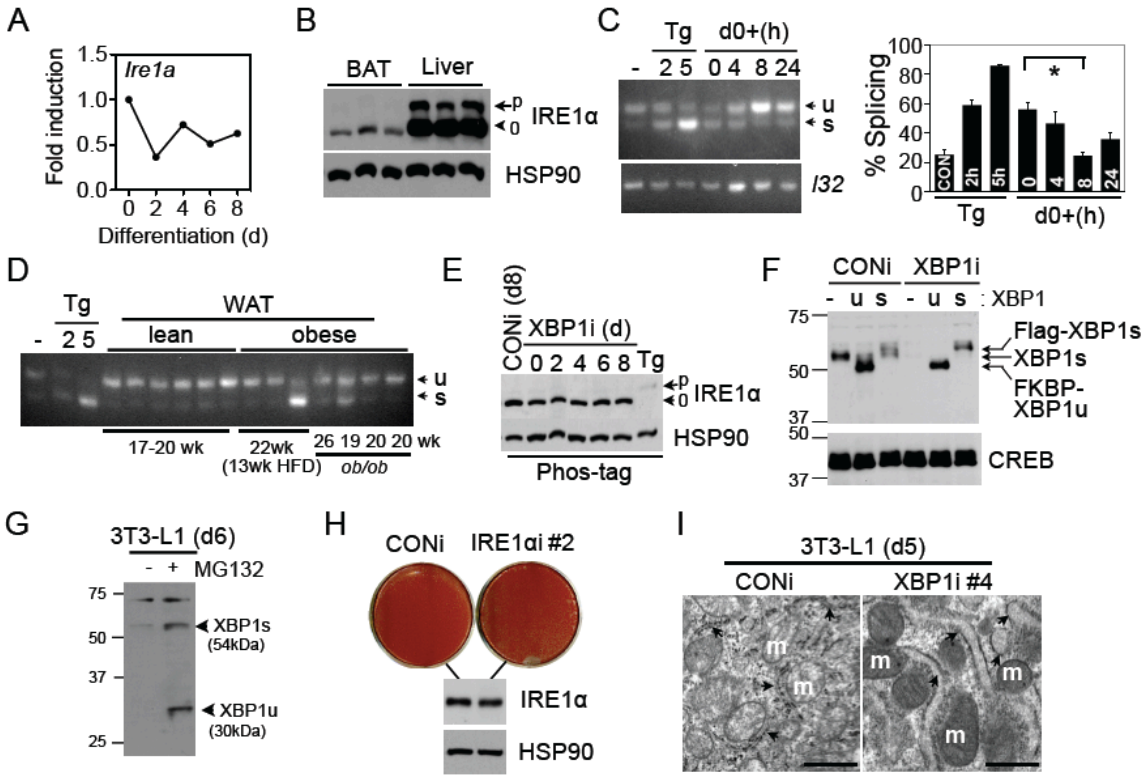
A
Ire1a
Fold induction
1.5
1.0
0.5
0.0
0 2 4 6 8
Differentiation (d)
B
BAT
Liver
p
0
IRE1α
HSP90
C
Tg
d0+(h)
- 2 5 0 4 8 24
u
s
I32
% Splicing
100
80
60
40
20
0
CON
2h
5h
0
4
8
24
*
Tg
d0+(h)
D
Tg
WAT
- 2 5
lean
obese
u
s
17-20 wk
22wk
(13wk HFD)
26 19 20 20 wk
ob/ob
E
CONi (d8)
XBP1i (d)
0 2 4 6 8 Tg
p
0
IRE1α
HSP90
Phos-tag
F
CONi
XBP1i
- u s - u s : XBP1
75
50
37
50
37
Flag-XBP1s
XBP1s
FKBP-
XBP1u
CREB
G
3T3-L1 (d6)
- + MG132
75
50
37
25
XBP1s
(54kDa)
XBP1u
(30kDa)
H
CONi
IRE1αi #2
IRE1α
HSP90
I
3T3-L1 (d5)
CONi
XBP1i #4
m
m
m
m
m

2.4.4 XBP1 directly regulates C/EBPα expression

We speculated that XBP1 may regulate the expression of an important adipogenic factor. Indeed, C/EBPα protein levels were significantly decreased in differentiating XBP1$^{-/-}$ MEFs while C/EBPβ levels remained largely unaffected (Fig. 2.7A). Similar observations were obtained in 3T3-L1 adipocytes (Fig. 2.8A). Furthermore, *Cebpa* mRNA levels on both d4 and d6 were significantly reduced by over 90% in 3T3-L1 XBP1i cells compared to CONi cells whereas both *Pparg1* and *Pparg2* mRNA levels were reduced by approximately 50% only on d6 (Fig. 2.7B). Supporting the notion that XBP1 targets are cell-type specific (Acosta-Alvear et al., 2007; Lee et al., 2005), expression of some known XBP1 targets *Erdj4* and *p58IPK* (Lee et al., 2003a) was not affected in XBP1i adipocytes (Fig. 2.7B).

XBP1 preferentially binds to CRE-like sequences containing an ACGT core (Acosta-Alvear et al., 2007; Clauss et al., 1996). Considering that the *Cebpa* proximal promoter region contains a highly conserved putative XBP1 binding element centered at -270 bp (Fig. 2.7C), we tested the role of XBP1 in modulating *Cebpa* expression in adipocytes. Pointing to a direct regulatory role for XBP1 *in vivo*, XBP1 was enriched on the *Cebpa* promoter on d4 (Fig. 2.7D); this binding was comparable to that of C/EBPβ on d4 and was completely abolished in XBP1i 3T3-L1 cells (Figs. 2.7D and 2.8B). Demonstrating the specificity of the antibody, the XBP1 antibody is highly specific for both XBP1s and XBP1u proteins in immunoprecipitation (Fig. 2.8D).

In further support of the notion that XBP1 transactivates *Cebpa* expression, XBP1s overexpression increased *Cebpa* promoter activity in luciferase reporter assays in XBP1$^{-/-}$ MEFs and HEK293T cells whereas XBP1u had no effect (Fig.

2.8E). The activity of XBP1s on the *Cebpa* promoter was comparable to that on the promoter of a known target gene *Edem1* (Fig. 2.8E); this activation was largely abolished by either mutation or deletion of the XBP1 binding element on the *Cebpa* promoter (Figs. 2.7E and 2.8C). In a rescue experiment, C/EBPα overexpression readily rescued the differentiation defects observed in XBP1i cells (Fig. 2.8F), suggesting that adipogenic attenuation in these cells may be in part due to the reduction in C/EBPα levels. Taken together, our data demonstrates that *Cebpa* is a bona fide target of XBP1s in adipocytes.

Figure 2.7. XBP1 controls *Cebpa* expression.

(A) Western blot analysis of C/EBPα and C/EBPβ protein levels in XBP1$^{-/-}$ and wild-type MEFs. GRP78 and GAPDH, loading controls. **(B)** Q-PCR analysis in differentiating 3T3-L1 expressing CONi and XBP1i #4. Data normalized to d0 time point of 3T3-L1 CONi adipocytes. **(C)** Conservation of XBP1 binding sites on the *Cebpa* promoter. The core binding element ACGT is underlined. **(D)** ChIP analysis showing the recovery of *Cebpa* promoter from immunoprecipitates of C/EBPβ, XBP1, or control IgG prepared from 3T3-L1 cells at d0, 8 hr postinduction and d4 as indicated. The amount of *Cebpa* promoter (-335 to -82 bp) recovered was quantitated using Q-PCR. Data normalized to the IgG controls at each point. **(E)** Luciferase assay showing effects of XBP1s on *Cebpa* reporter activity (-320 to +45 bp) in HEK293T cells transiently transfected with control GFP (CON) and XBP1s. The *Cebpa* reporter constructs with either mutation (XBPmt) or deletion (ΔXBP) of the XBP1 binding sites were included. Data represented as mean ± SEM. *$p<0.05$ using unpaired two-tailed Student's t test comparing the samples included by the brackets. **(F)** Model showing the role of IRE1α-XBP1 in adipogenesis. The new findings described in this paper are highlighted in bold. See text for details.

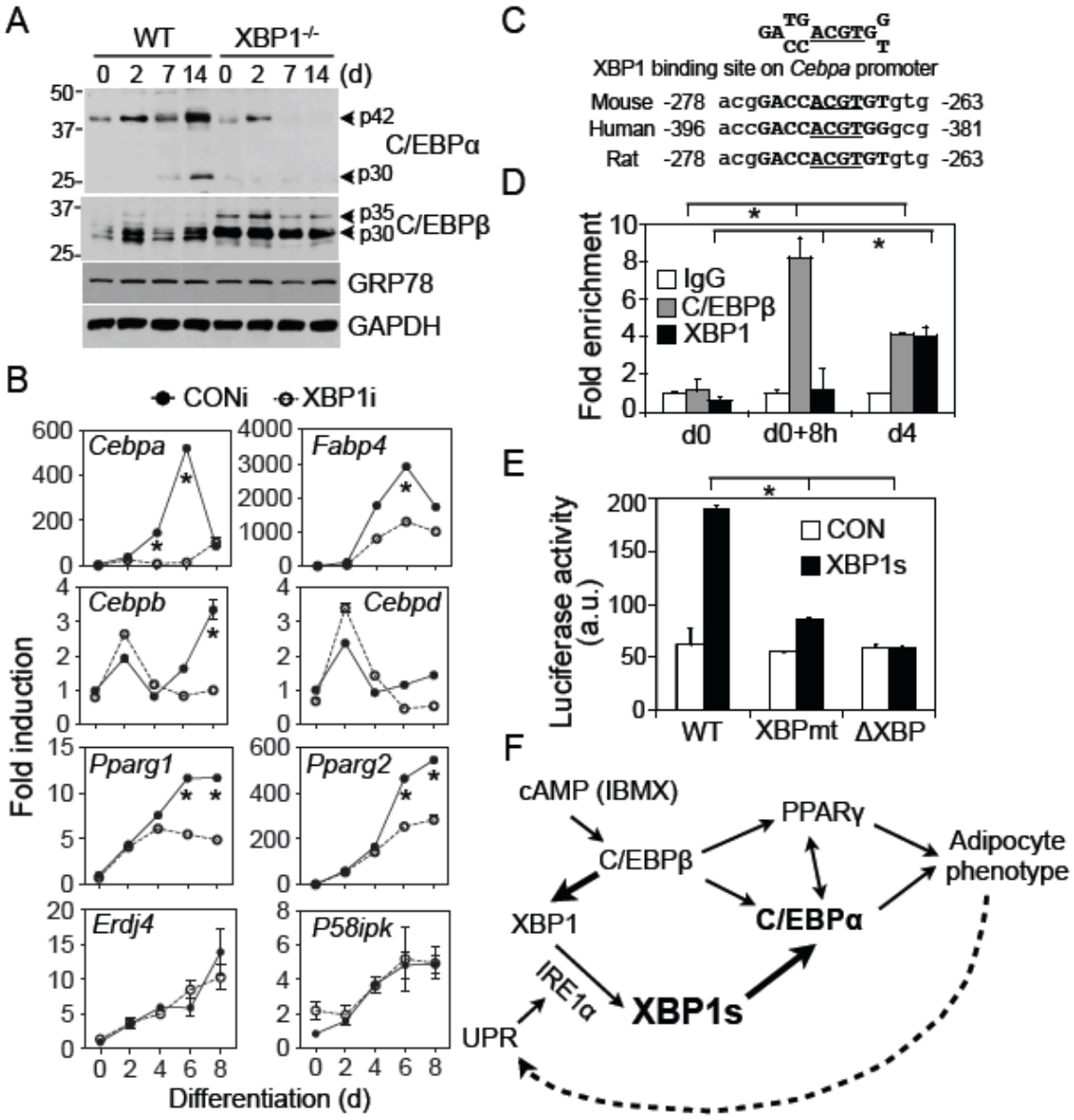
A
WT
XBP1-/-
0 2 7 14 0 2 7 14 (d)
50
37
25
p42
C/EBPα
p30
37
25
p35
p30
C/EBPβ
GRP78
GAPDH
B
CONi
XBP1i
Cebpa
Fabp4
Cebpb
Cebpd
Pparg1
Pparg2
Erdj4
P58ipk
Fold induction
Differentiation (d)
C
XBP1 binding site on Cebpa promoter
Mouse -278 acgGACCACGTGTgtg -263
Human -396 accGACCACGTGGgcg -381
Rat -278 acgGACCACGTGTgtg -263
D
Fold enrichment
IgG
C/EBPβ
XBP1
d0
d0+8h
d4
E
Luciferase activity (a.u.)
CON
XBP1s
WT
XBPmt
ΔXBP
F
cAMP (IBMX)
C/EBPβ
PPARγ
Adipocyte phenotype
XBP1
C/EBPα
IRE1α
XBP1s
UPR

Figure 2.8. XBP1 binds to the *Cebpa* promoter and induces its expression.

(A) Immunoblot assay showing the level of C/EBPα and C/EBPβ in differentiating 3T3-L1 adipocytes at d8 expressing CONi, XBP1i, IRE1αi, and C/EBPβi. **(B)** ChIP analysis showing the recovery of *Cebpa* promoter from immunoprecipitates of control IgG or XBP1-specific antibody prepared from differentiating 3T3-L1 CONi or XBP1i cells at d4. The amount of *Cebpa* promoter (-335 to -82 bp) recovered was quantitated using Q-PCR. Data was normalized to IgG control of each sample. **(C)** Mutagenesis of XBP1 binding elements. The core ACGT nucleotides were either deleted (ΔXBP) or mutated to AAAA (XBPmt). **(D)** Left, Immunoblot assay showing recovery of endogenous XBP1 from immunoprecipitates of XBP1 prepared from HEK293T cells treated with 5 μg/ml Tm for 6 hr. Note the lack of the 30 kDa XBP1u protein in the IP samples, presumably because XBP1u protein is quickly degraded. Right, Western blot showing XBP1s and XBP1u in pancreatic lysates from wild-type mice. The same antibody was used in the ChIP studies shown in Figs. 2.7D and 2.8B. **(E)** Reporter assay of $XBP1^{-/-}$ MEFs transfected with *Cebpa* reporter (-320 to +45 bp) and XBP1u or XBP1s. *Edem* reporter (-336 to +15 bp), a positive control. Data was normalized to control GFP-transfected samples. **(F)** Macroscopic images of differentiation of 3T3-L1 expressing CONi or XBP1i plus pBabe-vector (CON) or pBabe-Flag-C/EBPα. Oil Red-O staining was carried out on d8.

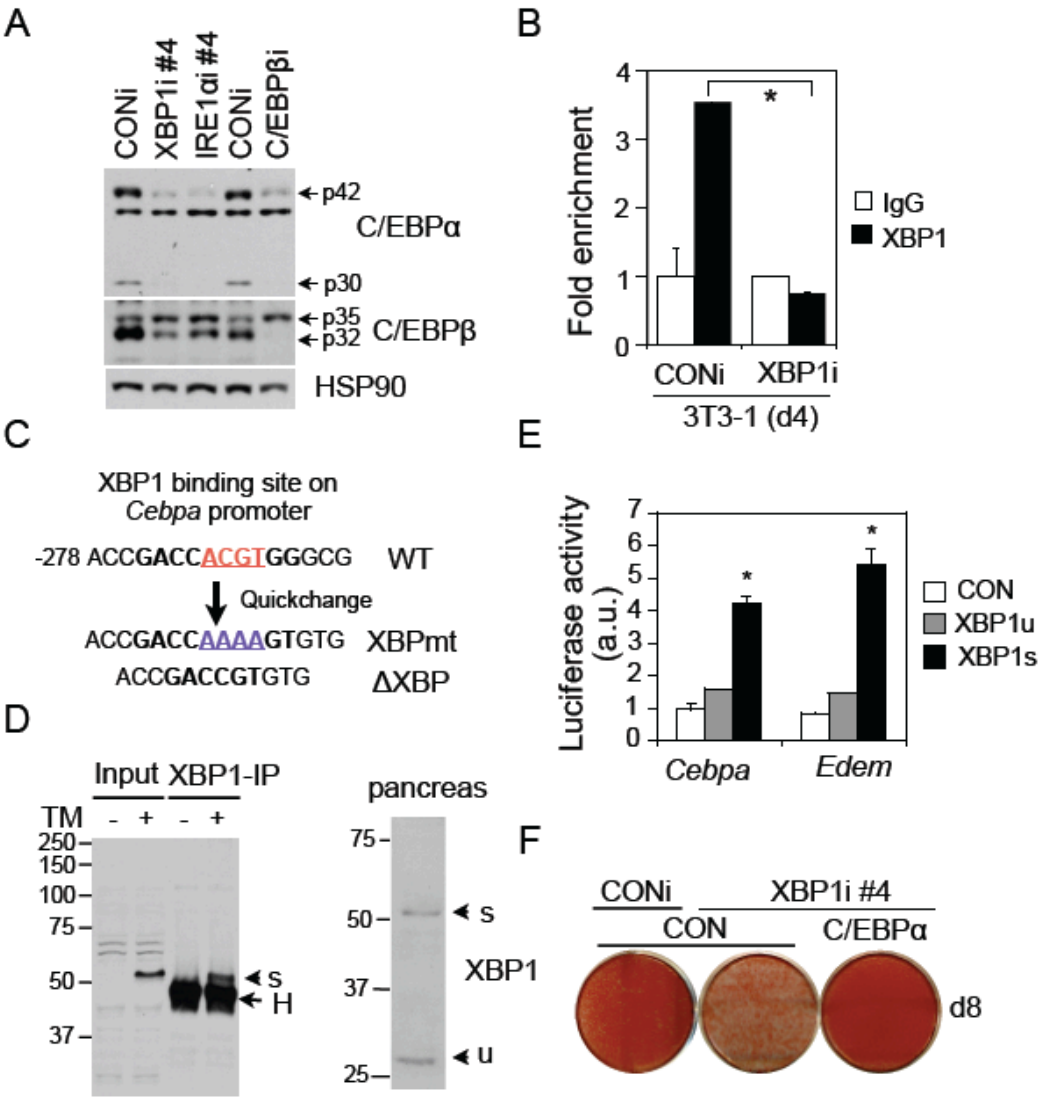
A
CONi
XBP1i #4
IRE1αi #4
CONi
C/EBPβi
p42
C/EBPα
p30
p35
p32
C/EBPβ
HSP90
B
Fold enrichment
4
3
2
1
0
*
IgG
XBP1
CONi
XBP1i
3T3-1 (d4)
C
XBP1 binding site on
Cebpa promoter
-278 ACCGACCACGTGGGCG WT
Quickchange
ACCGACCAAAAGTGTG XBPmt
ACCGACCGTGTG ΔXBP
D
Input XBP1-IP
TM - + - +
250
150
100
75
50
37
s
H
pancreas
75
50
37
25
s
XBP1
u
E
Luciferase activity
(a.u.)
7
6
5
4
3
2
1
0
*
*
CON
XBP1u
XBP1s
Cebpa
Edem
F
CONi
XBP1i #4
CON
C/EBPα
d8

2.5 DISCUSSION

Adipocytes are specialized cell types that integrate lipid metabolism with protein synthesis in a very compact cellular space. Here we show that the IRE1α-XBP1 pathway, the most conserved branch of the UPR, is indispensable for the cellular transformation into adipocytes (Fig. 2.7F). Investigation of the underlying mechanism uncovered a number of discoveries about the function of the IRE1α-XBP1 branch in adipogenesis that increased our understanding of this pathway in adipocytes.

First, we show that adipogenesis is associated with a low level of UPR – termed as "physiological" UPR. IRE1α activity peaks during early adipogenesis with nearly 55% of *Xbp1* mRNA being spliced. Subsequently, splicing is reduced to 10–20% in mature adipocytes. Indeed, the splicing in fully differentiated adipocytes in our culture system is equivalent to that in mature adipocytes from wild-type lean mice. Upon induction of obesity, there is approximately a 2-fold increase in *Xbp1* mRNA splicing with only a minor fraction of the IRE1α proteins being hyper-phosphorylated. In support of our observations, UPR activation was detected mainly in the pancreas and skeletal muscles in a UPR-reporter transgenic mouse model with ~50% and 26% *Xbp1* mRNA splicing, respectively; no UPR was detected in any other organs including adipose tissues (Iwawaki et al., 2004). Thus, we conclude that UPR is activated at an early stage of adipogenesis and maintained at a relatively low physiological level in mature adipocytes. Moreover, obesity is associated with elevated UPR, but the level of UPR activation incurred in adipose tissues is not as high as anticipated.

Second, we show that the majority of IRE1α proteins are not

hyperphosphorylated during adipogenesis even as *Xbp1* mRNA splicing approaches 55% on d0 of adipocyte differentiation. We speculate that hyperphosphorylation may not be required for activation of IRE1α RNase activity under physiological UPR. Indeed, although several structural studies have implicated the importance of dimerization and trans-autophosphorylation of IRE1α in activation of its RNase activity (Lee et al., 2008a; Zhou et al., 2006), an earlier study showed that the kinase-defective IRE1α K599A mutant has intact RNase activity (Tirasophon et al., 2000). Furthermore, a recent structural study on the cytosolic domain of yeast IRE1α (Korennykh et al., 2009) suggests that trans-autophosphorylation of IRE1α is not required for its RNase activation. As our data show that IRE1α RNase activity is dynamically regulated during adipogenesis, some intriguing questions arise: Is IRE1α activated by misfolded proteins during adipogenesis? How is IRE1α RNase activity affected by trans-autophosphorylation during this process? Does oligomerization of IRE1α proteins and formation of IRE1α foci occur under physiological UPR in mammals as shown in drug-treated yeast? Many detailed biochemical studies are required before we can fully appreciate the mechanisms of mammalian IRE1α activation under physiological conditions.

Third, we show that C/EBPβ regulates *Xbp1* expression, which in turn modulates the expression of a key adipogenic factor C/EBPα. Cells or animals lacking XBP1 have profound defects in adipogenesis and adipose development [this study and (Lee et al., 2005)], similar to the phenotypes of C/EBPα-deficient cells or adipose tissues (Farmer, 2006; Tontonoz and Spiegelman, 2008). As

PPARγ and C/EBPα are critical for the induction and maintenance of each other, further studies are required to determine whether regulation of *Cebpa* by XBP1 and PPARγ occurs independently or in concert. Additionally, generation of adipose-specific IRE1α or XBP1 null animals will elucidate the role of UPR in the pathogenesis of obesity and insulin resistance.

Fourth, we show that the IRE1α-XBP1 pathway of the UPR is important for adipogenic differentiation. In light of the observations made in this study, it is interesting to compare the roles of XBP1 in governing adipogenesis with that of myogenesis or plasma cell differentiation. In myogenic differentiation, two key myogenic factors, MyoD and myogenin, transactivate *Xbp1* expression (Blais et al., 2005), which in turn transactivates *Mist1*, a negative regulator of MyoD, leading to decreased differentiation (Acosta-Alvear et al., 2007). During early B cell differentiation, IRF4 and Blimp-1 regulate *Xbp1* expression (Klein et al., 2006; Shaffer et al., 2004), which in turn induces the expression of IL-6, a key growth factor for driving B cell differentiation (Iwakoshi et al., 2003). Thus, these results suggest that the IRE1α-XBP1 pathway may act as a critical regulatory component of diverse cellular differentiation events. Further studies of the activation of the different UPR components during adipocyte differentiation and their mechanisms of action will clarify how pre-adipocytes undergo their amazing transformation into adipocytes and provide insights into the nature of physiological UPR.

2.6 ACKNOWLEDGEMENTS

We thank Drs. L. Glimcher, L. Kraus and J. Pleiss for reagents; Drs. K. L. Guan, S. Lee, M. Montminy, and three anonymous reviewers for insightful comments and suggestions. The Qi laboratory is supported by the Cornell start-up package and grants from American Federation for Aging Research (RAG08061), American Diabetes Association (ADA) (7-08-JF-47), and National Institutes of Health (R01DK082582).

I specifically thank Haibo Sha for his mentorship on this project, Cindy Wang and Hui Chen for technical assistance and the entire Qi lab for helpful discussions. I thank the National Institutes of Health Training Grant to Cornell University (Department of Molecular Biology and Genetics) for funding.

The author contributions are as follows: Figs. 2.1, 2.2, 2.3C, F-G, 2.4C, 2.5A-C, H-I, K, 2.6B, E-H, 2.7 A-B, 2.8A, D, F were contributed by H. Sha. H. Chen optimized conditions for Phos-tag gels. A. Zenno contributed Figs. 2.5G and 2.6I.

CHAPTER 3*

NON-MUSCLE MYOSIN IIB LINKS CYTOSKELETON TO IRE1α SIGNALING DURING ER STRESS

3.1 ABSTRACT

Here we identify and characterize a cytoskeletal myosin protein required for IRE1α oligomerization, activation, and signaling. Proteomic screening identified non-muscle myosin heavy chain IIB (NMHCIIB), a subunit of non-muscle myosin IIB (NMIIB), as an ER stress-dependent interacting protein specific to IRE1α. Loss of NMIIB compromises XBP1s and UPR target gene expression with no effect on the PERK pathway. Mechanistically, NMIIB is required for IRE1α aggregation and foci formation under ER stress. The NMIIB-mediated effect on IRE1α signaling is in part dependent on the phosphorylation of myosin regulatory light chain and the actomyosin contractility of NMIIB. Biologically, the function of NMIIB in ER stress response is conserved as both mammalian cells and *C. elegans* lacking NMIIB exhibit hypersensitivity to ER stress. Thus, optimal IRE1α activation and signaling require concerted coordination between the ER and cytoskeleton.

* This chapter has been published as **He, Y**., Beatty, A., Han, X., Ji, Y., Ma, X., Adelstein, R.S., Yates III, J.R., Kemphues, K., and Qi, L. *Developmental Cell* **23**, 1141-1152 (2012) and is reprinted here with permission.

3.2 INTRODUCTION

Perturbations in endoplasmic reticulum (ER) homeostasis culminate in ER stress and activate an ER-to-nucleus signal transduction cascade termed the unfolded protein response (UPR) (Hetz et al., 2011; Walter and Ron, 2011). In mammals, the ER luminal environment is sensitively monitored by three transmembrane sensors: inositol-requiring enzyme 1α (IRE1α), PKR-like endoplasmic reticulum kinase (PERK), and activating transcription factor 6 (ATF6), with IRE1α as the most conserved (Hetz et al., 2011; Walter and Ron, 2011). A current model of mammalian IRE1α activation speculates that upon alterations in ER homeostasis, the luminal domain of IRE1α undergoes a conformational change and subsequent homodimerization. Juxtaposition of IRE1α proteins promotes trans-autophosphorylation and may facilitate higher-order oligomerization of IRE1α dimers, followed by activation of its ribonuclease (RNase) domain to splice 26 nucleotides from the X-box binding protein 1 (*Xbp1*) mRNA (Walter and Ron, 2011). This processing event produces a transcription factor XBP1 spliced (XBP1s) required for UPR target gene induction (Acosta-Alvear et al., 2007; He et al., 2010). Given that activation of the IRE1α-XBP1 pathway is emerging as a central paradigm underlying human pathologies, such as cancer, diabetes, and conformational diseases (Hetz et al., 2011; Sha et al., 2011), a comprehensive and mechanistic understanding of IRE1α activation is of critical therapeutic value.

One model for IRE1α activation proposes that under non-stress conditions, IRE1α is bound in an inactive state by the ER chaperone, glucose-

regulated protein 78 (GRP78/BiP) (Bertolotti et al., 2000; Kimata et al., 2003). Accumulation of misfolded proteins promotes BiP dissociation, allowing for IRE1α homodimerization and activation. Alternatively, misfolded proteins may activate IRE1α through direct binding (Credle et al., 2005; Gardner and Walter, 2011; Kimata et al., 2007) to promote its oligomerization and optimal activation (Korennykh et al., 2009; Li et al., 2010; Walter and Ron, 2011). These two models are not mutually exclusive and may have different implications for yeast and mammalian IRE1α proteins (Oikawa et al., 2009). Here we identify a cytosolic factor required for mammalian IRE1α aggregation and optimal activation of this pathway.

Non-muscle myosin II (NMII), a member of the myosin II motor superfamily (Ma and Adelstein, 2012), is a hexameric molecule composed of a pair of heavy chains (NMHCs), a pair of regulatory light chains (RLCs), and a pair of essential light chains (Vicente-Manzanares et al., 2009). In mammals, the identity of the heavy chain, NMHCIIA, NMHCIIB, or NMHCIIC determines the overall NMII isoform (Vicente-Manzanares et al., 2009). NMII activation is largely mediated by phosphorylation of its RLC at serine residue 19 (Ser19) (Adelstein and Conti, 1975) and to a lesser extent by increased transcriptional activity (Vicente-Manzanares et al., 2009). NMII has been widely studied in distinct biological processes that require remodeling of the actin cytoskeleton, such as cell migration, polarity determination, cell adhesion, and clustering of signal transduction molecules (Ma and Adelstein, 2012; Vicente-Manzanares et al., 2009). Consequently, NMII-dependent processes span diverse physiological functions, including tumor-necrosis factor signaling, T cell antigen receptor

clustering, and viral entry (Arii et al., 2010; Flynn and Helfman, 2010; Ilani et al., 2009). Here, we report an indispensable role of NMIIB in IRE1α signaling of UPR.

3.3 MATERIALS AND METHODS

Cell lines and drug treatment

NMHCIIB$^{-/-}$ MEFs were generated as previously described (Meshel et al., 2005). XBP1$^{-/-}$ and IRE1α$^{-/-}$ MEFs were generously provided by Drs. L. Glimcher (Weill Cornell) and D. Ron (University of Cambridge), respectively. Matching WT MEFs were used in this study. T-REx293 IRE1-3F6HGFP was previously described (Li et al., 2010; Xue et al., 2011) and generously provided by Dr. P. Walter (UCSF). MEFs, HEK-293T, Phoenix, and T-REx293 IRE1-3F6HGFP cells were maintained in DMEM supplemented with 10% FBS (Hyclone) and 1% penicillin/streptomycin (Cellgro). Tg and Tm (EMD Calbiochem), Blebbistatin (Cayman Chemical), and ML-7 (Sigma) were dissolved in DMSO. Cytochalasin D (Enzo Life Sciences) and doxycycline (EMD Millipore) were dissolved in H_2O. In most experiments, cells were treated with 150 - 300 nM Tg or 2.5 - 5 μg/ml Tm for 4 - 8 hr. A drug concentration titer was performed in one experiment to examine the dose-response curve.

Plasmids

pMSCV-IRE1α–HA encoding WT human IRE1α (Hetz et al., 2006) was provided by Dr. C. Hetz (University of Chile). IRE1α mutants D123P, K599A and P830L

were previously generated and described (Xue et al., 2011). CMV-GFP-NMHCII-B was purchased from Addgene Inc. CMV-GFP-NMHCII-B R709C was previously described (Kim, 2005). pcDNA3-Flag-mouse XBP1s was described previously (Chen and Qi, 2010).

Transfection

Transfections of HEK293T were performed as we recently described (Chen and Qi, 2010). Transfections of MEFs were performed using Lipofectamine 2000 (Invitrogen) per supplier's protocol. Cells were snap-frozen in liquid nitrogen 24-36 hr post-transfection followed by Western blot.

IRE1α immunopurification and mass spectrometry

IRE1$\alpha^{-/-}$ MEFs stably expressing human pMSCV-IRE1α-HA were treated with 300 nM Tg for 2 hr. Cells were harvested in lysis buffer (150 mM NaCl, 1% Triton X-100, 1 mM EDTA, 50 mM Tris HCl pH 7.5) supplemented with protease inhibitor cocktail (Sigma) and allowed to lyse on ice for 25 min. Cells were sonicated 10 s once with Branson Digital 250 Cell Disruptor at 10% amplitude followed by centrifugation. Supernatant was harvested and loaded on a 6% polyacrylamide SDS-PAGE gel. Gel was incubated with Coomassie Brilliant Blue (0.5 g Coomassie Brilliant Blue R-250 in 450 ml methanol, 450 ml MQ water, and 100 ml acetic acid) with gentle rocking for 30 min at room temperature followed by 2 washes with MQ water 5 min each. Gel was destained in destaining solution (45% methanol, 45% MQ water, and 10% acetic acid) that was changed every 30 min until bands could be clearly visualized. Protein bands were excised from

Coomassie-stained gels and destained, and subjected to an in-gel trypsin digestion. Briefly, digestion was performed with 12.5 ng/μL of trypsin in 50 mM ammonium bicarbonate and incubated overnight at 37°C. The resultant peptides were extracted with 50% acetonitrile/5% formic acid and dried in a vacuum centrifuge. Prior to measurements, dried peptides were dissolved in 0.1% formic acid.

The peptide mixtures were analyzed by online nanoflow liquid chromatography tandem mass spectrometry (LC-MS/MS) on an Agilent 1200 quaternary HPLC system (Agilent, Palo Alto, CA) connected to an LTQ-Orbitrap mass spectrometer (Thermo Fisher Scientific) through an in-house built nanoelectrospray ion source. The peptide mixtures were pressure-loaded onto a capillary column (75 μm i.d.) packed with 15 cm of 3 μm Aqua C18 resins (Phenomenex, Ventura, CA). They were separated with a 3 hr gradient from 5% to 60% acetonitrile in 0.1% formic acid and a flow rate of 300 nL/min (through split). As peptides were eluted from the analytical column, they were electrosprayed (distal 2.5 kV spray voltage) into the mass spectrometer. MS instrument method consisted of an FT full-scan MS analysis (400-1600 m/z, 60000 resolution) followed by data-dependent MS/MS scans of the 8 most intense precursors at a 35% normalized collision energy with dynamic exclusion for 60 s. Application of mass spectrometer scan functions and HPLC solvent gradients was controlled by the Xcalibur data system (Thermo Fisher Scientific).

MS/MS spectra were extracted using RawXtract (version 1.9.9) (McDonald et al., 2004) and searched with the ProLuCID algorithm against a human UniProt database concatenated to a decoy database in which the

sequence for each entry in the original database was reversed (Peng et al., 2003). ProLuCID search results were assembled and filtered using the DTASelect (version 2.0) algorithm (Tabb et al., 2002) with a false positive rate below one percent.

siRNA knockdown and retroviral transduction

Retroviral transduction and stable cell lines were carried out as described (Sha et al., 2009). Stable cell lines expressing siRNA were selected in hygromycin at 200 μg/ml or puromycin at 5 μg/ml. Stable cell lines were made and tested independently at least twice.

siRNA sequences for mouse *myh-10* (in MEFs)

shIIB#1: 5′ GAGAAGAAACTGAAAGAAA 3′

shIIB#3: 5′ GGAACAAGGCTGAGAAACA 3′

siRNA sequences for human *myh-10* (in HEK293T cells)

shIIB#1: 5′ GAGAAGAAGCTGAAAGAAA 3′

shIIB#2: 5′ CCAAAGATGATGTGGGAAA 3′

Immunoprecipitation

Whole cell lysate was harvested in lysis buffer (150 mM NaCl, 1% Triton X-100, 1 mM EDTA, and 50 mM Tris HCl pH 7.5) supplemented with protease inhibitor cocktail (Sigma) and 5 mM ATP (Sigma) and incubated on ice for 25 min. Samples were sonicated 10 s once with Branson Digital 250 Cell Disruptor at

amplitude 10%. For endogenous IP, supernatant was pre-cleared with Protein A-agarose (Invitrogen) for 30 min and rocked with 2 μg primary antibody overnight at 4^0C. Immune complexes were recovered with Protein A-agarose for 2 h at 4^0C with rocking. Beads were washed four times with wash buffer (20 mM Tris HCl pH 7.5, 137 mM NaCl, 20 mM EDTA, 1% Triton X-100, 10% glycerol), eluted in boiling 2X SDS sample buffer followed by SDS-PAGE and Western blot. In the case of overexpressed tagged proteins, the only difference was that cells were incubated overnight with HA- or Flag-agarose at 4^0C with rocking followed by washes as described above.

Western blot and image quantitation

Preparation of cell lysates and Western blot were performed as we previously described (Sha et al., 2009). Primary antibodies were diluted in 5% milk/TBST or 2% BSA/TBST and incubated with PVDF membrane overnight at 4^0C, while secondary antibodies were incubated at room temperature for 45 min. To study IRE1α phosphorylation, we used a Phos-tag based Western blot method described by our group that can sensitively monitor the phosphorylation status of UPR sensors (Qi et al., 2011; Sha et al., 2009; Yang et al., 2010). Membranes were routinely strip-reprobed for HSP90 as a positional control. In addition, a Phos-tag based method was also used to visualize total RLC phosphorylation as previously described (Aguilar et al., 2011). Of note, to ensure sufficient signal for cleaved caspase 3, the membrane for caspase 3 was cut around the 25 kDa line and then probed separately with caspase 3 antibody. Band density was quantitated using the Image Lab software on the ChemiDOC XRS$^+$ system (Bio-

Rad) and presented as mean ± SEM from several independent experiments or as representative data from at least two independent experiments.

Antibodies for western blots and immunoprecipitations

MYH10/NMIIB (sc-99210, 1:1000), MYH9/NMIIA (sc-98978, 1:1000), XBP1 (sc-7160, 1:1000), HSP90 (sc-7947, 1:6000), HA-HRP (sc-7392, 1:8000) were obtained from Santa Cruz. eIF2α (9722, 1:1000), p-eIF2α (9721, 1:1000), Caspase 3 (H277, 1:1000), p-Ser19 RLC/MLC (3671/3675, 1:1000), RLC/MLC (3672, 1:1000), IRE1α (14C10, 1:2000), PERK (3192, 1:2000) were obtained from Cell Signaling. Flag-HRP (1:8000) was obtained from Sigma. GAPDH (NB600-502, 1:20,000) was obtained from Novus Biologicals. Goat-anti-rabbit/mouse IgG HRP (1:5000) were obtained from Biorad. Donkey anti-goat IgG HRP (1:5000) was obtained from Jackson ImmunoResearch. Antibodies against GFP, CREB and PARP were gifts from Drs. Fenghua Hu (Cornell University), Marc Montminy (Salk Institute) and Lee Kraus (UT Southwestern), respectively.

RNA extraction and qPCR

These experiments were performed as previously described (Sha et al., 2009). For nematodes, WT (N2) or *nmy-2(ne3409)* worms were shifted to 25^0C and grown on 6 μg/ml Tm. 72 h later, approximately 300 animals of each genotype and condition were washed off plates with M9 buffer, pelleted and mixed with 10X volume of Trizol. qPCR was performed with primers in Tables 3.1 and 3.2 for mouse and worm genes, respectively.

Immunofluorescence

MEFs were plated and grown on collagen-coated coverslips in 6-well plates overnight followed by treatment with indicated concentration and time of Tg. After a brief wash with PBS, cells were fixed in fresh 3.7% formaldehyde in PBS for 10 min and washed 3 times with PBS 5 min each. Cells were lysed with 0.2% Triton X-100 in PBS for 5 min and washed 3 times with PBS 5 min each. Cells were blocked in 5% BSA in PBS for 10 min and incubated 1 hr at room temperature with anti-myosin IIB at 1:50 dilution (Developmental Studies Hybridoma Bank, CMII23) (Conrad et al., 1991). Cells were washed 3 times with PBS 5 min each followed by 1 hr incubation with donkey anti-mouse Cy3 (Jackson ImmunoResearch) with or without anti-rabbit FITC (Jackson ImmunoResearch) at 1:200 dilution in the dark. Cells were washed and mounted with Prolong Gold Antifade Reagent with DAPI (Invitrogen). Fluorescent microscopic images were taken with a Zeiss 710 Confocal microscope using a 63x/1.4 objective (Cornell Microscopy and Imaging Facility).

Foci imaging

T-REx293 IRE1-3F6HGFP cells were treated and processed as described (Xue et al., 2011). Fluorescent microscopic images were taken with a Zeiss 710 Confocal microscope using a 63x/1.4 objective (Cornell Microscopy and Imaging Facility). Foci-positive was calculated as the number of cells with one or more foci out of total number of cells.

Quantitative-PCR primers

Table 3.1. Primers for *M. musculus* genes for qPCR.

Gene (mouse)	Forward	Reverse
xbp1s	GAGTCCGCAGCAGGTG	GTGTCAGAGTCCATGGGA
erdj4	CTTAGGTGTGCCAAAGTCTGC	GGCATCCGAGAGTGTTTCATA
grp78	TGTGGTACCCACCAAGAAGTC	TTCAGCTGTCACTCGGAGAAT
myh10	GGAGCTGCTGAAGGTGAAAG	CTCCAGTTCCTGCTTTTTGG
p58ipk	GTGGCATCCAGATAATTTCCAG	GAGTTCCAACTTCTGTGGAAGG
hrd1	AGCTACTTCAGTGAACCCCACT	CTCCTCTACAATGCCCACTGAC
herp	AACCAGGACCCCAACAATAAC	CTGGAAGAAGAGAGGCAAAGAA
l32	GAGCAACAAGAAAACCAAGCA	TGCACACAAGCCATCTACTCA

Table 3.2. Primers for *C. elegans* genes for qPCR.

Gene (worm)	Forward	Reverse
xbp1s	TGCCTTTGAATCAGCAGTGG	ACCGTCTGCTCCTTCCTCAATG
hsp-4	AGTTGAAATCATCGCCAACG	GCCCAATCAGACGCTTGG
act-1	ACGACGAGTCCGGCCCATCC	GAAAGCTGGTGGTGACGATGGTT

Sucrose gradient sedimentation

Confluent WT and NMHCIIB$^{-/-}$ MEFs in 10-cm plates non-treated or treated with 300 nM Tg for 3 hr were harvested and lysed in 300 µl lysis buffer (see above). Extracts were centrifuged through 20-40% sucrose gradients prepared freshly by progressively layering higher to lower density sucrose fractions in 5% increments in polyallomar tubes of 11 x 60 mm (Beckman Coulter). Extracts were centrifuged at 60,000 rpm for 14.5 hr at 4^{0}C using a Beckman Coulter swinging bucket SW 60 Ti rotor. Each 4 ml gradient was divided evenly into 16 fractions (250 µl) and aliquots of fractions 3-16 (labeled 1-14 in Figures 3H-I) were subjected to SDS-PAGE analysis. IRE1α-containing complexes were detected using anti-IRE1α antibody. The density of IRE1α in each fraction was quantitated using the Image Lab software on the ChemiDOC XRS$^+$ system (Bio-Rad) and the % of IRE1α in each fraction was calculated as the amount of IRE1α in a fraction relative to the total IRE1α levels in all 14 fractions.

Cell survival assay

WT and NMHCIIB$^{-/-}$ or shCON and shIIB#1 MEFs were grown in 6-well plates and treated with 150-300 nM Tg for the indicated time. For rescue experiments, NMHCIIB$^{-/-}$ MEFs were transfected with WT or R709C NMHCIIB plasmids using Lipofectamine 2000 per supplier's protocol for 24 hr prior to Tg treatment. Cells were counted by hemocytometer and 1.5X10^5 cells were re-plated onto 10-cm plates. 4 days later, the cells were briefly washed in PBS and fixed in 3.7% formaldehyde in PBS (freshly prepared) for 15 min followed by 30 min incubation in 0.05% crystal violet in distilled water (filtered before use) with

gentle rocking at room temperature. Cells were washed 3 times for 5 min each with ddH_2O, permeabilized with methanol for 15 min and sampled aliquots were read at OD 540 nm with Bio-Tek Synergy 2 plate reader (Bio-Tek Inc.).

Brefeldin-A BODIPY and flow cytometry

WT and various mutant MEFs were grown in 24-well plates overnight followed by treatment with 150 nM Tg or 2.5 μg/ml Tm for the indicated time. For rescue experiments, $NMHIIB^{-/-}$ MEFs were transfected with WT, R709C NMHCIIB or XBP1s plasmids with Lipofectamine 2000 per supplier's protocol for 24 hr followed by Tg treatment. Cells were incubated at 37^0C for 30 - 45 min with 0.4 μg/ml Brefeldin A-BODIPY (Invitrogen) in culture media followed by trypsinization and flow cytometric analysis using a BD FACSCalibur flow cytometer. Data was analyzed using the CellQuest and FlowJo software.

ER stress resistance in *C. elegans*

Nematodes were cultured using standard conditions (Brenner, 1974), with N2 (Bristol) as wild type. The mutations used in this analysis include *nmy-2(ne3409)* (Liu et al., 2010) and *xbp-1(zc12)* (Calfon et al., 2002). For ER stress resistance assays, embryos were laid onto plates containing 0 or 6 μg/mL Tm. After 18 hr, the number of hatching larvae was noted and compared to the number of L4/adult stage worms after 72 hr. In experiments using *nmy-2(ne3409)*, embryos were allowed to complete embryogenesis at the permissive temperature of 16°C and then shifted to the restrictive temperature of 25°C after hatching. Some nematode strains used in this work were provided by the Caenorhabditis

Genetics Center (University of Minnesota), which is funded by the NIH National Center for Research Resources.

Statistical analysis

Results are expressed as mean ± SEM unless indicated otherwise. Comparisons between groups were made by unpaired two-tailed Student's t-test, where $p < 0.05$ was considered as statistically significant. All experiments were repeated at least two to three times and representative data are shown.

3.4 RESULTS

3.4.1 NMHCIIB physically interacts with IRE1α upon ER stress

To investigate mechanisms regulating mammalian IRE1α signaling, we performed a proteomic screen using IRE1α$^{-/-}$ mouse embryonic fibroblasts (MEFs) stably expressing hemagglutinin (HA)-tagged IRE1α to identify potential IRE1α-interacting proteins. Coomassie blue staining revealed a band approximately 250 kDa in size that was responsive to thapsigargin (Tg)-induced ER stress (Fig. 3.1A). Tandem mass spectrometry (MS/MS) identified this factor as the heavy chain of non-muscle myosin II (NMHCII) with 35.4% identity to NMHCIIB, 31.6% to NMHCIIA, and 5.4% to NMHCIIC; peptide coverage spanned all functional domains (Fig. 3.1B).

As endogenous NMHCIIB interacted with IRE1α much more strongly than NMHCIIA (Fig. 3.1C), the remainder of our study focused on NMIIB. The ER stress-dependent interaction between NMHCIIB and IRE1α was verified in HEK293T cells overexpressing IRE1α-HA and GFP-NMHCIIB, or IRE1α-HA alone (Figs. 3.1C-D). Treatment with another ER stress agent tunicamycin (Tm) also promoted the interaction (Fig. 3.1E), demonstrating that this event is ER stress-dependent and independent of non-specific Ca^{2+} effects. Lastly, immunoprecipitation in MEFs with anti-IRE1α antibody confirmed the ER stress-dependent interaction between endogenous proteins (Fig. 3.1F).

Figure 3.1. NMIIB is an ER stress-induced IRE1α-interacting factor.

(A) Coomassie blue staining of immunoprecipitates (IPs) of IRE1α$^{-/-}$ MEFs stably expressing C-terminal hemagglutinin (HA)-tagged IRE1α untreated or treated with 300 nM Tg for 2 hr. Unknown Tg-specific band at ~250 kDa was excised and identified as NMHCII using tandem mass spectrometry (MS/MS) analysis. **(B)** Schematic of the functional domains of the three mammalian isoforms of NMHCII with respective peptide coverage recovered (indicated by lines below) from MS/MS. Figure is drawn to scale using sequence annotation data from UniProt. **(C)** Western blot showing recovery of endogenous NMHCIIB and NMHCIIA from immunoprecipitates of HA-tagged IRE1α prepared from transiently transfected HEK293T cells treated with 150 nM Tg for the indicated time. **(D and E)** Western blot showing recovery of GFP-tagged NMHCIIB from IPs of HA-tagged IRE1α prepared from transfected HEK293T cells treated with 300 nM Tg for the indicated time **(D)** or 300 nM Tg or 5 μg/ml Tm for 2 hr **(E).** Arrowhead points to endogenous protein. **(F)** Western blot showing recovery of endogenous NMHCIIB from IPs of endogenous IRE1α prepared from MEFs treated with 150 nM Tg for the indicated time. For **(C)-(F),** similar results were observed in 2-3 independent experiments.

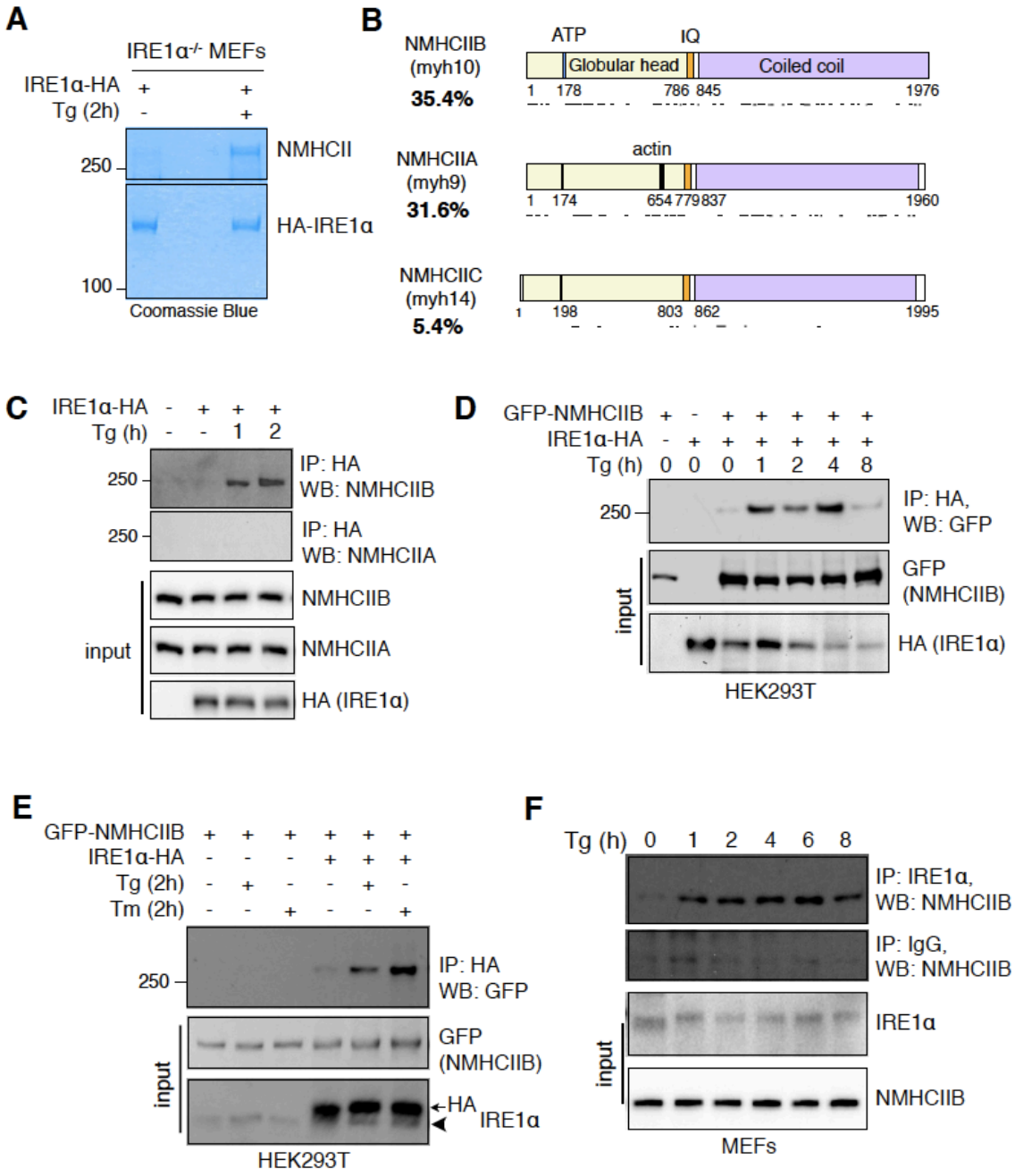
A
IRE1α-/- MEFs
IRE1α-HA + +
Tg (2h) - +
250
100
NMHCII
HA-IRE1α
Coomassie Blue
B
NMHCIIB
(myh10)
35.4%
ATP
IQ
Globular head
Coiled coil
1 178 786 845 1976
NMHCIIA
(myh9)
31.6%
actin
1 174 654 779 837 1960
NMHCIIC
(myh14)
5.4%
1 198 803 862 1995
C
IRE1α-HA - + + +
Tg (h) - - 1 2
250
IP: HA
WB: NMHCIIB
250
IP: HA
WB: NMHCIIA
input
NMHCIIB
NMHCIIA
HA (IRE1α)
D
GFP-NMHCIIB + - + + + + +
IRE1α-HA - + + + + + +
Tg (h) 0 0 0 1 2 4 8
250
IP: HA,
WB: GFP
input
GFP
(NMHCIIB)
HA (IRE1α)
HEK293T
E
GFP-NMHCIIB + + + + + +
IRE1α-HA - - - + + +
Tg (2h) - + - - + -
Tm (2h) - - + - - +
250
IP: HA
WB: GFP
input
GFP
(NMHCIIB)
HA
IRE1α
HEK293T
F
Tg (h) 0 1 2 4 6 8
IP: IRE1α,
WB: NMHCIIB
IP: IgG,
WB: NMHCIIB
input
IRE1α
NMHCIIB
MEFs

3.4.2 NMIIB is required and sufficient for optimal IRE1α activation

To study the functional role of NMIIB in IRE1α signaling, we used loss- and gain-of-function models. Induction of *Xbp1s* mRNA, a substrate of IRE1α, was blunted in NMHCIIB$^{-/-}$ and knock-down MEFs (Fig. 3.2A). Concomitantly, nuclear XBP1s protein production was defective and delayed in NMHCIIB$^{-/-}$ MEFs (Fig. 3.2B), NMHCIIB knock-down MEFs (Fig. 3.2C) and cells treated with the NMII-specific inhibitor blebbistatin (Straight et al., 2003) (Fig. 3.2D). A similar observation was made in NMHCIIB$^{-/-}$ MEFs treated with Tm (Fig. 3.2E). Further pointing to defects in the IRE1α-XBP1 pathway, the expression of a subset of XBP1 target genes were attenuated in NMHCIIB knock-down (Fig. 3.2F) and NMHCIIB$^{-/-}$ MEFs (Fig. 3.2G).

Conversely, overexpression of NMHCIIB in HEK293T cells increased XBP1s protein (Fig. 3.2H) and overexpression in NMHCIIB$^{-/-}$ MEFs rescued the levels of XBP1s protein (Fig. 3.2I). Notably, the gain-of-function effect was observed only under conditions of ER stress, further supporting the notion that NMIIB-mediated IRE1α signaling is ER stress-dependent.

To determine the specificity of NMIIB for IRE1α, we aimed to study its impact on the other two major UPR branches. Upon ER stress, PERK undergoes trans-autophosphorylation and subsequently phosphorylates Ser51 on eukaryotic initiation factor 2α (eIF2α), leading to attenuation of global protein synthesis. Paradoxically, this event selectively upregulates the translation of a subset of genes including *Chop* (Walter and Ron, 2011). Upon ER stress, no interaction occurred between PERK and NMHCIIB (Fig. 3.3A). Furthermore,

PERK activation and signaling was unaffected in NMHCIIB knock-down MEFs as phosphorylation of PERK and eIF2α, and *Chop* transcript levels were unchanged (Figures 3.3B-D). We were unable to study the relationship between NMIIB and ATF6 activation due to the lack of a good antibody against the endogenous active form of ATF6. Nonetheless, our data points to a functional role of NMHCIIB specifically in IRE1α signaling and dispensable for the PERK pathway.

Figure 3.2. NMIIB is required for optimal IRE1α-XBP1 signaling.

(A) Quantitative real-time PCR analysis of *Xbp1s* expression from NMHCIIB$^{-/-}$ or shIIB#1 MEFs treated with 150 nM Tg for the indicated time. **(B and C)** Western blot of nuclear (XBP1s) and cytosolic extracts (NMHCIIA/B) from **(B)** WT and NMHCIIB$^{-/-}$ MEFs treated with 150 nM Tg for the indicated time or **(C)** WT MEFs stably expressing shRNA against control (shCON) or murine NMHCIIB (shIIBi#1 and shIIBi#3) treated with 150 nM Tg for the indicated time. **(D)** Western blot of XBP1s in HEK293T cells untreated or pretreated with 50 μM blebbistatin followed by treatment with 150 nM Tg for 3 hr. **(E)** Western blot of XBP1s in WT and NMHCIIB$^{-/-}$ MEFs treated with 5 μg/ml Tm for the indicated time. **(F and G)** Quantitative real-time PCR analysis of UPR genes in **(F)** shCON and shIIBi#1 MEFs treated with 150 nM Tg for 5 hr or **(G)** WT and NMHCIIB$^{-/-}$ MEFs treated with 150 nM Tg for the indicated time. **(H and I)** Western blot of nuclear (XBP1s) and cytosolic extracts (NMHCIIA/B) from **(H)** HEK293T cells transiently overexpressing GFP vector or GFP-NMHCIIB treated with 150 nM Tg for the indicated time, or **(I)** WT or NMHCIIB$^{-/-}$ MEFs transiently overexpressing GFP vector or GFP-NMHCIIB treated with 150 nM Tg for the indicated time. Arrowhead points to endogenous protein. Quantitation of XBP1s protein levels shown below the gel after normalization to CREB. In western blots, CREB and HSP90 are loading controls. In quantitative real-time PCR analysis, data are shown as mean ± SEM. *$p < 0.05$, **$p < 0.01$, ***$p < 0.001$. For all, similar results were observed in 2-3 independent experiments.

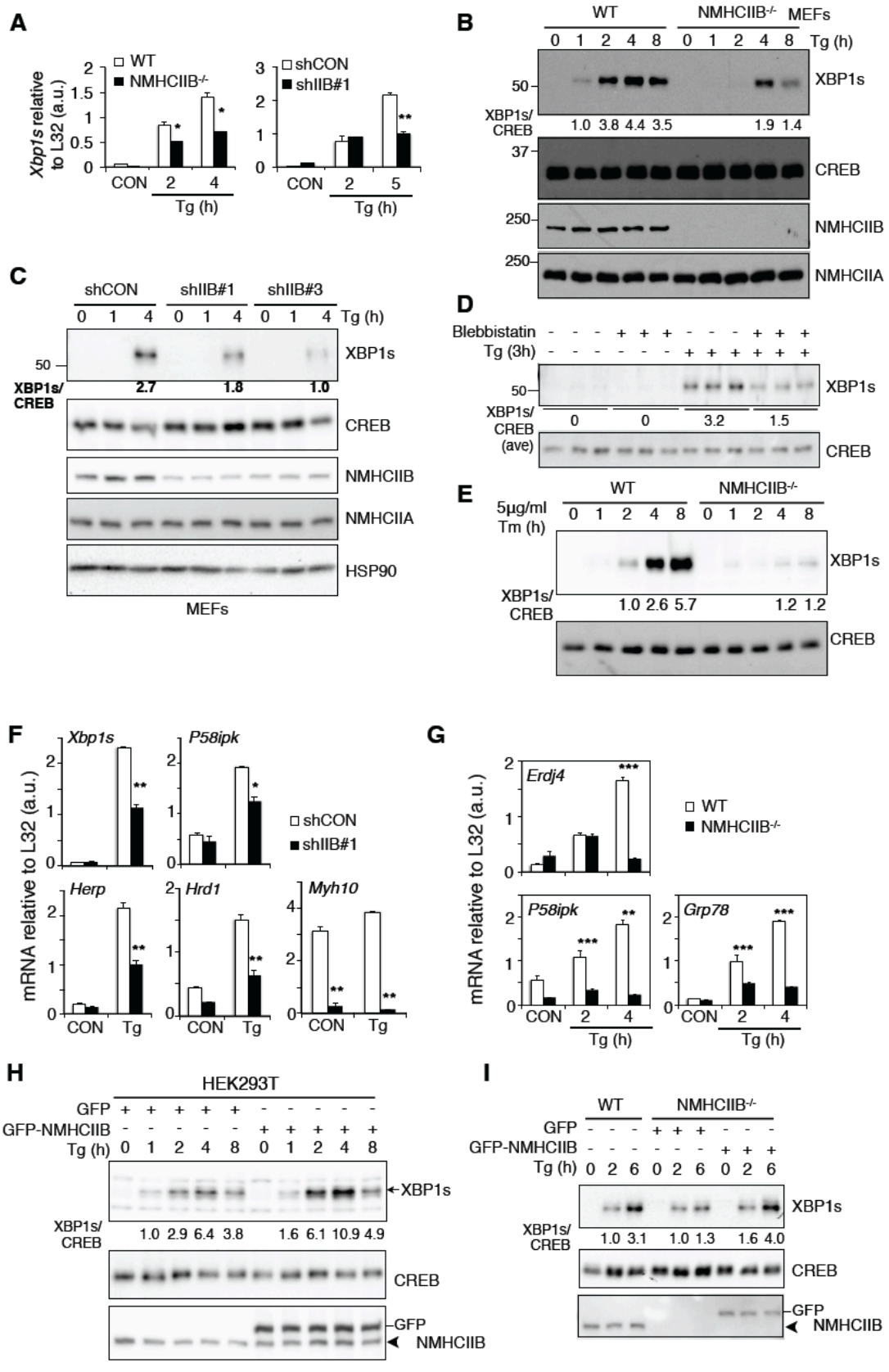
A
Xbp1s relative to L32 (a.u.)
WT
NMHCIIB-/-
shCON
shIIB#1
CON
Tg (h)
B
WT
NMHCIIB-/-
MEFs
Tg (h)
XBP1s
XBP1s/ CREB
CREB
NMHCIIB
NMHCIIA
C
shCON
shIIB#1
shIIB#3
Tg (h)
XBP1s
CREB
NMHCIIB
NMHCIIA
HSP90
MEFs
D
Blebbistatin
Tg (3h)
XBP1s
XBP1s/ CREB (ave)
CREB
E
5μg/ml Tm (h)
XBP1s
CREB
F
Xbp1s
P58ipk
Herp
Hrd1
Myh10
mRNA relative to L32 (a.u.)
shCON
shIIB#1
CON
Tg
G
Erdj4
P58ipk
Grp78
WT
NMHCIIB-/-
Tg (h)
H
HEK293T
GFP
GFP-NMHCIIB
Tg (h)
XBP1s
XBP1s/ CREB
CREB
GFP
NMHCIIB
I
WT
NMHCIIB-/-
GFP
GFP-NMHCIIB
Tg (h)
XBP1s
XBP1s/ CREB
CREB
GFP
NMHCIIB

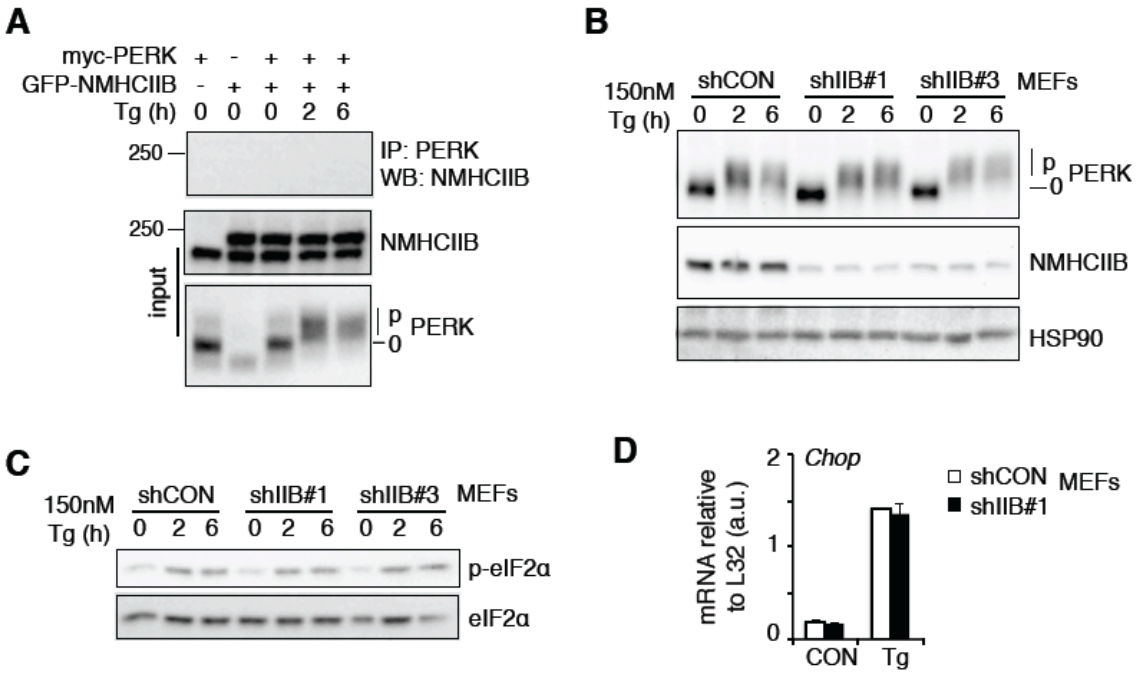

Figure 3.3. NMIIB is dispensable for PERK pathway activation and signaling. **(A)** Co-immunoprecipitation of myc-tagged PERK and GFP-tagged NMHCIIB upon ER stress shows no association. **(B)** Western blot analysis of PERK phosphorylation in control (shCON) and NMHCIIB knock-down MEFs (shIIB#1 and #3) treated with 150 nM Tg for indicated time. **(C)** Western blot analysis of p-eIF2α in shCON, shIIB#1 and #3 MEFs treated with 150 nM Tg for indicated time. **(D)** Quantitative real-time PCR analysis of PERK downstream target, *Chop*, in shCON and shIIB#1 MEFs treated with 150 nM Tg for 4 hr.

3.4.3 IRE1α foci formation and oligomerization require NMIIB

To understand mechanistically how NMIIB affects IRE1α signaling, we investigated two key steps in IRE1α activation, namely dimerization/trans-autophosphorylation and oligomerization/RNase activity (Walter and Ron, 2011). Upon ER stress, IRE1α phosphorylation (Qi et al., 2011; Yang et al., 2010) was not affected in NMHCIIB$^{-/-}$ MEFs (Fig. 3.4A), cells exposed to blebbistatin (Fig. 3.4B) or cells overexpressing NMHCIIB (not shown), suggesting that NMIIB is dispensable for IRE1α trans-autophosphorylation. As ER stress persists, mammalian IRE1α dimers oligomerize to form foci (Credle et al., 2005; Korennykh et al., 2009) that may correlate with RNAse activation and *Xbp1* splicing (Li et al., 2010); this event can be visualized using a T-REx293 cell system in which expression of a GFP-tagged IRE1α protein, IRE1-3F6HGFP, is driven by a doxycycline-inducible promoter (Li et al., 2010). In line with previous studies (Korennykh et al., 2009; Li et al., 2010), IRE1α distribution changed dramatically upon ER stress from diffuse to strong punctate foci beginning as early as 1 hr and peaking at 4 hr (Fig. 3.4C). Knock-down of NMHCIIB (shIIB#1) drastically reduced foci formation from 73.3 ± 10.6% in control cells (shCON) to 20.2 ± 7.7% foci-positive cells in shIIB#1; cells with a shRNA targeting sequence that failed to deplete NMHCIIB (shIIB#2) retained the ability to form foci with 70.0 ± 17.6% foci-positive cells (Figs. 3.4D-G). This effect was consistently observed at various stages of ER stress (Fig. 3.5). Of note, IRE1α-GFP protein levels in all cell lines were comparable (Fig. 3.4E), thus excluding the possibility that reduced protein levels accounted for diminished foci formation.

To confirm this observation under endogenous conditions, we examined oligomerization of endogenous IRE1α proteins using sucrose gradient fractionation. In support of a role for NMIIB in IRE1α aggregation and activation, loss of NMIIB reduced the formation of higher-order complexes of endogenous IRE1α under ER stress (Figs. 3.4H-I). Overall, these results indicate that NMIIB regulates IRE1α aggregation and foci formation during ER stress.

Figure 3.4. NMIIB promotes IRE1α foci formation upon ER stress.

(A and B) Phos-tag western blot of IRE1α phosphorylation prepared from lysates of **(A)** WT or NMHCIIB$^{-/-}$ MEFs treated with 150 nM Tg for the indicated time, and **(B)** MEF cells pretreated with Blebbistatin prior to treatment with Tg at the indicated concentration for 3 hr. **(C)** Confocal microscopic images of IRE1α-GFP in T-REx293 IRE1-3F6HGFP cells untreated (CON) or treated with 300 nM Tg for the indicated time. **(D)** Western blot of NMHCIIB in T-REx293 IRE1-3F6HGFP cells stably expressing shRNA against control (shCON) or human NMHCIIB (shIIB#1 and shIIB#2). HSP90, loading control. **(E)** Western blot of GFP in T-REx293 cells treated with 10 nM doxycycline for 24 hr. **(F and G)** Confocal microscopic images of IRE1α-GFP in T-REx293 IRE1-3F6HGFP cells stably expressing shCON, shIIB#1, or shIIB#2 cells untreated (CON) or treated with 300 nM Tg for 4 hr. Quantitation of the number of foci-positive cells from at least 30 fields with 500-1,000 cells per group are shown in **(G).** Data are shown as the mean ± SEM. ***$p < 0.001$. **(H and I)** Western blot showing the distribution of IRE1α **(H)** and quantitation **(I)** in fractions 1-14 prepared from WT and NMHCIIB$^{-/-}$ MEFs treated with 300 nM Tg for 3 hr and centrifuged using 20%-40% sucrose gradients. For all, similar results were observed in 2-3 independent experiments.

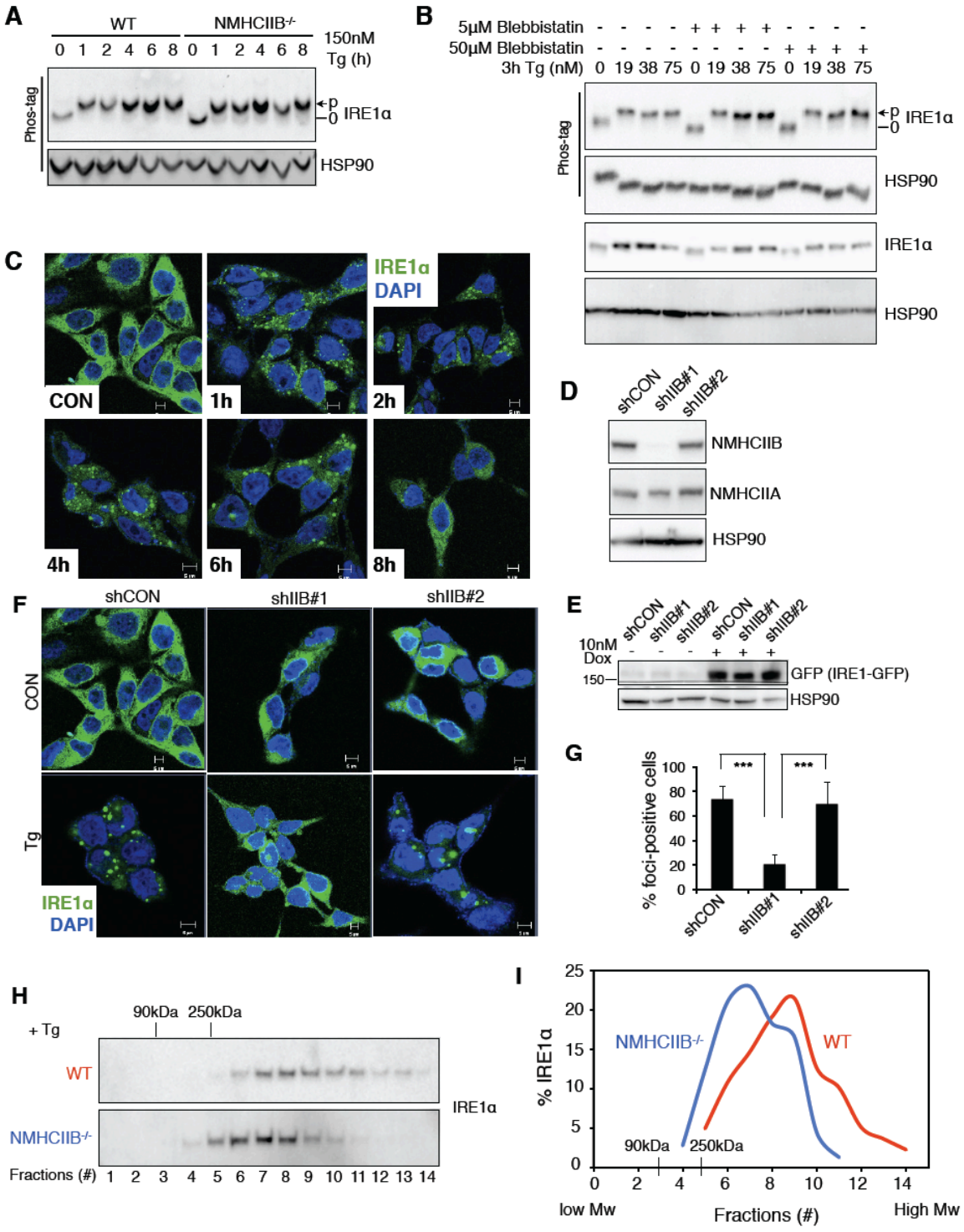
A
WT
NMHCIIB-/-
0 1 2 4 6 8 0 1 2 4 6 8
150nM Tg (h)
Phos-tag
p
0 IRE1α
HSP90
B
5μM Blebbistatin - - - - + + + + - - - -
50μM Blebbistatin - - - - - - - - + + + +
3h Tg (nM) 0 19 38 75 0 19 38 75 0 19 38 75
Phos-tag
p
0 IRE1α
HSP90
IRE1α
HSP90
C
IRE1α
DAPI
CON
1h
2h
4h
6h
8h
D
shCON
shIIB#1
shIIB#2
NMHCIIB
NMHCIIA
HSP90
E
shCON
shIIB#1
shIIB#2
shCON
shIIB#1
shIIB#2
10nM Dox - - - + + +
150
GFP (IRE1-GFP)
HSP90
F
shCON
shIIB#1
shIIB#2
CON
Tg
IRE1α
DAPI
G
% foci-positive cells
100
80
60
40
20
0
***
***
shCON
shIIB#1
shIIB#2
H
90kDa 250kDa
+ Tg
WT
NMHCIIB-/-
IRE1α
Fractions (#) 1 2 3 4 5 6 7 8 9 10 11 12 13 14
I
% IRE1α
25
20
15
10
5
0
NMHCIIB-/-
WT
90kDa
250kDa
0 2 4 6 8 10 12 14
low Mw
Fractions (#)
High Mw

Figure 3.5. Knock-down of NMHCIIB disrupts IRE1α aggregation.

Confocal microscopic analysis of T-REx293 IRE1-3F6HGFP cells stably expressing shRNA against **(A)** control (shCON) or **(B)** human NMHCIIB (shIIB#1) treated with 300 nM Tg for 2-4 hr. Images are representative of 25 fields. Similar results were observed in three separate experiments. Scale bar, 5 μm.

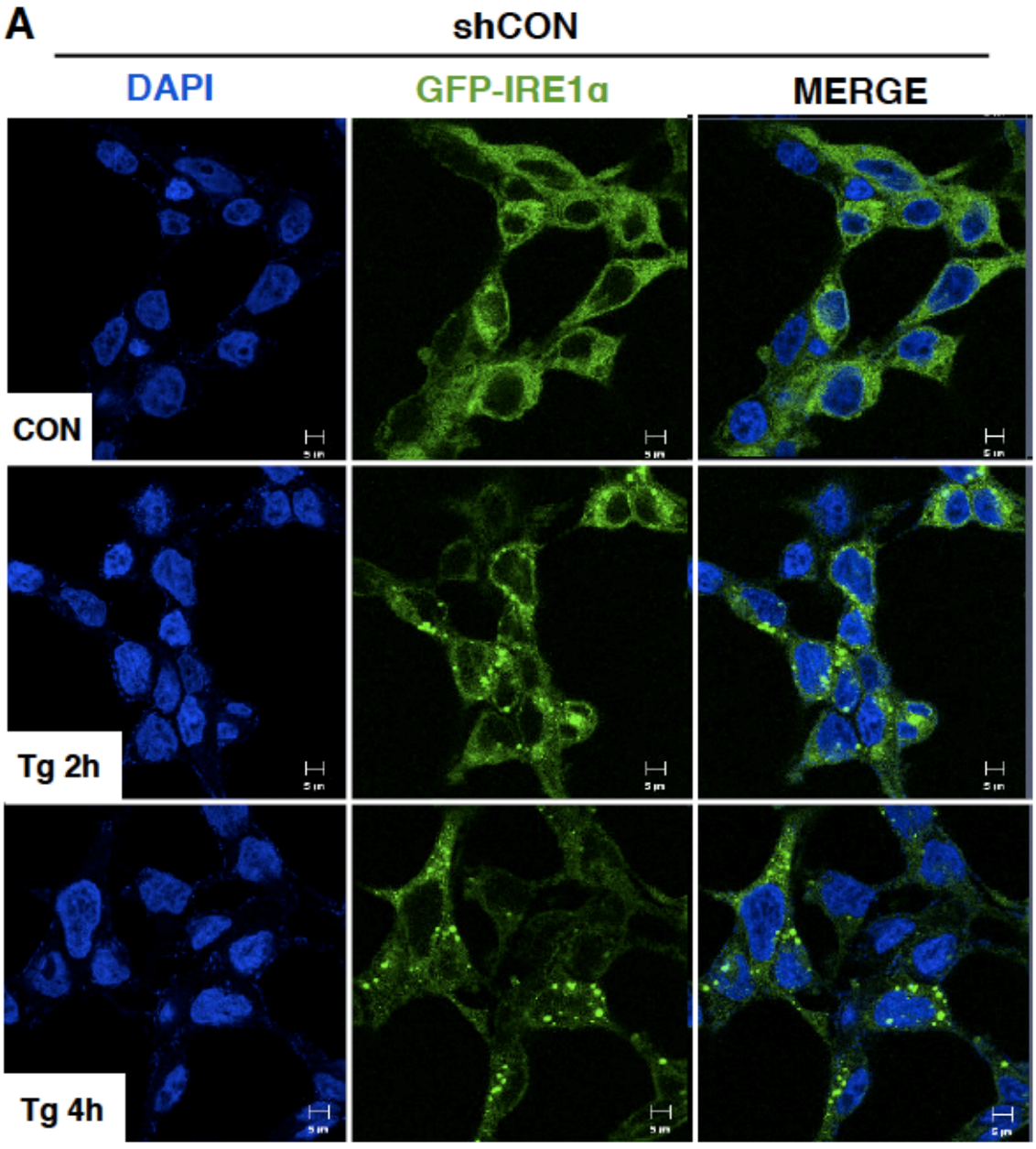
A
shCON
DAPI
GFP-IRE1α
MERGE
CON
Tg 2h
Tg 4h

Figure 3.5 (Continued)

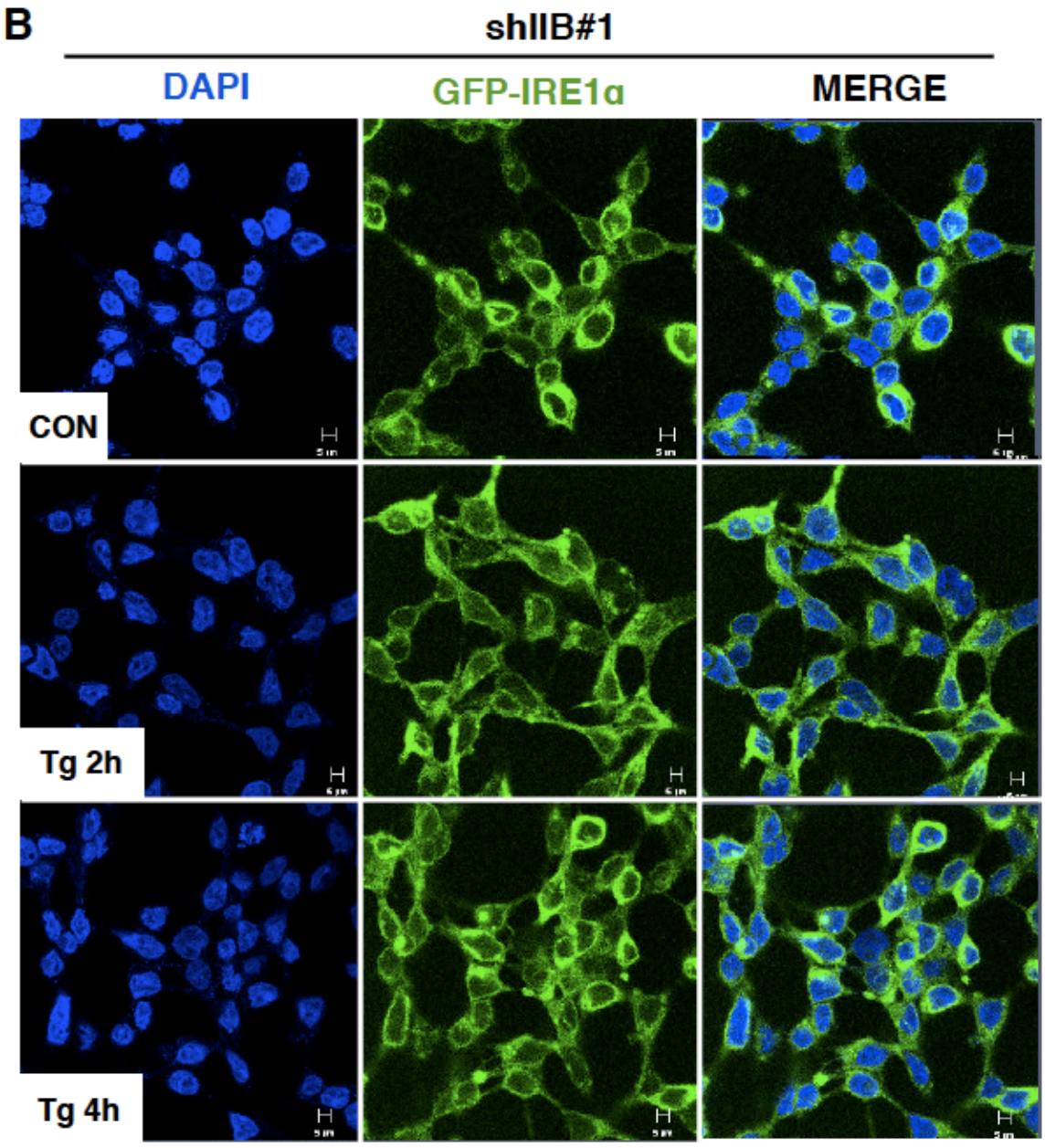

3.4.4 Effect of NMIIB on IRE1α signaling requires RLC phosphorylation

To understand the mechanistic basis of the ER stress-induced NMIIB-IRE1α complex, we first queried whether the interaction was contingent upon the activation status of IRE1α. We used to our advantage two IRE1α mutants: a kinase-dead mutant K599A (Tirasophon et al., 1998) and a loss-of-function mutant P830L lacking both kinase and RNase functions (Xue et al., 2011). Surprisingly, both mutants interacted just as strongly with NMHCIIB as WT IRE1α (Fig. 3.6A), suggesting that the interaction occurs independently of the kinase function of IRE1α. Unexpectedly, the dimerization-defective D123P IRE1α mutant was able to undergo trans-autophosphorylation in HEK293T cells (Figure 3.6A), presumably due to the presence of endogenous IRE1α (Xue et al., 2011).

Next, we examined changes in NMIIB upon ER stress. While ER stress had no noticeable effects on the intracellular distribution (Fig. 3.6B) or protein levels (Fig. 3.6C) of NMHCIIB, it dramatically induced phosphorylation of RLC at Ser19 (Fig. 3.6D), a critical triggering event in NMII activation (Adelstein and Conti, 1975; Ma and Adelstein, 2012; Vicente-Manzanares et al., 2009). Additionally, an independent Phos-tag-based method examining total RLC phosphorylation (Figure 3.6E) demonstrated that RLC phosphorylation peaked within 60 min following ER stress (Figures 3.6D-E), preceding IRE1α foci formation ((Li et al., 2010) and Fig. 3.4C).

Further demonstrating the importance of RLC phosphorylation, treatment with a myosin light chain kinase (MLCK)-specific inhibitor ML-7 (Saitoh et al., 1987) abolished ER stress-dependent IRE1α foci formation (Fig. 3.6F), reduced

the interaction between NMHCIIB and IRE1α (Fig. 3.6G) and dramatically attenuated XBP1s protein levels by over 6-fold (Fig. 3.6H). Thus, the physical interaction between NMIIB and IRE1α as well as the effect of NMIIB on IRE1α aggregation and signaling are largely dependent on MLCK-mediated RLC phosphorylation. How ER stress signals emanating from the ER lumen are transmitted to the cytosolic MLCK requires further investigation.

3.4.5 Motor activity of NMIIB is indispensable for IRE1α activation and signaling

As NMIIB contains several functional domains (Vicente-Manzanares et al., 2009), we next queried whether the motor function was required for optimal IRE1α signaling. Unlike wild-type NMHCIIB, a motor defective mutant R709C with diminished ATPase activity (Kim, 2005; Takeda et al., 2003) did not exhibit ER stress-dependent association with IRE1α (Fig. 3.6I) and overexpression of the mutant failed to enhance XBP1s protein expression upon ER stress (Fig. 3.6J).

As myosin molecules propel along actin filaments to provide movement through the energy of ATP hydrolysis (Vicente-Manzanares et al., 2009), we next addressed the role of actin in IRE1α signaling. Consistently, cells pre-treated with an actin inhibitor cytochalasin D also exhibited attenuated XBP1s levels (Fig. 3.6K). A similar observation was obtained in cells treated with blebbistatin (Fig.3.2D), a highly-specific drug that inhibits the ATPase activity and in vitro motility of NMII proteins (Straight et al., 2003). Therefore, our data collectively

suggest that the actomyosin contractility of NMIIB is required for IRE1α signaling.

3.4.6 NMIIB deficient mammalian cells are defective in ER stress response

We studied the biological consequences of NMIIB on UPR at three levels: organelle, cellular and organismal. At the organelle level, in line with the role of IRE1α-XBP1s in ER biogenesis (Hetz et al., 2006; Sriburi et al., 2004), loss of NMIIB, similar to the loss of IRE1α or XBP1, led to prominent defects in ER expansion in response to both Tg and Tm-induced ER stress (Figs. 3.7A and 3.8). This defect was rescued by overexpression of WT NMIIB, but not the R709C NMHCIIB mutant (Figs. 3.7B-C), further supporting a functional requirement of the motor activity of NMIIB. Importantly, overexpression of XBP1s in NMIIB$^{-/-}$ MEFs rescued the ER expansion defect to a level similar to WT MEFs exposed to Tg (Figs. 3.7B-C). Taken together, these data demonstrate that NMIIB is a critical component of ER stress response via IRE1α activation and XBP1s production.

At the cellular level, NMHCIIB$^{-/-}$ MEFs were unable to recover appropriately after an ER stress challenge (Fig. 3.7D), in line with a pro-survival role attributed to the IRE1α-XBP1s pathway (He et al., 2010). Consistent with the ER expansion phenotype, WT but not R709C NMHCIIB completely rescued cell survival defects (Fig. 3.7E). This was further supported by an increase of caspase-3 cleavage, a marker for apoptosis, in NMHCIIB-deficient cells upon prolonged Tg treatment (Fig. 3.7F).

Figure 3.6. RLC phosphorylation and the actomyosin contractility of NMIIB are required for optimal IRE1α signaling.

(A) Western blot showing recovery of GFP-tagged NMHCIIB from immunoprecipitates of HA-tagged WT and mutant IRE1α (D123P, K599A, P830L) prepared from transfected HEK293T cells treated with 300 nM Tg for 2 hr. Bottom panel shows Phos-tag western blot analysis of IRE1α phosphorylation in HEK293T cells overexpressing WT or mutant IRE1α. ACC (acetyl-CoA carboxylase), loading control. **(B)** Confocal microscopic analysis of endogenous NMHCIIB in MEF cells treated with 300 nM Tg for the indicated time. Images are representative of 25 fields. Scale bar, 5 μm. **(C)** Western blot of NMHCIIB from HEK293T cells treated with 150 nM Tg for the indicated time. **(D)** Western blot of p-Ser19 and total RLC in whole-cell lysates prepared from MEFs treated with 300 nM Tg for the indicated time. **(E)** Phos-tag western blot analysis of total RLC phosphorylation in MEFs treated with 150 nM Tg for the indicated time. Quantitation of p-RLC shown belown. **(F)** Confocal microscopic images of IRE1α-GFP in T-REx293 IRE1-3F6HGFP cells pretreated with 25 μM ML-7 for 30 min prior to treatment with 300 nM Tg for 4 hr. Data is representative of at least 30 fields with 500-1,000 cells per group. Scale bar, 5 μm. **(G)** Western blot showing recovery of endogenous NMIIB from immunoprecipitates of HA-tagged IRE1α prepared from transiently transfected HEK293T cells untreated or pretreated with 25 μM ML-7 for 30 min prior to treatment with 300 nM Tg for 2 hr. Note that ML-7 pretreatment abolishes the interaction between IRE1α and NMIIB. **(H)** Western blot analysis of nuclear XBP1s in HEK293T cells treated as in **(F). (I)** Western blot showing recovery of GFP-tagged WT or the motor-defective R709C NMHCIIB mutant from immunoprecipitates of HA-tagged IRE1α prepared from transfected HEK293T cells treated with 150 nM Tg for the indicated time. **(J and K)** Western blot of XBP1s in **(J)** MEFs transfected with GFP-tagged WT or R709C NMHCIIB treated with 150 nM Tg for 4 hr or **(K)** MEFs pretreated with an actin inhibitor, cytochalasin D, for 30 min prior to treatment with 150 nM Tg for 5 hr. For all, similar results were observed in 2-3 independent experiments. CREB/GAPDH/HSP90, loading controls.

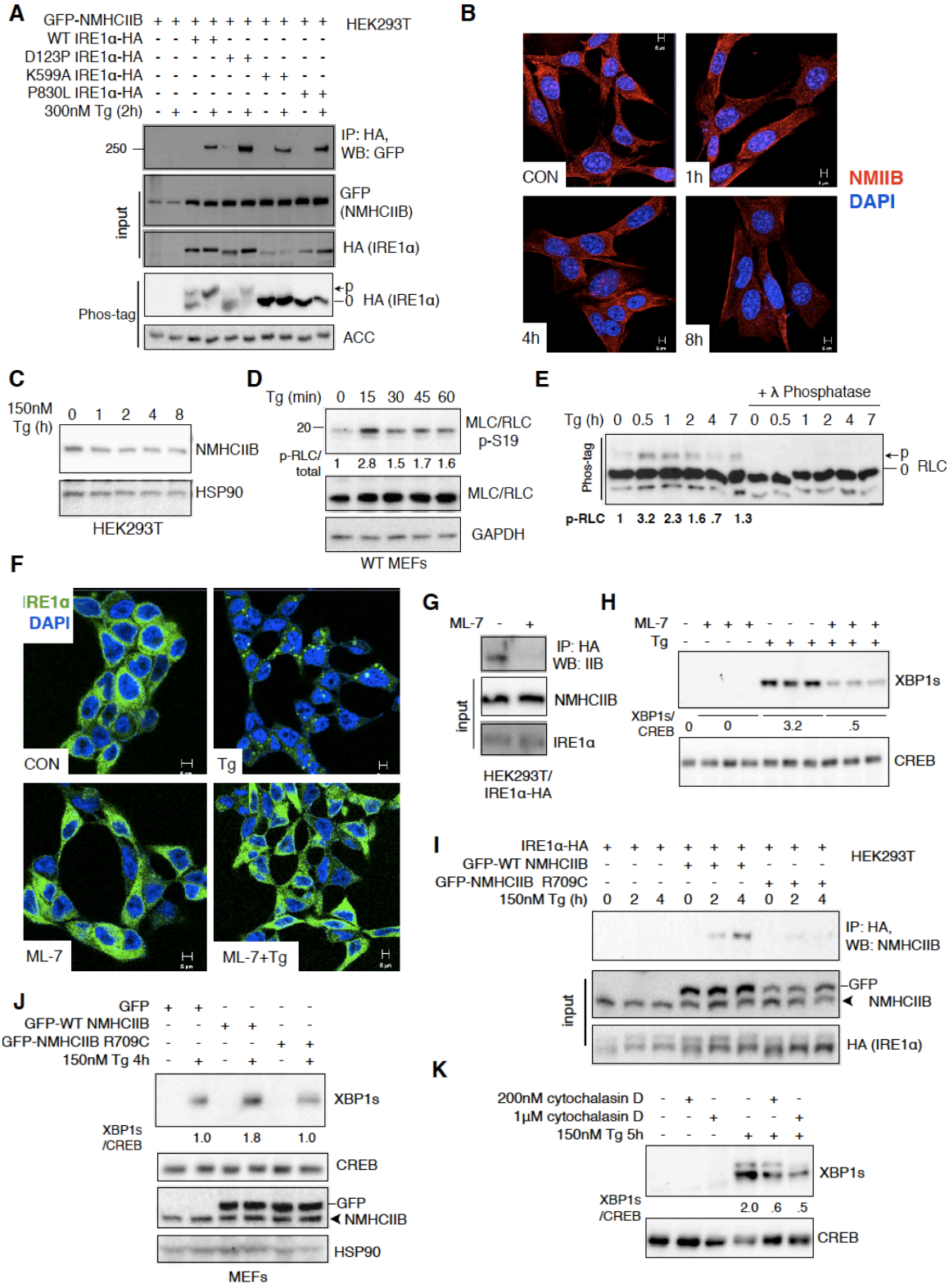
A
GFP-NMHCIIB
WT IRE1α-HA
D123P IRE1α-HA
K599A IRE1α-HA
P830L IRE1α-HA
300nM Tg (2h)
HEK293T
250
IP: HA, WB: GFP
input
GFP (NMHCIIB)
HA (IRE1α)
Phos-tag
p
0
HA (IRE1α)
ACC
B
CON
1h
4h
8h
NMIIB
DAPI
C
150nM Tg (h) 0 1 2 4 8
NMHCIIB
HSP90
HEK293T
D
Tg (min) 0 15 30 45 60
20
MLC/RLC p-S19
p-RLC/ total
1 2.8 1.5 1.7 1.6
MLC/RLC
GAPDH
WT MEFs
E
+ λ Phosphatase
Tg (h) 0 0.5 1 2 4 7 0 0.5 1 2 4 7
Phos-tag
p
0
RLC
p-RLC 1 3.2 2.3 1.6 .7 1.3
F
IRE1α
DAPI
CON
Tg
ML-7
ML-7+Tg
G
ML-7 - +
IP: HA WB: IIB
input
NMHCIIB
IRE1α
HEK293T/ IRE1α-HA
H
ML-7 - + + + - - - + + +
Tg - - - + + + + + +
XBP1s
XBP1s/ CREB 0 0 3.2 .5
CREB
I
IRE1α-HA + + + + + + + + +
GFP-WT NMHCIIB - - - + + + - - -
GFP-NMHCIIB R709C - - - - - - + + +
150nM Tg (h) 0 2 4 0 2 4 0 2 4
HEK293T
IP: HA, WB: NMHCIIB
input
GFP
NMHCIIB
HA (IRE1α)
J
GFP + + - - - -
GFP-WT NMHCIIB - - + + - -
GFP-NMHCIIB R709C - - - - + +
150nM Tg 4h - + - + - +
XBP1s
XBP1s /CREB 1.0 1.8 1.0
CREB
GFP
NMHCIIB
HSP90
MEFs
K
200nM cytochalasin D - + - - + -
1μM cytochalasin D - - + - - +
150nM Tg 5h - - - + + +
XBP1s
XBP1s /CREB 2.0 .6 .5
CREB

3.4.7 NMIIB deficient worms are hypersensitive to ER stress

Lastly, we explored the physiological implications of NMIIB in ER stress response at the organismal level. As NMHCIIB$^{-/-}$ mouse embryos die before birth (Takeda et al., 2003), we turned to the nematode *C. elegans*, in which NMY-2, a protein required for polarity establishment during worm embryogenesis, is a homolog of NMHCIIB (Guo and Kemphues, 1996). We examined the ability of temperature-sensitive NMII mutant worms *nmy-2(ne3409)* (Liu et al., 2010) to reach L4 and adulthood in response to ER stress after shifting to the restrictive temperature following embryogenesis. In the absence of Tm, 99% ± 1% WT and 95% ± 3% *nmy-2(ne3409)* reached L4 or adulthood. However, in the presence of ER stress, a dramatic difference was consistently observed after 72 hr between the percent of WT (85% ± 4%) and *nmy-2(ne3409)* (23% ± 13%) animals that developed to L4 (Fig. 3.7G), suggesting that *nmy-2(ne3409)* worms were hypersensitive to ER stress. This effect was similar to that of a Xbp1 deficiency as previously reported (Henis-Korenblit et al., 2010), though less severe (Fig. 3.7G). At the molecular level, ER stress-dependent induction of *Xbp1s* and its target *hsp-4*, the worm homolog of the ER chaperone GRP78/BiP, was completely abrogated in *nmy-2(ne3409)* (Fig. 3.7H). Together, these in vivo studies reveal a functional and conserved role for NMII specifically in IRE1α signaling.

Figure 3.7. NMIIB deficiency renders cells and worms hypersensitive to ER stress.

(A-C) Flow cytometric analysis of ER/Golgi mass of **(A)** WT and various mutant MEFs or **(C)** NMHCIIB$^{-/-}$ MEFs transfected with WT, R709C NMHCIIB, or XBP1s, followed by treatment with 300 nM Tg for 8 hr and stained with Brefeldin A-BODIPY. Numbers indicate mean channel fluorescence. Western blot analysis of protein levels in transfected cells shown in **(B)** with WT MEFs treated with 150 nM Tg for 3 hr in the far right lane. HSP90 and CREB, loading controls whole-cell extract and nuclear extract, respectively. **(D and E)** Cell survival assays: Quantitative reading of crystal violet staining of WT and NMHCIIB$^{-/-}$ MEFs treated with 150 nM Tg for the indicated time, followed by recovery for 4-5 days. y axis indicates cell or colony numbers. In **(E),** MEFs expressing shCON or shIIB#1, or WT, NMHCIIB$^{-/-}$, and NMHCIIB$^{-/-}$ MEFs rescued with WT or R709C NMHCIIB were used. Data are shown as mean ± SEM. **p<0.01, ***p<0.001. **(F)** Western blot of active and procaspase 3 from WT and NMHCIIB$^{-/-}$ MEFs treated with 150 nM Tg for the indicated time. Quantitation of cleaved caspase 3 levels shown below the gel after normalization to procaspase 3. **(G and H)** WT (N2) or *nmy-2(ne3409)* worms were shifted to 25°C after embryogenesis and grown on 6 μg/ml Tm to assay development at 72 hr. *xbp-1(zc12)* worms were included as controls. Data are shown as mean ± SD ($p = 0.004$ for *nmy-2(ne3409)* versus WT and $p < 0.001$ for *xbp-1(zc12)* versus WT). **(H)** Quantitative real-time PCR analysis of UPR genes in WT (N2) or *nmy-2(ne3409)* worms grown on 6 μg/ml Tm for 72 hr at 25°C. Data are shown as mean ± SEM. **(I)** Model for the role of NMIIB in IRE1α aggregation and signaling. Our data suggest that optimal IRE1α activation and signaling require concerted coordination between the ER and cytoskeleton in the cytosol. Findings from this study are highlighted in red, whereas known activating signals from the ER are in blue. For all, similar results were observed in 2-3 independent experiments

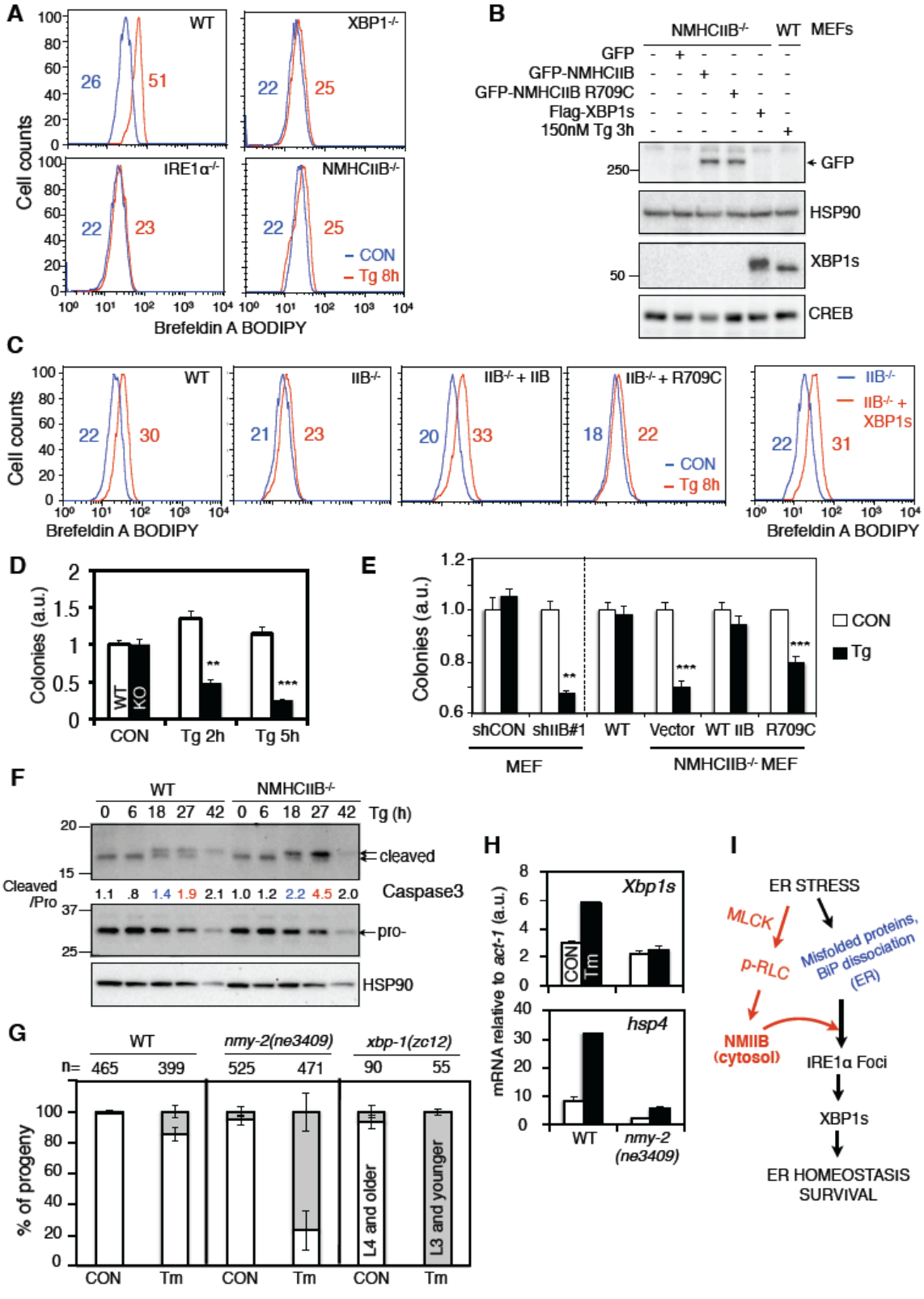
A
WT
XBP1-/-
IRE1α-/-
NMHCIIB-/-
26
51
22
25
22
23
22
25
CON
Tg 8h
Cell counts
Brefeldin A BODIPY
B
NMHCIIB-/-
WT
MEFs
GFP
GFP-NMHCIIB
GFP-NMHCIIB R709C
Flag-XBP1s
150nM Tg 3h
250
GFP
HSP90
50
XBP1s
CREB
C
WT
IIB-/-
IIB-/- + IIB
IIB-/- + R709C
IIB-/- + XBP1s
22
30
21
23
20
33
18
22
22
31
CON
Tg 8h
Cell counts
Brefeldin A BODIPY
Brefeldin A BODIPY
D
Colonies (a.u.)
WT
KO
CON
Tg 2h
Tg 5h
E
Colonies (a.u.)
CON
Tg
shCON
shIIB#1
WT
Vector
WT IIB
R709C
MEF
NMHCIIB-/- MEF
F
WT
NMHCIIB-/-
0 6 18 27 42 0 6 18 27 42 Tg (h)
cleaved
Cleaved /Pro
1.1 .8 1.4 1.9 2.1 1.0 1.2 2.2 4.5 2.0
Caspase3
pro-
HSP90
G
WT
nmy-2(ne3409)
xbp-1(zc12)
n= 465 399 525 471 90 55
% of progeny
L4 and older
L3 and younger
CON
Tm
H
Xbp1s
hsp4
mRNA relative to act-1 (a.u.)
CON
Tm
WT
nmy-2 (ne3409)
I
ER STRESS
MLCK
p-RLC
Misfolded proteins, BiP dissociation (ER)
NMIIB (cytosol)
IRE1α Foci
XBP1s
ER HOMEOSTASIS SURVIVAL

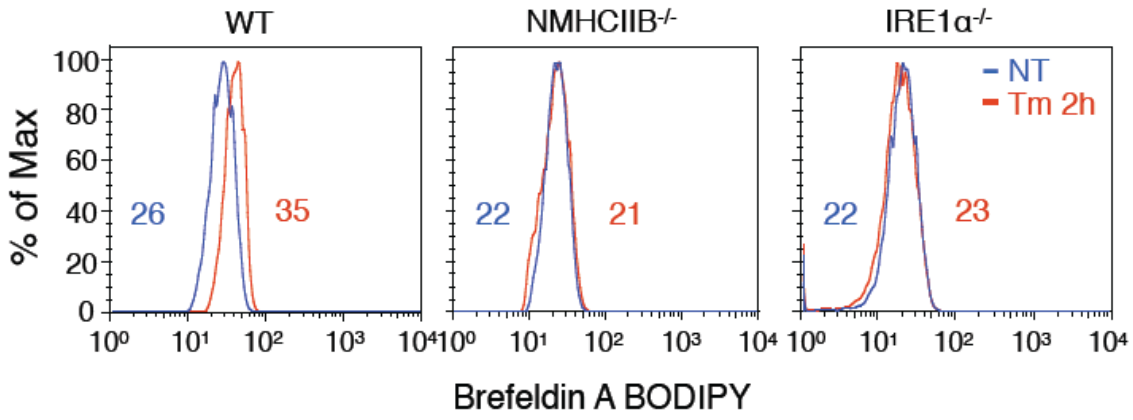

Figure 3.8. NMHCIIB is required for ER stress-induced ER expansion.

Flow cytometric analysis of ER/Golgi mass of WT, NMHCIIB$^{-/-}$ and IRE1α$^{-/-}$ MEFs treated with 5 μg/ml Tm for 2 hr and stained with Brefeldin A-BODIPY. Numbers indicate mean channel fluorescence. Similar results were observed in three independent experiments.

3.5 DISCUSSION

Our study has identified and characterized NMIIB as a specific and essential component of the IRE1α-XBP1 signaling axis of UPR. We propose a model in which ER stress promotes an IRE1α-NMIIB interaction and subsequently, NMIIB facilitates the oligomerization, activation, and signaling of IRE1α (Fig. 3.7I). This model is supported by our findings that NMIIB is required for IRE1α aggregation and foci formation, induction of XBP1s protein and downstream UPR targets, and cellular and organismal responses to ER stress in vivo. The actomyosin contractility of NMIIB is required as both the motor domain and involvement of the actin filament are indispensable.

Our data point to a concerted coordination between the ER and cytoskeleton that is essential for optimal IRE1α activation and cell fate determination in response to ER stress (Fig. 3.7I). Upon ER stress, RLC phosphorylation is required for NMIIB activation and its regulation of IRE1α; these events are at least in part dependent on MLCK. How MLCK or other RLC kinases respond to ER stress remains unclear. An intriguing possibility is that IRE1α itself may serve as a kinase for MLCK directly or indirectly, and thus form a feedback regulatory loop. Although other scenarios, such as NMIIB-mediated *Xbp1* mRNA trafficking or ER membrane reorganization, are exciting possibilities that remain to be explored, our data demonstrate that NMIIB directly impacts IRE1α activation and signaling by interacting with IRE1α and regulating its oligomerization and activation.

A number of studies have identified a repertoire of IRE1α regulatory

cofactors that modulate its activity, including BAX/BAK, Bax inhibitor-1, RACK1, HSP90, and others (Hetz et al., 2011; 2006; Lisbona et al., 2009; Qiu et al., 2010). Collectively, these interacting proteins comprise the ''UPRosome,'' a scaffolding complex believed to dynamically regulate IRE1α in a cell or tissue-specific manner (Hetz et al., 2011; Hetz and Glimcher, 2009). Identification of these regulatory cofactors of IRE1α signaling has greatly advanced our understanding of how IRE1α activity and output can be regulated mechanistically. Unlike other IRE1α-interacting proteins that have been identified, NMIIB is unique in that it is an essential component involved in the oligomerization step of IRE1α activation. Speculatively, NMIIB may not only promote IRE1α aggregation but also recruit other regulatory components to the foci. The interplay between NMIIB and the ''UPRosome'' is an open but exciting question.

Findings from this study and others showed that IRE1α foci can be visualized as early as 1 hr, peaked around 4 hr and are resolved by 8 hr of ER stress (Fig. 3.4C and (Li et al., 2010)). However, questions such as how foci dispersion and deoligomerization are regulated and whether NMIIB or other cytoskeletal proteins are involved in this process remain unaddressed. Interestingly, our data convey that NMIIB activation as indicated by RLC phosphorylation is extremely dynamic and transient, peaking within the first hour and resolved after prolonged ER stress (Figs. 3.6D-E), suggesting an intimate relationship between NMIIB activation and the kinetics of IRE1α foci formation and dispersion. A recent study in yeast reported that the kinase

activity of IRE1α is important for its deactivation and foci dispersion (Rubio et al., 2011). Whether and how NMIIB are linked to the activation and inactivation of IRE1α during ER stress remains to be elucidated, and future studies are warranted to tease out the mechanistic details and dynamics of IRE1α foci formation and dispersion.

IRE1α has been reported to cleave other nonspecific mRNAs upon ER stress in a process termed regulated IRE1-dependent decay (RIDD), presumably to decrease ER load (Han et al., 2009; Hollien and Weissman, 2006; Hollien et al., 2009; So et al., 2012). However, the molecular mechanism and signals by which IRE1α regulates RIDD remain largely unknown. For example, does IRE1α RNase activation depend on the substrate (i.e., *Xbp1* versus RIDD targets) and is IRE1α aggregation a prerequisite for RIDD? As NMIIB regulates IRE1α oligomerization, it will be of great interest to determine whether and how NMIIB regulates IRE1α RIDD activity.

Although IRE1α dimers may possess RNase activity to splice *Xbp1* mRNA, IRE1α oligomers are believed to have maximal splicing efficiency as the arrangement of dimers into oligomers brings multiple *Xbp1* mRNA binding pockets into close proximity (Korennykh et al., 2009; Li et al., 2010; Walter and Ron, 2011). This is supported by our observation that a NMIIB deficiency does not completely abolish XBP1s production. Nonetheless, NMIIB-mediated IRE1α oligomerization is significant as shown by our in vivo data on the cellular and organismal response to ER stress in which NMIIB is essential for initiating and engaging an optimal IRE1α signaling and UPR.

One outstanding question is whether the involvement of NMIIB in IRE1α activation and signaling is relevant in vivo under physiological conditions, where ER stress can be much milder relative to the pharmacological insults used in cell culture to disrupt ER homeostasis (Pfaffenbach et al., 2010; Sha et al., 2011; Yang et al., 2010). Because of the lack of a good antibody for immunostaining, the question of whether endogenous IRE1α forms foci in vivo under physiological UPR remains unanswered. This is important as it will shed light on the activating mechanism of IRE1α under physiological and pathophysiological settings. Overall, our finding linking the IRE1α branch of the UPR and the cytoskeletal machinery of the cell enhances our comprehension of the cellular and molecular basis of mammalian ER stress response and may shed light on therapeutic targets for UPR-associated diseases.

3.6 ACKNOWLEDGEMENTS

We thank Drs. C. Hetz, D. Ron, P. Walter, M. Montminy, L. Glimcher, L. Kraus, F. Hu, A. Bretscher, and V. Vogt for reagents and equipment; A. Bretscher for suggestions; M. Montminy, J.T. Lis, and M.A. Conti for reading of the manuscript; D. Garbett and R. Dick for assistance with sucrose gradient; D. Morton for assistance with *C. elegans* experiments; S. Sun for the drawing of the graphical abstract; and members of the Qi laboratory for technical assistance and discussions. L.Q. is the recipient of the Junior Faculty and Career Development Awards from American Diabetes Association (ADA). This study is supported by the NIH (HL004228 to X.M. and R.S.A.; R01GM079112 to K.K.; P41 GM103533 to J.R.Y.; and R21AA020351 and R01DK082582 to L.Q.) and the ADA (1-12-CD-04 to L.Q.).

I thank Alex Beatty, Diane Morton and the entire Kemphues lab for their assistance with establishing and conducting *C. elegans* experiments. I thank Yewei Ji for help with flow cytometric assays, Cindy Wang for technical assistance and all members of the Qi lab for helpful discussions and comments. I thank Carol Bayles for confocal training.

Tandem mass spectrometry and identification of NMII was performed by X. Han in the Yates Lab. Fig. 3.7G was contributed by A. Beatty in the Kemphues Lab. Figs. 3.7A,C and Fig. 3.8 were assisted by Y. Ji.

CHAPTER 4

GENERAL DISCUSSION AND FUTURE DIRECTIONS

4.1 DISCUSSION AND WORKING MODEL

The overarching aim of this dissertation is to conduct a thorough investigation of the underlying mechanisms regulating mammalian IRE1α activation and signaling as well as to characterize the physiological implications and significance of this pathway. Although the general outcomes of IRE1α activation and signaling and their corresponding sequence of events have been reported and reviewed, a comprehensive understanding of the underlying regulatory mechanisms was incomplete. Each chapter and appendix of this dissertation provides new insight and understanding into the activation, signaling, regulation and physiological function of the IRE1α-XBP1 pathway. In Chapter 2 and Appendix A, we uncover novel functions of IRE1α-XBP1 signaling in regulating two fundamental biological processes: differentiation of pre-adipocytes into mature fat cells (Chapter 2) and ER stress-induced inflammation in macrophages (Appendix A). Both adipogenesis and inflammation activate the IRE1α-XBP1 pathway but in distinct manners. During adipogenesis, IRE1α is phosphorylated and activated at a low basal level as opposed to an overt activation typically observed with ER stress (Chapter 2). This basal level of IRE1α activation is sufficient to efficiently splice *Xbp1u* mRNA and generate XBP1s protein. On the contrary, ER stress-associated inflammation clearly promotes IRE1α phosphorylation and activation (Appendix A). These findings contribute

to and expand the current knowledge of cellular signaling pathways that integrate with UPR and specifically IRE1α. However, the source and type of signals that activate IRE1α during adipogenesis are not clear and it is uncertain whether canonical ER stress signals such as accumulation of misfolded proteins play a role in this process.

In addition to contributing to our basic understanding of the physiological importance of IRE1α-XBP1 signaling, our proteomics-based screen coupled with molecular and functional characterizations greatly enhanced our mechanistic understanding of how IRE1α is regulated. In Chapter 3 and Appendix C, we used tandem mass spectrometry as a screening tool to identify novel IRE1α-interacting proteins. From the screen, NMIIB, a cytoskeleton-associated factor, was identified and shown to exert a conserved functional role essential for IRE1α oligomerization and foci formation (Chapter 3). NMIIB selectively interacts with IRE1α upon ER stress and its motor domain, along with the actin cytoskeleton, coordinately pull IRE1α proteins into higher-order oligomers that efficiently splice *Xbp1* mRNA. Although several IRE1α-interacting factors have been reported thus far and are proposed to comprise the IRE1α interactome (see Chapter 1 and Fig. 1.4), NMIIB is the first interactor identified to regulate IRE1α activation at the step of aggregation and foci formation. In addition to NMIIB, several other factors were also identified from the screen with putative biological roles in mRNA splicing and processing, nucleosome remodeling and nonsense-mediated decay (Appendix C). Interestingly, most of these factors and their interactions with IRE1α were selectively enriched for either control non-stress

conditions or ER stress conditions, suggesting that both positive and negative regulators of IRE1α signaling were identified. Although purely speculative at this point, it is very exciting to note the role of so many of these factors in mRNA processing and maturation given the role of IRE1α RNase activity in splicing *Xbp1u* and RIDD mRNAs, and potentially even microRNAs. All together, these findings expand our current knowledge of the repertoire of the IRE1α interactome and may identify potential factors as drug targets for therapeutic intervention in conformational diseases.

Lastly, in addition to uncovering novel regulatory factors of IRE1α signaling, our mass spectrometry analysis also identified a novel motif on IRE1α protein that may be required to direct its trans-autophosphorylation. Currently, despite efforts to identify targets of IRE1α kinase activity under ER stress, the only known target is itself. Yet descriptions of the exact phosphorylation residues and their importance and contribution to overall mammalian IRE1α activation remain incomplete. Our Phos-tag based Western blots typically reveal one fast-migrating band denoted as the phosphorylated form of IRE1α, suggesting that phosphorylation may not be very extensive [Chapter 3 and (Sha et al., 2009; Yang et al., 2010)]. This is in stark contrast with PERK phosphorylation, which is visualized as a smear on the gel (Qi et al., 2011; Yang et al., 2010). Excitingly, mass spectrometry identified a unique motif on IRE1α protein located on the cytosolic linker region following the transmembrane domain that undergoes extensive phosphorylation upon ER stress. Peptides containing mono-, di- and even tri-phosphorylation were detected on an "SSPS"

motif at amino acid positions 548-551 of human IRE1α protein (977 total amino acids) (Appendix B). To our knowledge, this is the first report of a motif on IRE1α that may be critical in directing its trans-autophosphorylation. However, future studies, in particular mutagenesis assays in which serine residues are mutated to loss-of-function alanine or gain-of-function/phospho-mimetic aspartic acid, are required to understand whether this motif plays a functional role in IRE1α signaling. Also, we are interested in determining the contribution of each serine residue to overall IRE1α phosphorylation and whether phosphorylation at SSPS represents an initiating event that can trigger a rapid cascade of downstream trans-autophosphorylation events. An in vivo knock-in mouse model will be essential in deciphering the physiological significance of this motif.

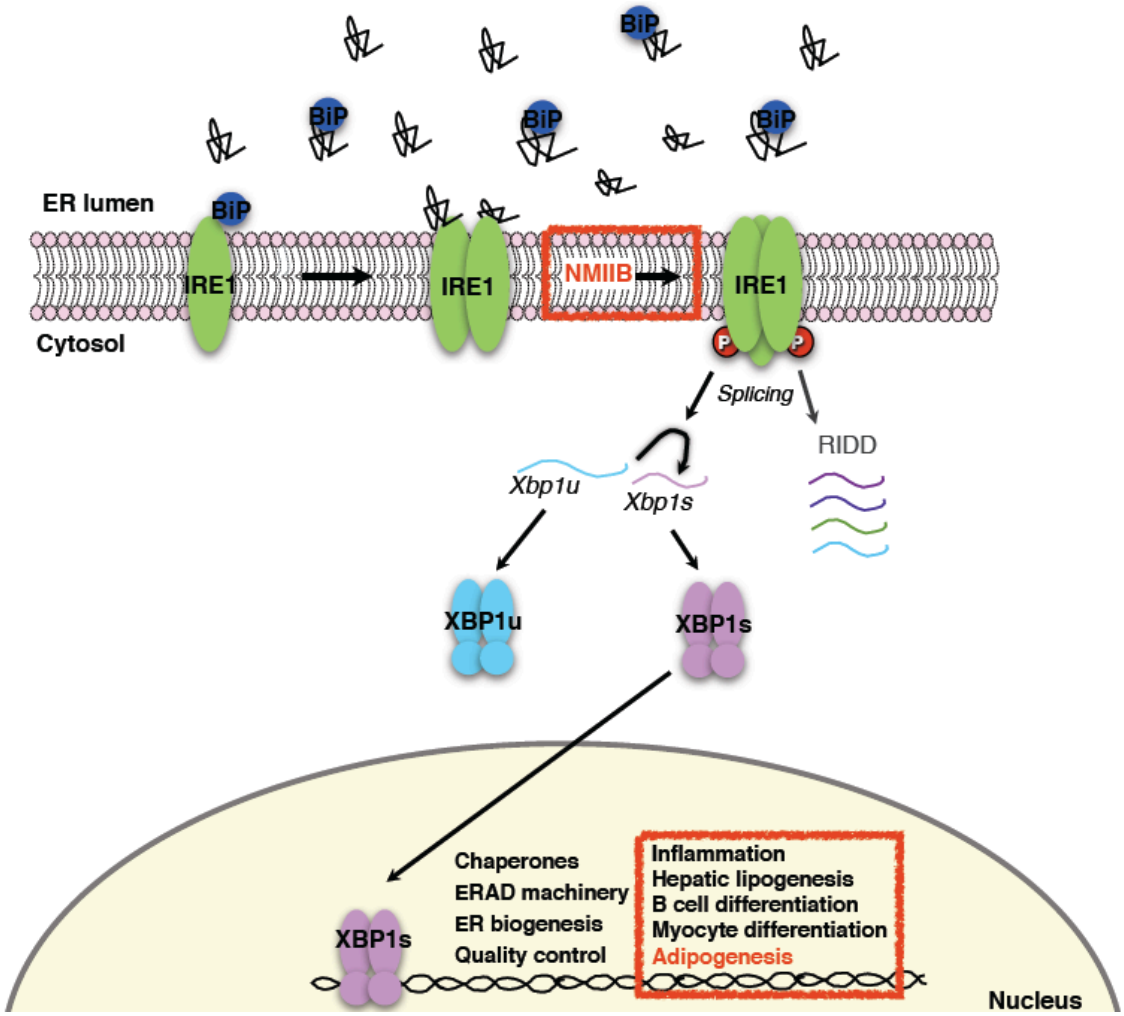

Figure 4.1. Contributions of this dissertation to the field of ER stress.

Under conditions of ER stress, metazoan IRE1α protein undergoes activation at the ER membrane through BiP dissociation and/or direct binding of misfolded proteins. This promotes IRE1α dimerization and trans-autophosphorylation via its cytosolic kinase domain. Further stacking of IRE1α dimers into efficient higher-order oligomers in a process termed foci formation requires a cytoskeleton protein NMIIB (Chapter 3). IRE1α processes and splices *Xbp1* mRNA to produce a critical UPR transcription factor XBP1s. In addition to regulating genes associated with ER homeostasis, XBP1s is also intimately linked to various cellular and physiologically-relevant processes including a key differentiation and developmental event that occurs in fat cells called adipogenesis as described in this dissertation (Chapter 2). Novel contributions from this dissertation are highlighted in red boxes.

4.2 FUTURE DIRECTIONS

Despite the advances and contributions made from this dissertation and the work of others to the field of ER stress and understanding IRE1α activation, many more questions remain in our efforts to characterize mammalian IRE1α signaling and the pathophysiological consequences that arise from its dysfunction. Cell culture models are essential for basic science as they provide researchers a tool to simplify and study complex underlying molecular and physiological networks of an organism at the cellular level. However, the use of animal models is essential to bridge the gap between basic science and translational and clinical research. Thus, the use of in vivo models based on the findings from this dissertation can greatly enhance our understanding of the pathophysiological role of the IRE1α-XBP1 pathway. For example, as IRE1α and UPR have been implicated in metabolic dysfunction, a tissue-specific NMIIB knock-out mouse model administered a high-fat diet (HFD) to induce obesity would provide substantial information on the impact of NMIIB in vivo. Similarly, an adipose-tissue specific knock-out mouse model of IRE1α or XBP1 will offer invaluable insight into the in vivo requirement of either of these UPR components in adipogenesis and the overall contribution of adipose tissue to the general metabolic status and parameters of the animal. Additionally, a knock-in mouse model containing the loss-of-function "AAPA" motif of IRE1α would address whether this motif functions as an in vivo cis regulator of IRE1α phosphorylation and activation.

Studies in the field of ER stress and UPR typically turn to the use of pharmacological agents such as Tg and Tm to induce ER stress. However, even low doses of these chemical agents can cause overt UPR activation concomitant with initiation of apoptosis. Indeed, studies from our lab using Phos-tag gels have shown that MEF cells incubated with 75 nM Tg for only 30 min was sufficient to induce IRE1α phosphorylation (Yang et al., 2010). Alarmingly, reports in the literature typically use a concentration and incubation period of 2 to 6-fold more than our report. Therefore, the question arises as to the relevance of these chemical agents in addressing and understanding UPR associated with pathophysiological conditions such as obesity. As expected, studies have demonstrated that physiological UPR is at times very minor and almost undetectable relative to chemical-induced UPR (Sha et al., 2009). Furthermore, physiological UPR may be reversible and sustainable in the cell for indefinite periods of time without inducing apoptosis, and may even lead to adaptations or a resetting of ER capacity and homeostasis. Therefore, observations arising from the use of pharmacological agents to induce ER stress should be cautiously interpreted. Future studies investigating the role of physiological UPR in various tissues will be essential for gaining a full understanding of the role of UPR in conformational diseases.

Although IRE1α-XBP1 signaling is essential for mounting a proper UPR upon misfolded protein accumulation, this pathway has recently emerged to engage in additional cellular processes including differentiation, metabolism and immunity. Thus, rather than simply acting as an adaptation mechanism against protein folding stress, UPR signaling may serve as a central hub that integrates

various cellular stress and metabolic inputs to determine cell fate. Likewise, others have proposed that UPR resembles a cellular rheostat that acts to fine-tune, integrate, and couple different signals with an appropriate output (Hetz, 2012). As the signals activating IRE1α-XBP1 in metabolism, cellular differentiation and immunity may not be directly associated with the canonical UPR inducing signals (defective protein folding or degradation, accumulation of misfolded proteins, etc.), the future of studying ER stress and UPR activation under pathophysiological conditions lies in identifying the initiating signals and understanding the mechanism by which they act to engage the IRE1α-XBP1 pathway.

Canonical UPR signaling acts on the premise that all three major pathways are activated, albeit to differing degrees corresponding to varying levels of ER stress. However, the studies presented in this dissertation and the work of others have suggested selective activation of UPR branches. First, the three major ER transmembrane sensors may exhibit different sensitivities to various types of ER stress. Changes in ER luminal Ca^{2+} concentrations have been suggested to selectively activate IRE1α and PERK branches more rapidly than ATF6 (DuRose et al., 2006). On the other hand, ATF6 appears to be preferentially activated first in response to alterations in glycosylation and the redox environment (Yoshida et al., 2003). Furthermore, many of the adaptor proteins comprising the IRE1α interactome have been reported to selectively form a complex with IRE1α and not PERK or ATF6 (Hetz, 2012). Indeed, our studies showed a selective interaction and regulation of IRE1α signaling by NMIIB (Chapter 3). Thus, the localization and tissue- or cell type-specific regulated

expression of these interacting factors may inherently act as specific modulators of IRE1α activation and signaling.

In conclusion, studies of IRE1α-XBP1 and UPR regulation are highly relevant to human health and conformational disorders. This dissertation characterized the novel physiological role of IRE1α-XBP1 signaling in fat cell differentiation and identified NMIIB as an essential modulator of IRE1α activation and ER stress response. Future work on understanding the pathophysiological role and contribution of UPR activation and ER stress to conformational diseases will be crucial in therapeutic development. Perhaps targeting NMIIB or using pharmacologic chaperones such as 4-PBA or TUDCA that ameliorate ER stress may prove to be effective treatments for conformational diseases.

APPENDIX A

MACROPHAGE XBP1 MODULATES ER STRESS-DEPENDENT INFLAMMATION THROUGH ATF3

A.1 ABSTRACT

Innate immunity is required for host defense, but dysregulation and prolonged activation can trigger chronic inflammatory diseases including obesity and atherosclerosis. Thus, a comprehensive understanding of the mechanisms underlying the regulation of innate immunity and inflammation is of fundamental and clinical relevance. Our microarray study showed that both lipopolysaccharide (LPS)- and thapsigargin (Tg)-induced activation of the IRE1α-XBP1 pathway in macrophages induced the expression of key pro-inflammatory mediators. However, the transcriptome induced in response to LPS or Tg showed vast differences in their dependency on XBP1 as well as their Gene Ontology-annotated biological functions. Surprisingly, of the genes induced under either condition, both treatments displayed similar percentages of target genes containing predicted XBP1 binding motifs in their proximal promoter regions. Mechanistically, XBP1 may modulate inflammatory gene expression through ATF3, a key regulator of inflammation. Loss of XBP1 in macrophages drastically attenuated *Atf3* expression and XBP1s overexpression transactivated an ATF3 promoter-construct. In conclusion, XBP1-mediated regulation of crucial inflammatory mediators upon ER stress may occur through modulation of ATF3.

A.2 INTRODUCTION

The innate immune system, of which inflammation comprises one of the earliest defenses, is a non-specific response that provides immediate protection against infection. This surveillance system recognizes conserved microbial structural motifs called pathogen-associated molecular patterns (PAMPs) through pattern recognition receptors, such as Toll-like receptors (TLRs) expressed on the surfaces of cells that respond immediately to infection including neutrophils, macrophages and dendritic cells (Gordon, 2002). A classic example of a PAMP is lipopolysaccharide (LPS) derived from the outer membrane of Gram-negative bacteria. Upon activation by PAMPs, TLR-mediated signaling primarily promotes the nuclear translocation of nuclear factor kappa-light-chain-enhancer of activated B cells (NF-κB) and downstream activation and secretion of pro-inflammatory cytokines including interleukin-1 (IL-1), IL-6, IL-12, and tumor necrosis factor-α (TNF-α) (Armant and Fenton, 2002; Hu et al., 2008; Medzhitov and Horng, 2009; Moynagh, 2005). Despite the vital role of the innate immune system as a sentinel in protecting the cell, a comprehensive understanding of the regulatory mechanisms governing inflammation as well as the interplay with other stress signaling pathways such as UPR remain largely uncharacterized.

Unfolded protein response (UPR) is an evolutionarily conserved quality-control mechanism activated by the accumulation of misfolded proteins in the endoplasmic reticulum (ER). Of the three primary ER-to-nucleus signaling pathways, the IRE1α-XBP1 branch is the most conserved (Calfon et al., 2002). Upon ER stress, ER-resident transmembrane protein inositol-requiring enzyme

1α (IRE1α) undergoes trans-autophosphorylation, leading to activation of its cytosolic RNAse domain. In turn, the RNAse domain splices 26 nucleotides from the mRNA of X-box binding protein 1 (*Xbp1*) to generate XBP1 spliced (XBP1s) (Lee et al., 2002; Yoshida et al., 2001). In contrast to XBP1u (unspliced), the XBP1s protein product is stable and contains a transactivation domain, allowing it to function as a potent basic leucine zipper (b-ZIP) transcription factor (Tirosh et al., 2006). XBP1s translocates to the nucleus and induces the expression of target genes not only involved in restoring ER homeostasis, but in many fundamental cellular processes as well including adipogenesis, myocyte differentiation and B cell maturation (Acosta-Alvear et al., 2007; Hetz et al., 2011; Iwakoshi et al., 2003; Lee et al., 2003a; Reimold et al., 2001; Sha et al., 2009).

The link between UPR and immunity has only been recently explored. In animal studies, XBP1 has been demonstrated to be essential for both the development of B-lymphocytes into plasma cells and the survival and function of dendritic cells (Iwakoshi et al., 2007; Reimold et al., 2001). Additionally, XBP1 was initially identified and named for its role in binding to the X-box motif found in the promoters of many human MHC class II genes (Liou et al., 1990). More recently, a link between UPR and immunity was established when the regulation of a gene involved in innate immunity and inflammation, *hepcidin*, was shown to be UPR-dependent (Vecchi et al., 2009). Finally, several recent reports have also alluded to a potential link between UPR and inflammation. First, the IRE1α pathway is correlated with phosphorylation of c-Jun N-terminal kinases (JNK) under inflammatory physiological conditions such as obesity (Ozcan et al., 2004). Moreover, another UPR signaling pathway mediated by

pancreatic ER kinase (PERK) was implicated in extracellular signal-regulated kinase-1/2 (ERK1/2) activation and pro-inflammatory IL-6 induction (Urano et al., 2000).

Most relevant to this study are two recent publications examining the interplay between IRE1α-XBP1 signaling and inflammatory responses. During *C. elegans* development, XBP1 was induced by innate immunity pathways and required for protection against microbes (Richardson et al., 2010). Additionally, lipopolysaccharide (LPS)-induced inflammation was shown to activate IRE1α-XBP1 signaling in macrophages and was essential for pro-inflammatory cytokine secretion (Martinon et al., 2010). Despite these advances in the field, precise characterization of the relationship between UPR activation and inflammatory gene expression as well as the role of canonical ER stress-induced activation of IRE1α-XBP1 in immune cells remain unknown.

Activating transcription factor 3 (ATF3) is a b-ZIP transcription factor that binds to CRE-like consensus sequences and can homo- or hetero-dimerize with other transcription factors to allow for specificity in modulating gene expression (Hai and Hartman, 2001; Hai et al., 1989). Whether ATF3 acts as a positive or negative transcriptional regulator may be dependent on its co-factor interactions (Hai et al., 1999). However, in immune cells, the dominant role of ATF3 has been as a repressor of gene expression. Indeed, ATF3 has been shown to regulate the expression of many LPS-responsive inflammatory genes including IL1β, IL-6, IL-12, TNFα, and CCL4 (MIP1β) (Gilchrist et al., 2006; Hai et al., 2010; Suganami et al., 2009; Whitmore et al., 2007; Zmuda et al., 2010). Due to its role in integrating various stress inputs with downstream responses, ATF3 has often been dubbed

as a hub in governing immune responses including inflammation. Indeed, ATF3 expression is highly stress-inducible and has been shown to be up-regulated in response to ER stress in various cell types and may serve broad functions associated with apoptosis and PERK downstream signaling (Jiang et al., 2004; Wang et al., 2009a; Zhang et al., 2001). However, the relationship between IRE1α signaling and ATF3 expression is not known. A thorough examination of the contribution of canonical ER stress and IRE1α-XBP1 activation to inflammation is critical for a comprehensive understanding of immune regulation and will permit for the manipulation of this pathway in inflammatory disease-associated drug interventions.

A.3 MATERIALS AND METHODS

Cell lines and drug treatment

HEK293T cells and RAW264.7 macrophages were maintained in DMEM supplemented with 10% FBS (Hyclone) and 1% penicillin/streptomycin (Cellgro). For passaging, RAW264.7 macrophages were washed once with PBS, trypsinized and gently scraped with a cell scraper (Corning Costar). Tg was purchased from EMD Calbiochem and LPS from Sigma.

Retroviral transduction and stable cell line generation

Phoenix cells were transfected with the plasmids encoding the gene of interest in pSuper or pBabe vectors and VSVG at 2:1 ratio for 16 hr, and then replaced with fresh culture media. Following 48 hr culture, media containing retroviruses were harvested and used to transduce RAW264.7 macrophages in the presence of 5

μg/ml polybrene (Sigma) for 24 hr. Stable cell lines were selected in the presence of 2 μg/ml puromycin (Sigma). Typically, puromycin-resistant cell lines developed in 6 days.

shRNA knockdown

pSuper/U6/retro (gift from Lee Kraus, UTSW) was used. Control RNAi was against the firefly luciferase gene. shRNA targeting sequences were designed using Dharmacon and specific for mouse XBP1 (GGATTCATGAATGGCCCTTA) at position nucleotide 1558-1577 at 3′ UTR.

Nuclear-cytosolic fractionation

Cells in a 6 cm dish were resuspended in 200 μl ice-cold hypotonic buffer (10 mM HEPES pH 7.9, 10 mM KCl, 0.1 mM EDTA, 0.1 mM EGTA, and 1 mM DT) and allowed to swell on ice for 15 min followed by addition of 10% NP-40 to a final concentration of 0.6%. Lysates were vortexed vigorously for 15 s prior to centrifugation. Supernatant was transferred to a fresh tube as the cytosolic fraction. Pellets were resuspended in 30-50 μl ice-cold high-salt buffer (20 mM HEPES pH 7.9, 0.4 M NaCl, 1 mM EDTA, 1 mM EGTA, and 1 mM DTT) and vortexed vigorously for 15 s every 5 min for a total of 25 min. Extracts were centrifuged at 4°C for 5 min and supernatant was collected as the nuclear fraction.

Western blot

Western blot was performed using 20-30-μg of total cell lysate or 10-15 μg nuclear extracts. Antibodies used in this study: XBP1 (rabbit, 1:1000, Santa Cruz), CREB (rabbit, 1:5000), ATF3 (rabbit, 1:500, Santa Cruz), and goat anti-rabbit IgG (1:5000, Jackson ImmunoResearch).

Phos-tag gels

Phos-tag gel was carried out in the same manner as regular Western blots except that 50 μM Phos-tag (NARD Institute) and 50 μM $MnCl_2$ (Sigma) were incorporated into 5% SDS-PAGE gels. Also, gels were soaked in 1 mM EDTA for 10 min prior to transfer onto a PVDF membrane.

Immunoprecipitation

Whole cell lysate was harvested in lysis buffer (150 mM NaCl, 1% Triton X-100, 1 mM EDTA, and 50 mM Tris HCl pH 7.5) supplemented with protease inhibitor cocktail (Sigma) and incubated on ice for 25 min. Samples were sonicated 10 s with Branson Digital 250 Cell Disruptor at amplitude 10%. Immune complexes were recovered with HA-agarose beads overnight at 4°C with rocking. Beads were washed three times with wash buffer (20 mM Tris HCl pH 7.5, 137 mM NaCl, 20 mM EDTA, 1% Triton X-100, and 10% glycerol), eluted in boiling 2X SDS sample buffer followed by SDS-PAGE and Western blot.

RNA extraction and qPCR

Total RNA was extracted using Trizol per supplier's protocol (Molecular Research Center) and reverse transcribed using Superscript III kit (Invitrogen). cDNA were analyzed using the Power SYBR Green PCR kit on the ABI PRISM 7900HT-QPCR machine (Applied Biosystems) or the SYBR Green PCR system on the iQ5 or Cfx384 Q-PCR machine (Bio-Rad). All data were normalized to the *l32* ribosomal gene. qPCR primers are listed below.

Atf3	Forward: 5′ GAGGATTTTGCTAACCTGACACC 3′ Reverse: 5′ TTGACGGTAACTGACTCCAGC 3′
***Xbp1* total**	Forward: 5′ ACATCTTCCCATGGACTCTG 3′ Reverse: 5′ TAGGTCCTTCTGGGTAGACC 3′
Xbp1s	Forward: 5′ GAGTCCGCAGCAGGTG 3′ Reverse: GTGTCAGAGTCCATGGGA 3′

Microarry analysis

RNA was extracted as described above and RNA quality was verified on an Agilent 2100 Bioanalyzer (Agilent Technologies, Amsterdam, The Netherlands) using 6000 Nano Chips according to supplier's protocol. 100 ng of RNA was used for Whole Transcript cDNA synthesis (Affymetrix, Santa Clara, CA). Hybridization, washing, and scanning of Affymetrix GeneChip Mouse Gene 1.0 ST Arrays were carried out according to standard Affymetrix protocols. Scans of the Affymetrix arrays were processed using packages from the Bioconductor project. Arrays were normalized using the Robust Multi-array Average method (Bolstad et al., 2003; Irizarry et al., 2003). Changes in gene expression were calculated as signal log ratios between treatment and control. These ratios were

used to create heatmaps within Excel. Affymetrix GeneChip analysis was carried out on WT and XBP1-knockdown RAW264.7 macrophages incubated with thapsigargin (Tg, 300 nM) for 2 hr or lipopolysaccharide (LPS, 10 ng/mL) for 2 hr.

Gene ontology (GO analysis)

The complete list of genes induced/up-regulated in response to Tg or LPS incubation in RAW264.7 macrophages was analyzed against a background of all *Mus musculus* genes using the Gene Ontology AmiGO tool (http://amigo.geneontology.org/).

Luciferase reporter assay

Following overnight transfection, cells were lysed in extraction buffer (Gly-Gly buffer, 1% Triton X-100, and 1 mM DTT) and 50 µl lysates were transferred to a 96-well plate containing equal volume of assay mix (Gly-Gly buffer, 16 mM K_2HPO_4, 2 mM DTT, and 2.5 mM ATP). 100 µl of 0.4 mM luciferin mix was added to each well through an injector and readings were collected using the Synergy 2 plate reader (Biotek). Luciferase activity was normalized to activity from co-transfected Rous sarcoma virus-β-galactosidase expression plasmid.

A.4 RESULTS AND DISCUSSION

Lipopolysaccharide (LPS)-induced inflammation activates UPR

A recent study by Martinon and colleagues showed that LPS-induced TLR2/4 signaling in macrophages specifically activated the IRE1α-XBP1 signaling pathway, which in turn was required for mounting an appropriate response to inflammation by regulating the production and secretion of a subset of pro-inflammatory cytokines (Martinon et al., 2010). Interestingly, LPS-induced activation of IRE1α-XBP1 in macrophages did not affect the expression of canonical UPR target genes. Rather, the production and secretion of select pro-inflammatory cytokines including IL-6, TNF and IFN-β required XBP1. Biologically, an XBP1 deficiency rendered macrophages more susceptible to bacterial infections by *F. tularensis* (Martinon et al., 2010). However, the role of canonical ER stress and IRE1α-XBP1 signaling in macrophages was not addressed. Hence, our study aimed to understand the relationship between classical activation of IRE1α-XBP1 signaling and inflammation in macrophages.

First, to compare the activation status of the IRE1α-XBP1 pathway by classical ER stress and LPS, we treated RAW264.7, a well-established macrophage cell line, with 10 ng/ml LPS to induce TLR2/4-associated inflammation and 300 nM thapsigargin (Tg) to induce canonical ER stress. As expected and consistent with Martinon et al.'s study, RAW264.7 macrophages incubated with both LPS and Tg displayed an increase in IRE1α phosphorylation as visualized by the Phos-tag Western blot system (Fig. A.1A). Notably, LPS-induced phosphorylation of IRE1α was not as extensive as canonical ER stress.

Consistently, both Tg and LPS incubation induced *Xbp1s* mRNA (Fig. A.1B) and protein levels (Fig. A.1C). Similar to IRE1α phosphorylation, XBP1s protein induction by LPS was not as pronounced as that in response to ER stress (Fig. A.1C). Thereby, IRE1α-XBP1 signaling in macrophages is responsive to and activated by both inflammation and canonical ER stress.

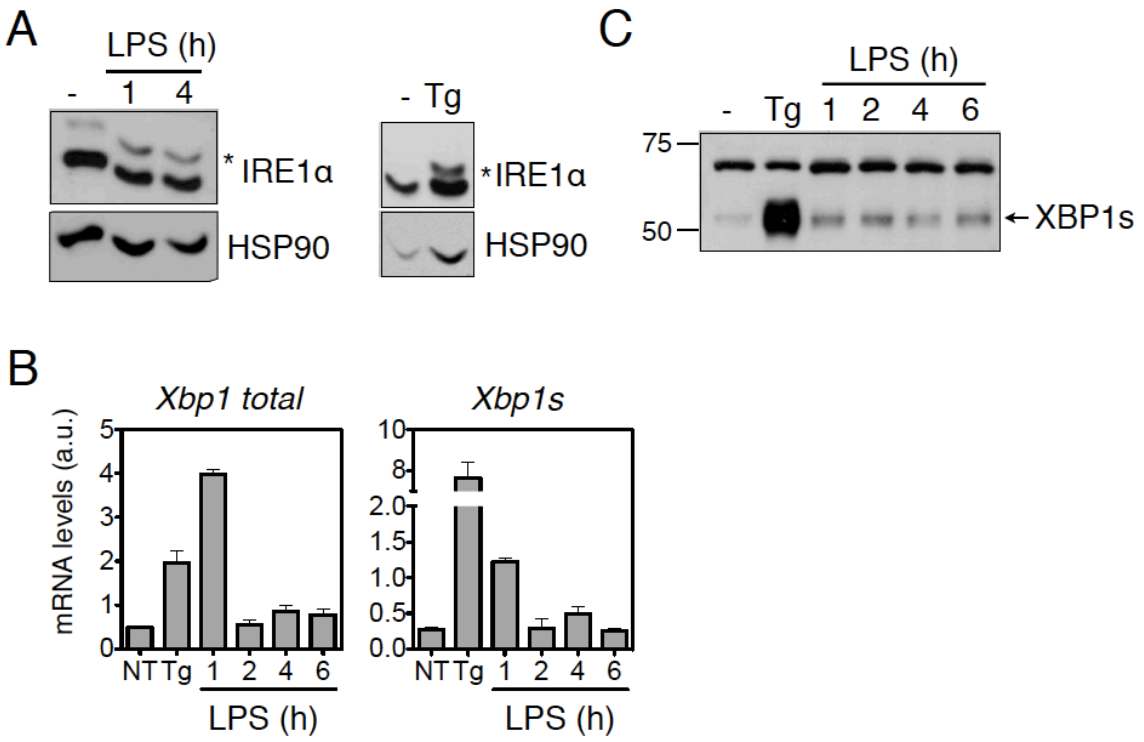

Figure A.1. LPS-associated inflammation activates the IRE1α-XBP1 pathway. **(A)** Phos-tag Western blot of RAW264.7 macrophages treated with 10 ng/ml LPS for indicated time or 300 nM Tg for 2 hr. *, phosphorylated IRE1α. HSP90, loading and positional control. **(B)** qPCR analysis of *Xbp1* total and *Xbp1s* mRNA expression in RAW264.7 macrophages treated with 300 nM Tg for 2 hr or 10 ng/ml LPS for the indicated time. All expression was normalized to the ribosomal *l32* gene. **(C)** Immunoblot of XBP1s protein from nuclear extracts harvested from RAW264.7 macrophages incubated with 300 nM Tg for 2 hr or 10 ng/ml LPS for the indicated time.

Canonical ER stress promotes inflammatory gene induction in macrophages

As both canonical ER stress and LPS can activate IRE1α-XBP1 signaling, we sought to examine the downstream effects by analyzing changes in the macrophage transcriptome. Microarray analysis was performed in collaboration with Dr. Sander Kersten's lab at Wageningen University on RAW264.7 cells treated with 300 nM Tg or 10 ng/ml LPS for 2 hr. LPS incubation induced the expression of over 300 genes and Tg treatment induced the expression of 210 genes (Fig. A.2A). Of the genes induced in response to either treatment, Tg and LPS shared 155 transcripts, indicative of a correlation between ER stress and inflammation (Fig. A.2A). Interestingly, when the dataset was sorted by the top 10 genes with the greatest induction, both ER stress and LPS treatment promoted the expression of key inflammatory mediators including *Il23a, Il1b* and *Il1a* (Fig. A.2B), which were validated by qPCR analysis (Fig. A.2C). We had previously anticipated that canonical ER stress would have the greatest impact on classical UPR target genes such as chaperones and degradation components. However, this data suggested a macrophage cell-type specificity in that canonical ER stress regulated the expression of pro-inflammatory cytokines. Thus, our transcriptomics data in macrophages showed that in response to both ER stress and LPS, a subset of inflammatory genes were highly induced, suggesting cross-talk between canonical ER stress activation and inflammation.

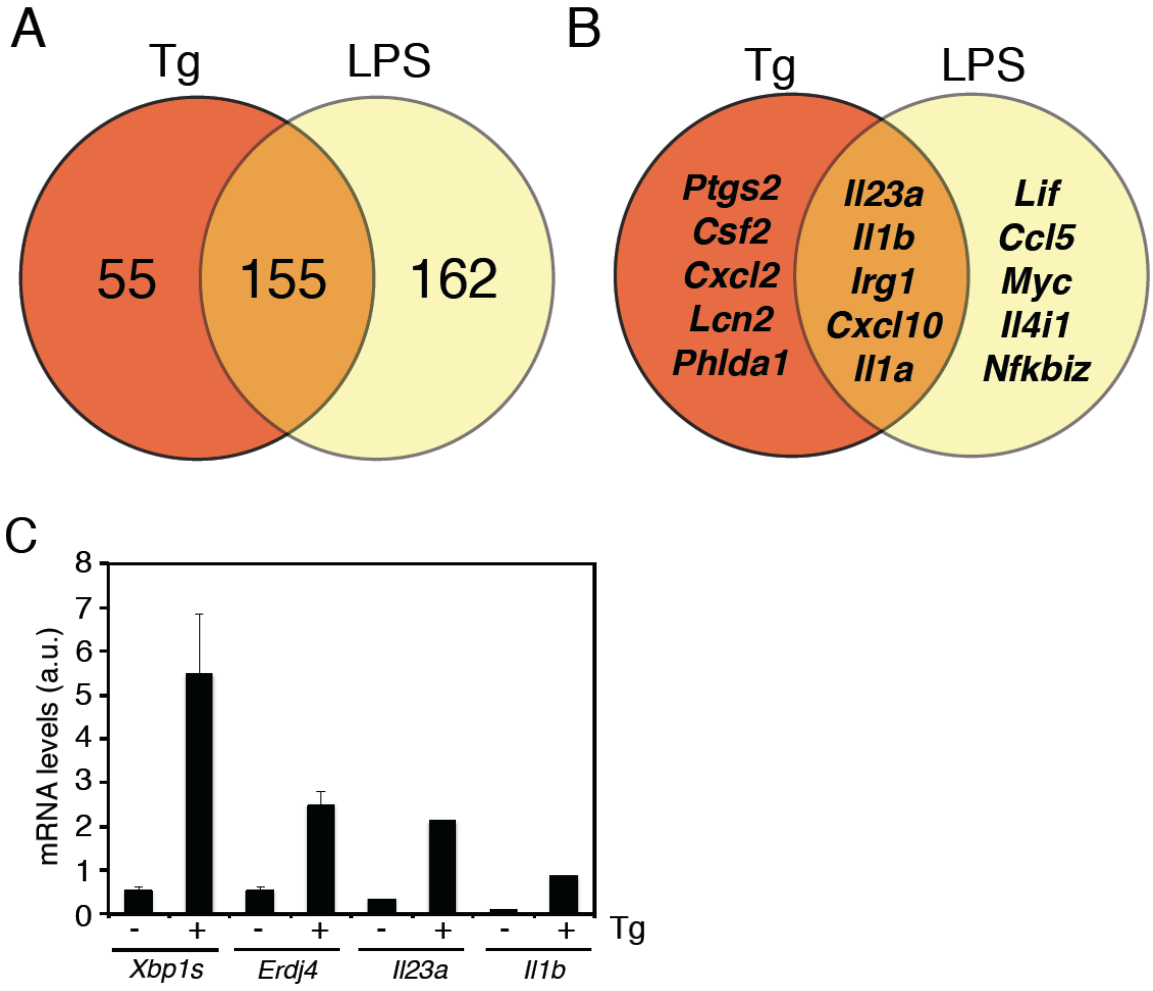

Figure A.2. Microarray of RAW264.7 macrophages in response to ER stress.
RAW264.7 cells treated with ER stress (Tg) or LPS, a known potent inducer of TLR2/4-associated inflammation, were subjected to microarray analysis. **(A)** Tg induced the expression of 210 genes and LPS induced 317 genes. However, there were 155 genes shared between the two treatments, suggesting a link between ER stress and inflammation. **(B)** Venn diagram depicting the top 10 genes induced upon Tg or LPS treatment and the transcripts shared between the two treatments. Interestingly, Tg and LPS treatment have 5 of the 10 genes in common and Tg up-regulates key inflammatory mediators, further reinforcing the model that ER stress promotes inflammation in macrophages. **(C)** qPCR analysis of RAW264.7 macrophages treated with 300 nM Tg for 2 hr. Tg strongly and expectedly induced the expression of *Xbp1s* and *Erdj4*, a canonical UPR target gene. In validation of the microarray, both *Il23a* and *Il1b* mRNA levels were induced by ER stress.

ER stress-associated inflammation in macrophages is dependent on XBP1

To determine the molecular mechanism underlying these transcriptional changes, we generated RAW264.7 cells stably expressing an shRNA targeting the 3' UTR of *Xbp1*, which resulted in a successful and potent knock-down of both *Xbp1* total and *Xbp1s* mRNA levels (Fig. A.3A) as well as XBP1s protein levels (Fig. A.3B). Microarray analysis in collaboration with the Kersten Lab (Wageningen University) was performed on both wild-type (CONi) and macrophages deficient for XBP1 (XBP1i). Surprisingly, of the 210 genes induced by ER stress (Fig. A.2A), approximately 90% of the induction was dependent on XBP1 (Fig. A.4). However, for LPS treatment, only 20% of the up-regulated genes showed XBP1 dependency (Fig. A.4), suggesting that although both conditions activated IRE1α-XBP1 signaling, modulation of inflammatory genes by LPS primarily occurred through mechanisms independent of XBP1. Indeed, a closer examination of the top 10 genes induced in response to canonical ER stress clearly illustrated a high XBP1 dependency that was almost completely absent with LPS treatment (Fig. A.5A). Furthermore, a comparison of the changes in expression of the top 10 genes in control (CONi) and XBP1-deficient macrophages (XBP1i) supported a role for XBP1 as a transcriptional activator (Fig. A.5A) consistent with its function in regulating canonical UPR genes. However, microarray analysis of a different cell type, 3T3-L1 pre-adipocytes, by Haibo Sha in collaboration with the Kersten Lab also showed strong XBP1 dependency, but in this case, XBP1 deficiency resulted in an up-regulation of inflammatory genes, suggesting a role for XBP1 as a repressor (Fig. A.5B).

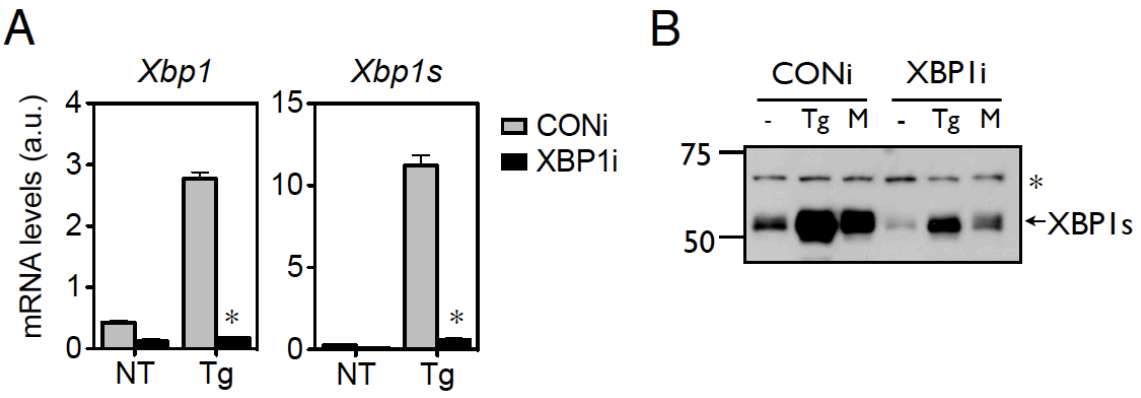

Figure A.3. Efficient knock-down of XBP1 in RAW264.7 macrophages.
(A) qPCR analysis of the transcript levels of *Xbp1* total and the active spliced form *Xbp1s* in response to Tg in control macrophages (CONi) and RAW264.7 macrophages expressing an shRNA against *Xbp1* to mediate knockdown (XBP1i). Xbp1 mRNA levels are dramatically attenuated in response to ER stress. * $p < 0.05$. **(B)** Western blot analysis of XBP1s protein levels in CONi and XBP1i macrophages in response to Tg and the proteasome inhibitor MG132 (M). Consistent with the mRNA levels, XBP1s protein is greatly reduced in response to Tg in XBP1i cells. * denotes non-specific band.

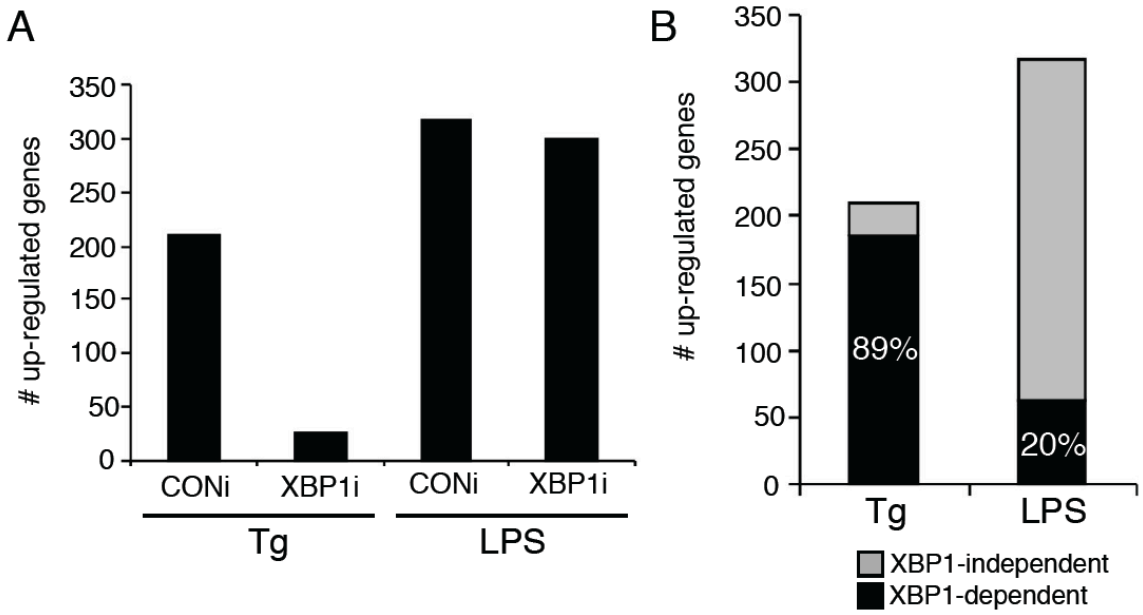

Figure A.4. XBP1 dependency profile of genes induced in response to Tg or LPS.

(A) Genes induced in response to Tg or LPS in macrophages were examined for their dependency on XBP1 by comparing the gene induction profiles of WT (CONi) and XBP1-depleted (XBP1i) RAW264.7 cells. Although Tg and LPS shared many up-regulated genes, their XBP1 dependency profiles were very different as the vast majority of Tg-induced genes were dependent on XBP1 (89%) whereas the majority of LPS-induced genes were XBP1 independent (80%). **(B)** Bar graph representation of data in **(A)** showing XBP1-dependency.

Figure A.5. Canonical ER stress-induced inflammatory mediators are XBP1-dependent.

(A) Our microarray data showed that the top 10 genes induced in response to classical ER stress (Tg) in RAW264.7 macrophages were highly dependent on XBP1. In contrast, although these genes were also up-regulated by LPS to varying degrees, XBP1-deficient macrophages (XBP1i) retained the ability to induce the majority of them, suggesting XBP1-independent transcriptional regulation in response to LPS. Data was normalized to the non-treated conditions. **(B)** Heat map representation of a microarray performed in our lab on 3T3-L1 pre-adipocytes by Haibo Sha demonstrated XBP1 to be a negative regulator of inflammatory genes, supporting the notion of cell-specificity transcriptional regulation.

A

	Tg (300 nM, 2 hr)			LPS (10 ng/ml, 2hr)		
Gene	CONi	XBP1i	CONi/XBP1i	CONi	XBP1i	CONi/XBP1i
Il23a	42.03	1.71	24.55	55.24	64.12	0.86
Il1b	39.46	1.09	36.13	92.87	68.97	1.35
Il1a	32.06	0.93	34.45	33.65	38.47	0.87
Ptgs2	28.69	1.96	14.65	26.95	11.27	2.39
Irg1	28.01	1.85	15.11	48.83	105.08	0.46
Csf2	24.56	0.78	31.55	14.74	28.09	0.52
Cxcl2	23.74	1.19	19.98	25.66	33.89	0.76
Lcn2	18.30	1.49	12.32	8.87	11.02	0.81
Cxcl10	16.90	1.25	13.48	108.96	88.53	1.23
Phlda1	15.12	1.50	10.11	18.13	25.88	0.70

B

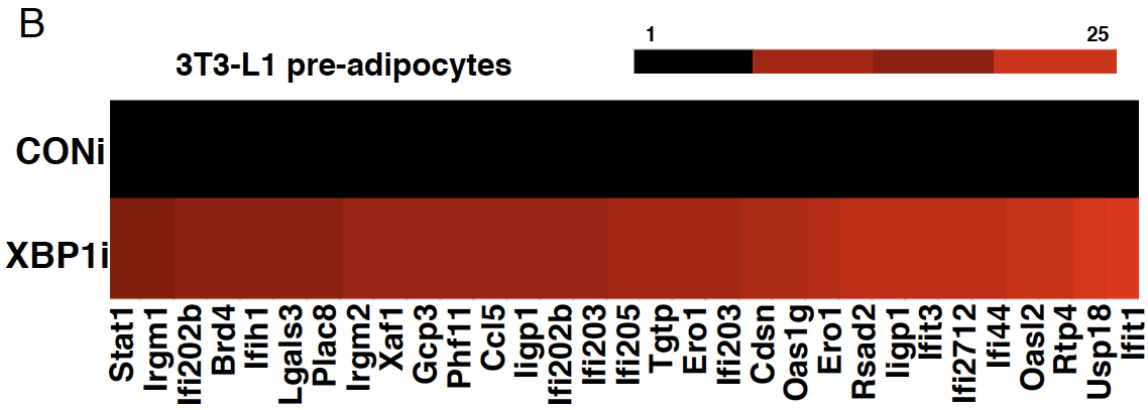

Next, to gain a deeper and more global view of the role of macrophage XBP1 in modulating gene expression, we queried whether specific functional categories of induced genes were enriched in either dataset. For Gene Ontology (GO) analysis, we turned to the AmiGO tool (Carbon et al., 2009) in collaboration with Dr. Huifeng Jiang in the Gu lab. GO analysis illustrated that XBP1-dependent gene induction in response to Tg was significantly enriched in genes related to inflammatory response, apoptosis and regulation of cell proliferation (Fig. A.6A). However, when the dataset was filtered for XBP1-dependent gene induction in response to LPS, the only two statistically significant GO categories that were enriched were T cell activation and immune system process (Fig. A.6B). This observation further reinforced the notion that inflammation in response to canonical ER stress may be mechanistically distinct from that of LPS –TLR 2/4-mediated inflammation.

As a transcription factor, XBP1 binds to the promoters of target genes containing a CRE site with an "ACGT" core consensus motif (Acosta-Alvear et al., 2007; Clauss et al., 1996). Because our data showed a huge discrepancy in the XBP1 dependency of Tg and LPS-regulated genes, we speculated that this may be due to the presence and/or distribution of XBP1 binding motifs in the promoter regions of target genes. In conjunction with Dr. Huifeng Jiang in the Gu Lab, we performed an analysis examining XBP1 binding site occupancy in the proximal promoter regions (-2000 to +200 bp relative to the transcription start site, TSS) of all genes induced in response to Tg or LPS treatment. As our search term, we used the XBP1 binding motif [T/C][G/C]ACGTG[G/T] containing the core ACGT element (underlined). The background frequency of encountering an XBP1 motif in the genome is approximately 11%. Interestingly, both Tg and LPS-

dependent genes had a significant increase in the frequency of XBP1 motif in their promoters, 15% and 14%, respectively (*p*-values for both = 0.02) (Fig. A.7). To gain additional insight into the position of the binding motif, we mapped it to the promoters of target genes (Fig. A.8). As expected for transcription factor binding, both Tg and LPS treatments showed a peak of motif enrichment around the TSS. However, the motif enrichment pattern for Tg and LPS were clearly different. Genes up-regulated in response to Tg showed a much broader peak around the TSS from +200 to -500 bp, but with no XBP1 binding motif at the TSS whereas LPS treatment displayed a much sharper peak centered at -100 bp (Fig. A.8). Furthermore, XBP1 binding motifs in Tg-induced genes revealed a more punctuated pattern containing peaks and valleys and in which the peaks were separated by regions of zero binding motif. This is in contrast with LPS-dependent genes that showed a more regular and steady motif enrichment throughout the entire proximal promoter region (Fig. A.8). From these promoter studies examining XBP1 binding site enrichment, we learned that despite large differences in the number of XBP1-dependent genes induced upon Tg or LPS, this discrepancy was unlikely to be attributed to a lack of XBP1 binding motifs in LPS-regulated genes. Hence, our data suggested that perhaps not all XBP1 binding motifs were occupied by XBP1. Rather, XBP1 recruitment to its binding site was being mediated through various interactions with different co-factors whose expression and regulation themselves may depend on diverse signals (i.e. Tg vs. LPS). Furthermore, the XBP1 binding motif used in our analysis was relatively short. As reported, XBP1 recognized and was bound to other motifs including the UPR element (UPRE) and a CCACG box, which may serve as additional *cis* regulators of XBP1 recruitment (Acosta-Alvear et al., 2007).

Figure A.6. GO enrichment of XBP1-dependent genes up-regulated in response to Tg or LPS in RAW264.7 cells.

Each of the categories listed were significantly enriched with a p-value listed next to the bars. The length of the bars determine the % cluster frequency. The most highly enriched biological processes that are XBP1-dependent upon Tg **(A)** are inflammatory response, apoptosis and regulation of multicellular organismal process. In contrast to XBP1-dependent gene induction in response to ER stress, LPS treatment **(B)** was only enriched for 2 biological processes: T cell activation and immune system process.

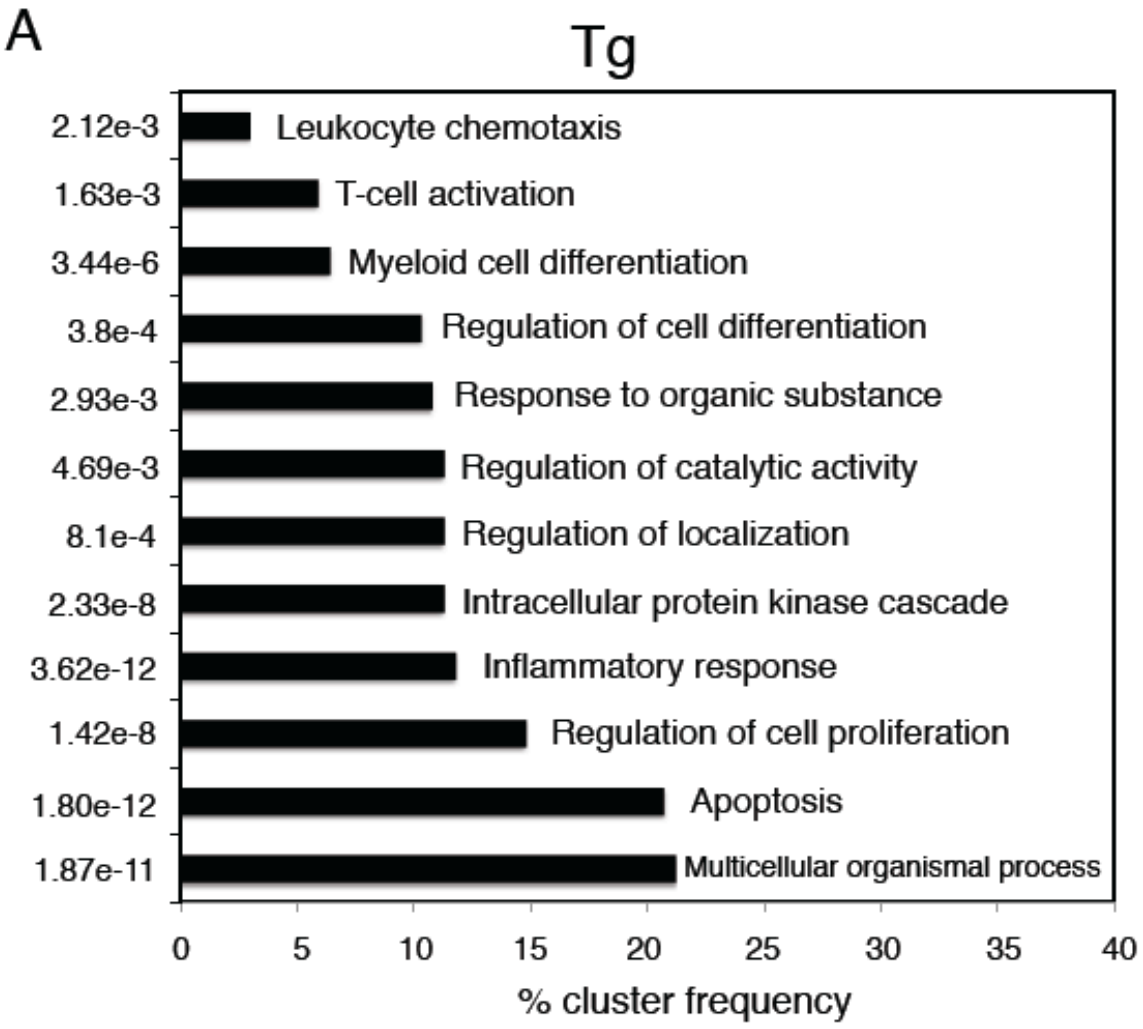
A
Tg
2.12e-3
Leukocyte chemotaxis
1.63e-3
T-cell activation
3.44e-6
Myeloid cell differentiation
3.8e-4
Regulation of cell differentiation
2.93e-3
Response to organic substance
4.69e-3
Regulation of catalytic activity
8.1e-4
Regulation of localization
2.33e-8
Intracellular protein kinase cascade
3.62e-12
Inflammatory response
1.42e-8
Regulation of cell proliferation
1.80e-12
Apoptosis
1.87e-11
Multicellular organismal process
0
5
10
15
20
25
30
35
40
% cluster frequency

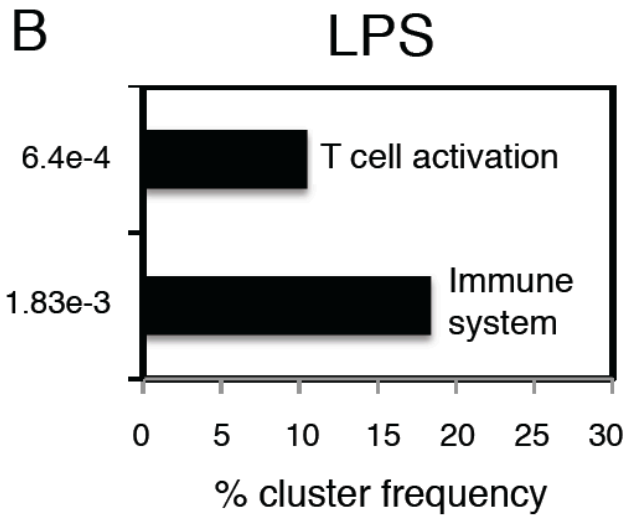
B
LPS
6.4e-4
T cell activation
1.83e-3
Immune system
0
5
10
15
20
25
30
% cluster frequency

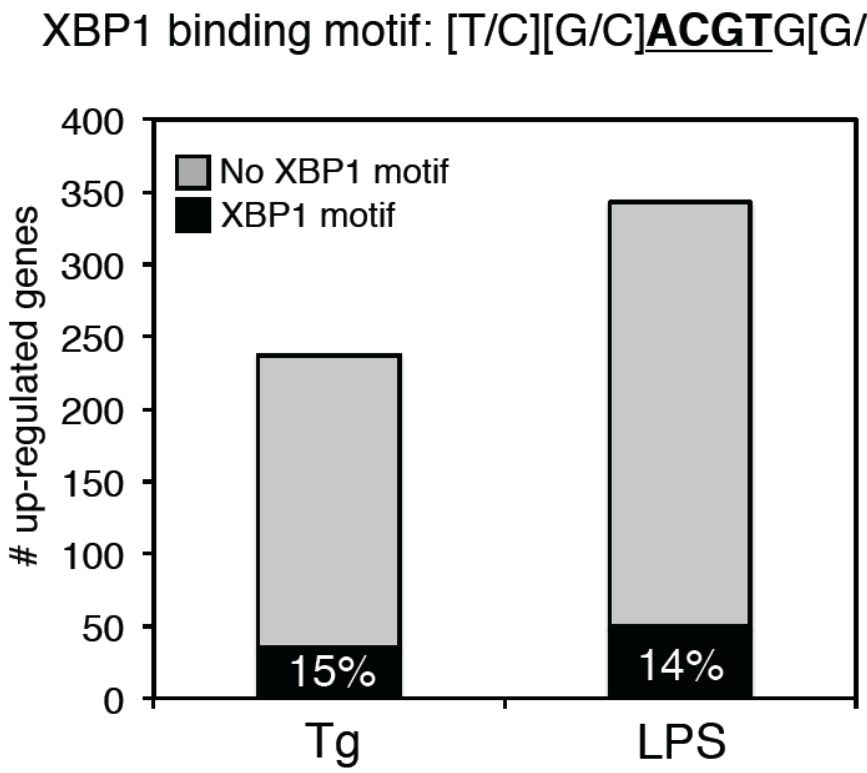

Figure A.7. XBP1 binding motif is enriched in Tg and LPS-induced genes.
Genes transcriptionally induced in response to Tg or LPS treatments were examined for the presence of an XBP1 binding motif in their proximal promoters (-2000 bp to +200 bp relative to the transcription start site). Although LPS-induced genes displayed significantly less dependency on XBP1 (Fig. A.4 and A.5) than Tg-dependent genes, both treatments displayed a similar percentage of up-regulated genes containing a putative XBP1 binding motif. The background frequency of containing an XBP1 binding motif is 11%. *p*-values = 0.02 for both treatments compared to the background frequency.

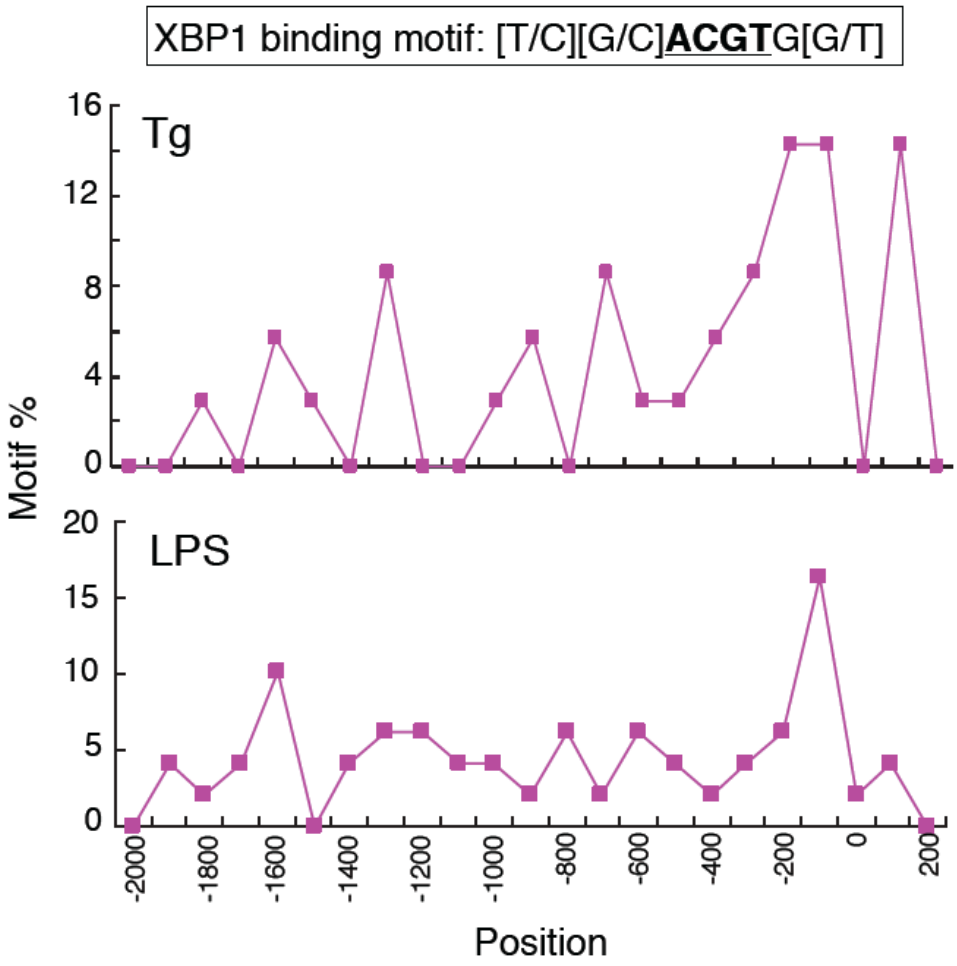

Figure A.8. Position of XBP1 motif in the promoters of induced genes.
Graphical representation displaying the position and frequency of an XBP1 binding motif in the proximal promoters (-2000 to +200 bp relative to the transcription start site, TSS) of up-regulated genes in response to Tg (top) and LPS (bottom). Notably, Tg treatment resulted in a much broader peak between the TSS and -500 bp whereas LPS treatment only showed a strong peak around -100 bp.

XBP1 regulates *Atf3* expression

To understand mechanistically how IRE1α-XBP1 activation and signaling may modulate inflammatory mediators, we turned to the literature. Recent studies have proposed that activating transcription factor 3 (ATF3), a stress-inducible transcription factor, may serve as an integration hub to modulate inflammatory signaling. First, to determine whether *Atf3* expression was responsive to ER stress (Jiang et al., 2004) and whether it was dependent on XBP1, we used wild-type (CONi) and RAW264.7 macrophages deficient for XBP1 (XBP1i) (Fig. A.3). Consistent with previous reports, *Atf3* expression was highly induced upon Tg treatment (Fig. A.9A). Although we failed to observe any differences in basal *Atf3* mRNA levels, ER stress-induced expression of *Atf3* was severely blunted in XBP1i macrophages, demonstrating that induction of *Atf3* gene expression under canonical ER stress was dependent on XBP1 (Fig. A.9A). In further support of a role for XBP1s in *Atf3* expression, XBP1s overexpression in HEK293T cells induced an *Atf3* proximal 300 bp promoter activity in a luciferase reporter assay whereas XBP1u had no effect; ATF3 overexpression repressed its own promoter activity as previously reported (Fig. A.9B) (Wolfgang et al., 2000). Taken together, our data demonstrated that ATF3 may be a transcriptional target gene of XBP1s in macrophages upon ER stress.

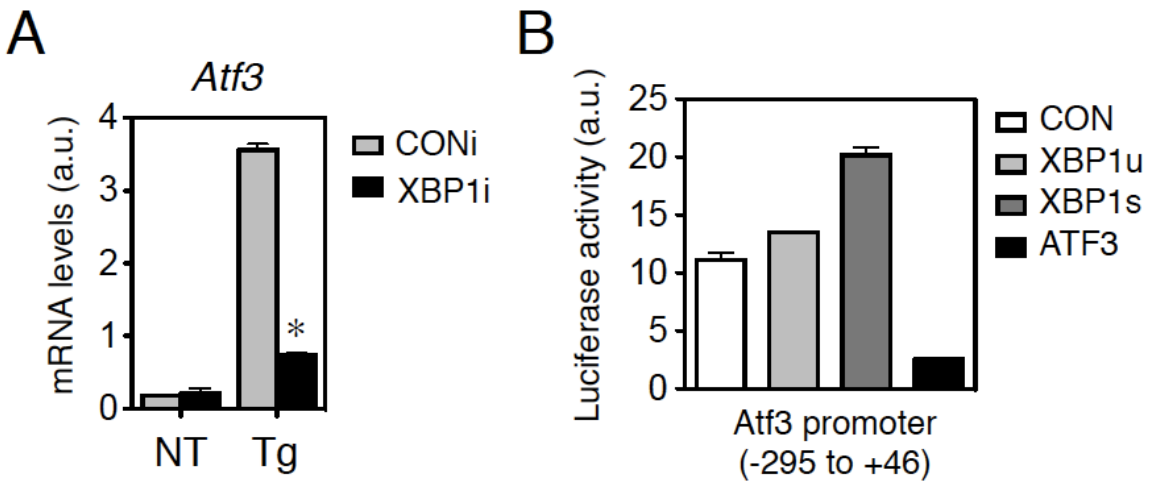

Figure A.9. XBP1 regulates *Atf3* gene expression.

(A) qPCR analysis of *Atf3* gene expression in RAW264.7 macrophages stably expressing shRNA against control luciferase (CONi) or XBP1 (XBP1i) un-treated (CON) or treated with 300 nM Tg for 2 hr. *Atf3* expression is drastically attenuated in XBP1i cells. * $p < 0.05$. **(B)** Luciferase activity of HEK293T cells transiently transfected with Atf3 promoter-luciferase construct (-295 to +46 bp relative to TSS) and XBP1u, XBP1s, or ATF3.

XBP1 and ATF3 form a complex

In a similar fashion as XBP1, ATF3 is a b-ZIP transcription factor that can homo- or hetero-dimerize with other transcription factors to allow for specificity in modulating gene expression (Hai and Hartman, 2001; Hai et al., 1989). Whether ATF3 acts as a positive or negative regulator of transcription may depend on its interactions with co-factors (Hai et al., 1999). However, in the context of regulating inflammation, ATF3 primarily serves as a repressor (Gilchrist et al., 2006; Hai et al., 2010; Suganami et al., 2009). Hence, we proposed that in response to canonical ER stress, ATF3 and XBP1 interact to coordinately activate inflammatory mediators by direct binding to their promoters. To this end, we first aimed to study the relationship between ATF3 and XBP1 proteins to delineate whether they can complex to jointly regulate inflammatory genes in macrophages.

To explore a potential interaction between XBP1 and ATF3, we overexpressed HA-tagged ATF3 and Flag-tagged XBP1 in HEK293T cells, immunoprecipitated with HA-agarose beads and probed for XBP1. Indeed, an interaction between ATF3 and XBP1 was detected only when both proteins were overexpressed (Fig. A.10A). Interestingly, ATF3 interacted with both XBP1u and XBP1s proteins (Fig. A.10A). Although this observation may not be physiologically relevant as XBP1u is highly unstable and rapidly degraded, this may provide insight into the interacting domains of ATF3 and XBP1 as the only shared overlapping regions between XBP1u and XBP1s are N-terminal of the splice site and inclusive of the DNA binding domain (Fig. A.10B).

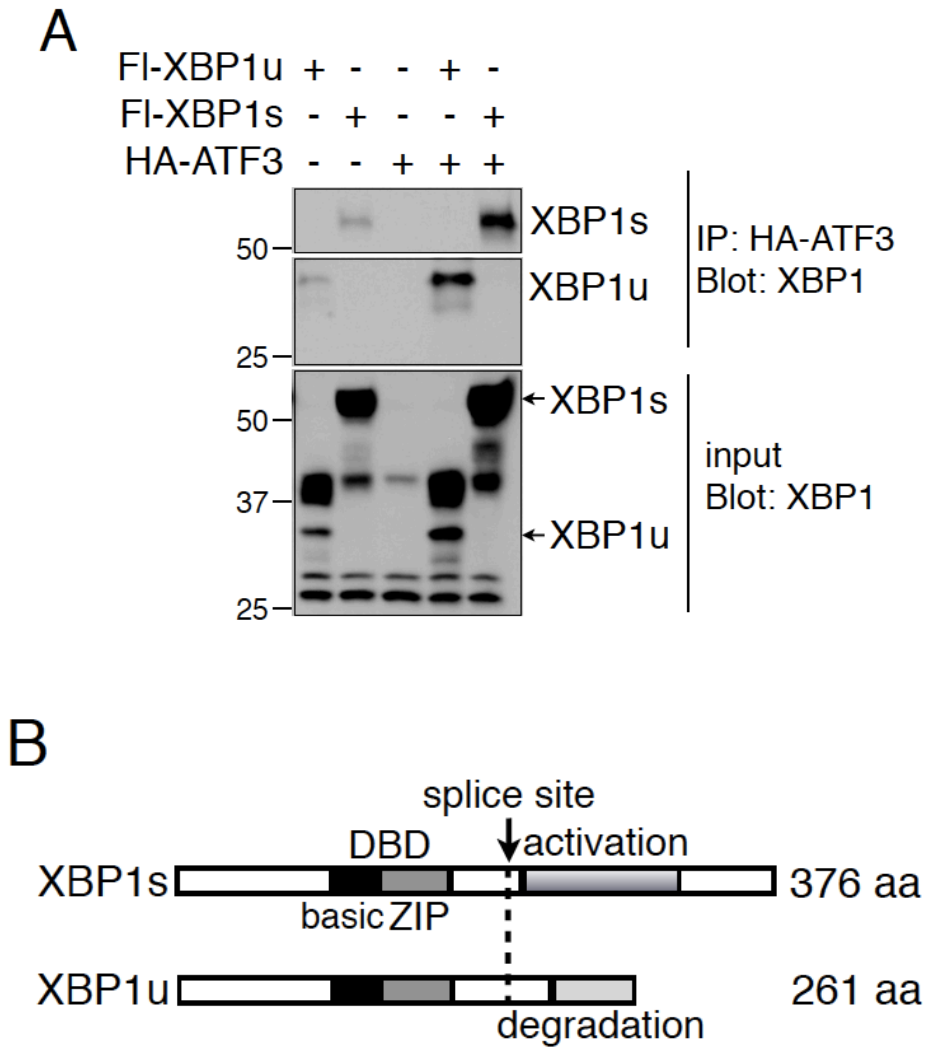

Figure A.10. ATF3 and XBP1 can form a complex.

(A) HEK293T cells transiently transfected with Flag-tagged XBP1u or XBP1s and HA-tagged ATF3 were immunoprecipitated with HA-agarose and immunoblotted for XBP1. Both XBP1u and XBP1s can interact with ATF3. **(B)** Schematic of mouse XBP1s and XBP1u proteins depicting the various domains and IRE1α splice site. Upon ER stress-induced splicing of 26 nucleotides from the *Xbp1u* mRNA, *Xbp1s* mRNA encodes a C-terminal transactivation domain absent from XBP1u. As XBP1s and XBP1s both appear to be able to interact with ATF3, the interacting domain of XBP1 is likely to be N-terminal to the splice site such as the conserved leucine zipper domain.

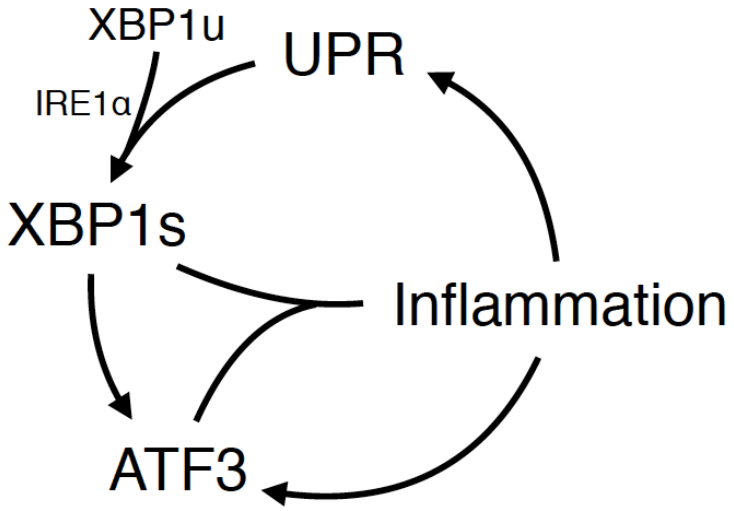

Figure A.11. Working model of XBP1 in ER stress and inflammation.
A previous report by Martinon and colleagues showed that LPS-TLR2/4 signaling activated the IRE1α-XBP1 pathway to govern the expression and secretion of key pro-inflammatory mediators. In this study, we examined the role of canonical ER stress in macrophages. From our data, we propose a model in which canonical ER stress activates IRE1α-XBP1s signaling in macrophages. XBP1s protein transcriptionally activates ATF3, a stress-inducible protein and important modulator of immune responses in many immune cell types including macrophages. XBP1s and ATF3, both b-ZIP transcription factors, act in conjunction to regulate a subset of critical inflammatory genes in response to canonical ER stress.

A.5 FUTURE DIRECTIONS

Here, we show that in murine macrophages, there exists a complex regulatory network underlying activation of the IRE1α-XBP1 pathway and inflammation. A previous study reported selective activation of the IRE1α-XBP1 pathway in response to LPS and TLR2/4 signaling (Martinon et al., 2010). However, the impact and consequence of canonical activation of IRE1α-XBP1 by ER stress were not addressed. In this study, we showed that both ER stress and LPS induced the expression of key inflammatory mediators in macrophages with striking overlap and similarity in target gene identity (Fig. A.11). Our gene expression profiling demonstrated that the presence of XBP1 is required to mediate the expression of critical inflammatory mediators in macrophages. Strikingly, ER stress-induced genes in macrophages were 89% dependent on XBP1 whereas LPS only exhibited 20% dependency. This distinction in XBP1 dependency suggests different underlying mechanisms regulating LPS and Tg-induced inflammation. However, both treatments contained a similar percentage of induced genes containing an XBP1 binding motif in their proximal promoters; this enrichment reached statistical significance relative to a background level of XBP1 binding motifs observed in the genome. Mechanistically, XBP1 was required for ER stress-dependent induction of ATF3, a critical mediator of inflammation in many immune cell types. We showed that *Atf3* expression was attenuated in the absence of XBP1 and XBP1s trans-activated an Atf3 promoter-construct. Furthermore, ATF3 and XBP1, both b-ZIP transcription factors, interacted in an overexpression immunoprecipitation assay. We propose a working model in which IRE1α-XBP1 activation by canonical ER stress

modulates key inflammatory factors through regulation and interaction with ATF3 (Fig. A.11).

Our observations present many possibilities and warrant future studies to determine how ER stress and IRE1α-XBP1 signaling may influence inflammation in macrophages. First, all of the studies presented here were performed in a macrophage cell line RAW264.7. In order to characterize the physiological relevance of these signaling events and to determine whether they can be recapitulated in vivo, we must turn to animal models or primary cell culture models including bone marrow-derived or peritoneal macrophages. Next, an extensive characterization of the interplay and cross-communication between TLR2/4- and ER stress-dependent IRE1α-XBP1 activation is required. Outstanding questions that remain include what are the signals induced by LPS-TLR2/4 that contribute to IRE1α-XBP1 activation and how does TLR2/4 communicate with UPR. Presumably, LPS activation of the IRE1α-XBP1 pathway is not directly related to protein misfolding as the downstream outputs are very different from that of canonical UPR signaling (Fig. A6).

In addition, to understand how ATF3 as a transcriptional repressor and XBP1 as an activator of inflammation can influence inflammatory gene expression, we need to investigate and compare the trancriptomes regulated by both to determine whether these two b-ZIP transcription factors can jointly modulate a unique subset of inflammatory mediators in macrophages. Lastly, the observation that a similar percentage of genes induced under either condition contained XBP1 binding motifs in their proximal promoters was very intriguing in light of their difference in XBP1 dependency. Only by addressing these critical

questions can we gain a more comprehensive understanding of the complex relationship between ER stress, IRE1α-XBP1 signaling and inflammation.

Previous reports linking canonical UPR activation and inflammation have attributed the cross-talk to be mediated through NF-κB or AP-1. Phosphorylation and degradation of IκB by IκB kinase (IKK) promoted NF-κB activation by allowing this transcription factor to enter the nucleus and transcriptionally induce classical pro-inflammatory gene expression (Bonizzi and Karin, 2004). AP-1 is also a transcription factor that can heterodimerize with members of the JUN, FOS and ATF families to specify the types of genes regulated (Eferl and Wagner, 2003). AP-1 targets that have been reported include TNF, IL-8 and other cytokines (Angel et al., 2001). Activated IRE1α interacting with TRAF2 can activate IκB kinase (IKK), which as described above results in nuclear translocation and activation of NF-κB and its pro-inflammatory targets (Hu et al., 2006; Urano et al., 2000). Furthermore, IRE1α signaling can intersect with AP-1 through the IRE1α-TRAF2-JNK complex. JNK engagement leads to phosphorylation AP-1 (Garg et al., 2012). Despite these advances, the physiological implications and underlying mechanisms of these findings are unknown. Given that some of the pro-inflammatory target genes identified from our microarray can also be regulated by NF-κB, additional studies delineating the interplay between these pathways are essential. Particularly interesting questions are whether IRE1α activation by canonical ER stress can initiate two parallel pathways (i.e. TRAF2-JNK interaction and XBP1s-ATF3) to mediate an inflammatory response, what are the transcriptional targets of each pathway and

how much overlap, if any, do they share, and whether ATF3 can jointly and differentially mediate inflammatory gene expression in response to diverse stimuli with various transcription factors such as XBP1 vs. AP-1.

A.6 ACKNOWLEDGEMENTS

I thank Lu Huang for providing the RAW264.7 macrophage cell line. I thank Sander Kersten and members of his lab at Wageningen University for microarray analysis, data interpretation and discussions. I thank Huifeng Jiang in the Gu Lab for GO analysis. I thank Cindy Wang for technical assistance and Qi Lab members for helpful comments. I thank Haibo Sha for sharing his microarray data on 3T3-L1 pre-adipocytes performed in collaboration with the Kersten Lab. Lastly, I thank my A-exam committee members, Lee Kraus, Tom Brenna, and Sylvia Lee, for suggestions on this project, which originated as an A-exam proposal.

APPENDIX B

IRE1α UNDERGOES ER STRESS-DEPENDENT PHOSPHORYLATION AT A UNIQUE "SSPS" MOTIF

B.1 ABSTRACT

Disruptions in ER homeostasis lead to activation of the unfolded protein response (UPR) and have been linked to a number of human diseases collectively called conformational disorders. To maintain equilibrium in the ER lumen, ER-to-nucleus signaling pathways have evolved that engage both transcriptional and translational responses. A key mammalian sensor of ER homeostasis is IRE1α. Although the general sequence of events in IRE1α activation has been resolved, the precise mechanistic details remain unknown. Here, we identify a novel post-translational motif on the IRE1α protein that may be required for its phosphorylation and activation. Tandem mass spectrometry identified a "SSPS" domain located on the linker cytosolic region of IRE1α that was heavily phosphorylated under ER stress. The "SSPS" site is conserved among mammals, suggesting a functional role for this motif in IRE1α trans-autophosphorylation. Thus, we propose that IRE1α activation upon ER stress requires phosphorylation at a unique and conserved "SSPS" motif, which may be an initiating event in the phosphorylation cascade.

B.2 INTRODUCTION

Protein misfolding in the ER activates the unfolded protein response (UPR). The most well-conserved signaling branch of UPR is the IRE1α-XBP1 pathway (Calfon et al., 2002). Upon sensing alterations in ER homeostasis either through direct binding of misfolded proteins or indirect dissociation of the ER chaperone GRP78/BiP, IRE1α activation occurs through dimerization, trans-autophosphorylation, oligomerization, and activation of its cytosolic RNase domain (Ron and Walter, 2007; Walter and Ron, 2011). However, the exact mechanistic details underlying mammalian IRE1α activation remain unclear. Several reports have provided some mechanistic insight into IRE1α activation and signaling by demonstrating that IRE1α regulation can occur in a cell or tissue-specific manner by its interaction with various co-factors, both activating and inhibitory (Hetz and Glimcher, 2009; Woehlbier and Hetz, 2011). Identification of these co-factors has provided valuable insight into how IRE1α may communicate and engage in cross-talk with other signaling pathways such as apoptosis and autophagy (Woehlbier and Hetz, 2011). In addition to co-factors, another avenue of regulation commonly occurs through post-translational modifications. Supporting this notion, IRE1α trans-autophosphorylation is well-accepted to be a key activating step (Ron and Walter, 2007; Walter and Ron, 2011). Furthermore, yeast studies on IRE1p have identified two neighboring serine residues, Ser840 and Ser841, located in the activation loop of the kinase domain to be critical for the trans-autophosphorylation activity of yeast IRE1p (Sicheri and Silverman, 2011).

However, no comprehensive characterization of mammalian IRE1α post-translational modification and specifically phosphorylation sites has been performed.

To gain a comprehensive and mechanistic understanding of IRE1α signaling, activating and regulation, we turned to tandem mass spectrometric (MS/MS) analyses of mammalian IRE1α protein. In addition to uncovering and characterizing novel IRE1α-interacting factors such as NMIIB as described in Chapter 3, we also aimed to examine the post-translational status of IRE1α protein and whether and how this changed in response to ER stress. To this end, we performed mass spectrometry analysis in collaboration with Dr. Xuemei Han from the Yates Lab at Scripps Research Institute to identify phosphorylation sites as well as determine the individual and joint contribution of these site(s) to overall IRE1α trans-autophosphorylation and activation.

B.3 MATERIALS AND METHODS

Cell lines and drug treatment

IRE1α$^{-/-}$ and wild-type control MEFs (gifts from Dr. L. Glimcher, Weill Cornell) were maintained in DMEM supplemented with 10% FBS (Hyclone) and 1% penicillin/streptomycin (Cellgro). Tg was acquired from EMD Calbiochem.

Plasmids and transfection

pMSCV-IRE1α-HA encoding WT human IRE1α was generously provided by Dr. C. Hetz (University of Chile).

IRE1α immunopurification and mass spectrometry

IRE1α$^{-/-}$ MEFs stably expressing human pMSCV-IRE1α-HA were treated with 300 nM Tg for 2 hr. Cells were harvested in lysis buffer (150 mM NaCl, 1% Triton X-100, 1 mM EDTA, and 50 mM Tris HCl pH 7.5) supplemented with protease inhibitor cocktail (Sigma) and allowed to lyse on ice for 20 min. Cells were sonicated 10 s with Branson Digital 250 Cell Disruptor at 10% amplitude followed by centrifugation. Supernatant was immunprecipiated overnight at 4°C with HA-agarose beads followed by washes the next day and immunoprecipitate was loaded on a 6% polyacrylamide SDS-PAGE gel. Gel was incubated with Coomassie Brilliant Blue (0.5 g Coomassie Brilliant Blue R-250 in 450 ml methanol, 450 ml MQ water, and 100 ml acetic acid) with gentle rocking for 30 min at room temperature followed by 2 washes with MQ water 5 min each. Gel was destained in destaining solution (45% methanol, 45% MQ water, and 10% acetic acid) that was changed every 30 min until bands could be clearly visualized. Protein bands were excised from Coomassie-stained gels and destained, and subjected to an in-gel trypsin digestion. Peptide mixtures were analyzed by online nanoflow liquid chromatrography tandem mass spectrometry (LC-MS/MS) on an Agilent 1200 quaternary HPLC system (Agilent, Palo Alto, CA) connected to an LTQ-Orbitrap mass spectrometer (Thermo Fisher Scientific) through an in-house built nanoelectrospray ion source.

B.4 RESULTS AND DISCUSSION

IRE1α is phosphorylated at a unique "SSPS" motif upon ER stress

Human IRE1α is a 977 amino acid type 1 ER transmembrane protein with multiple functional domains (Fig. B.1). The N-terminal domain resides in the ER lumen and contains an MHC-like region believed to be involved in direct binding of misfolded proteins. This is followed by a transmembrane region that tethers the IRE1α protein to the ER membrane. C-terminal of the transmembrane domain lies a short linker, kinase, and RNase regions. The kinase domain promotes trans-autophosphorylation of adjacent IRE1α proteins, a critical event in IRE1α activation upon ER stress. As yeast IRE1 protein has been reported to be extensively phosphorylated, the same has been speculated for mammalian IRE1α. However, outstanding questions such as the exact residue(s) and the individual contribution of each phosphorylation site to overall IRE1α activation and signaling remain unknown.

In an attempt to resolve IRE1α post-translational modification sites, we performed a mass spectrometry analysis of IRE1α in collaboration with Dr. Xuemei Han in the laboratory of Dr. John Yates at The Scripps Research Institute and obtained over 81% overall coverage of the human IRE1α protein (Fig. B.1). Surprisingly, our mass spectrometry only identified a few sites of phosphorylation, including a unique "SSPS" motif located in the linker region (Fig. B.2). Upon treatment with thapsigargin (Tg), a potent ER stress inducer, IRE1α phosphorylation occurred *simultaneously* at two and even all three of the Ser residues on the SSPS motif, suggesting that extensive phosphorylation at this

motif is ER stress-dependent (Fig. B.2). Alignment using the DNA Strider software demonstrated that this motif was highly conserved within mammalian IRE1, including the gut-specific IRE1β protein (Fig. B.3).

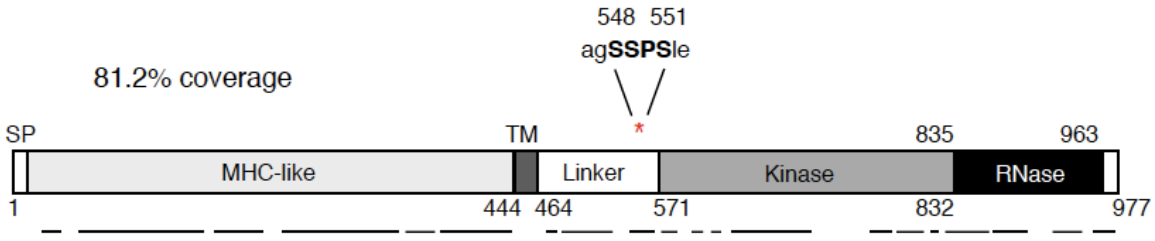

Figure B.1. Schematic of human IRE1α protein and its functional domains.

Human IRE1α protein is depicted to scale with numbers 1-977 denoting the respective amino acids. Mass spectrometric analysis with the Yates Lab identified a unique "SSPS" motif at amino acids 548 to 551 in the linker region undergoing di- or tri-phosphorylation upon ER stress. Lines beneath indicate peptides recovered from mass spectrometry with 81.2% overall coverage.

Non-treated	300 nM Tg for 2 hr	Phosphorylation sites
	K.IQLLQQQQ..SESSGTSSP**pS**TSPR.A	**S527**
K.AGSSPSLEQDDGDEET**pS**VVIVGK.I	K.AGSSPSLEQDDGDEET**pS**VVIVGK.I	**S562**
K.AG**pS**SPSLEQDDGDEETSVVIVGK.I	K.AG**pS**SPSLEQDDGDEETSVVIVGK.I	**S548**
K.AGS**pS**PSLEQDDGDEETSVVIVGK.I	K.AGS**pS**PSLEQDDGDEETSVVIVGK.I	**S549**
K.AGSSP**pS**LEQDDGDEETSVVIVGK.I	K.AGSSP**pS**LEQDDGDEETSVVIVGK.I	**S551**
	K.AGSSP**pS**LEQDDGDEE**pT**SVVIVGK.I	**S551, T561**
	K.AG**pS**SP**pS**LEQDDGDEETSVVIVGK.I	**S548, S551**
	K.AGS**pS**P**pS**LEQDDGDEETSVVIVGK.I	**S549, S551**
	K.AG**pSpS**PSLEQDDGDEETSVVIVGK.I	**S548, S549**
	K.AG**pSpS**P**pS**LEQDDGDEETSVVIVGK.I	**S548, S549, S551**

Figure B.2. Peptides recovered from mass spectrometry depicting ER stress-induced IRE1α phosphorylation sites.

IRE1α$^{-/-}$ MEFs stably expressing HA-tagged human IRE1α were untreated or treated with 300 nM Tg (ER stress agent) for 2 hr, immunoprecipitated with HA-agarose beads and lysates were run on a gel. Coomassie Blue staining revealed the IRE1α band at approximately 110 kDa, which was excised and submitted to our collaborator Dr. Xuemei Han in the Yates lab for MS/MS analysis of phosphorylation sites. Peptides recovered demonstrate mono-, di- and tri-phosphorylation at the SSPS (amino acids 548-551) motif as well as additional unique serine (Ser527, Ser 562) and threonine (Thr561) phosphorylation sites.

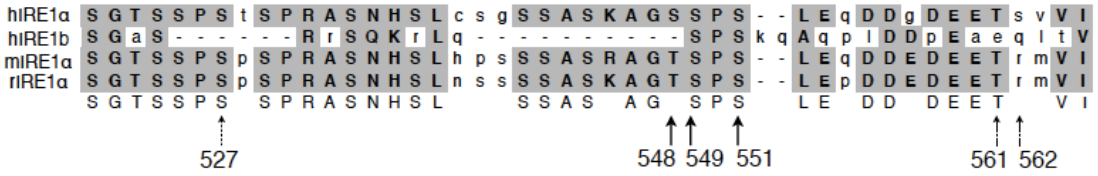

Figure B.3. SSPS is a conserved motif in mammalian IRE1α.

Sequence alignment of IRE1 protein from amino acids 521 to 565 in human, mouse and rat using the DNA Strider software. Gray shaded boxes indicated conserved amino acid. Arrows and numbers indicate the serine or threonine residue identified by MS/MS as an ER stress-dependent phosphorylation site.

B.5 FUTURE DIRECTIONS

Further studies are warranted to follow up on this exciting but preliminary observation. First and foremost, Quick-change mutagenesis assays will be performed to determine the functional significance of phosphorylation at this motif. As the MS/MS analysis demonstrated that tri-phosphorylation at SSPS can occur upon ER stress and in an attempt to study the most exaggerated mutant, we will first mutate all three Ser residues (SSPS) to either Ala (AAPA) to generate a loss-of-function mutant or to Asp (DDPD) to generate a gain-of-function/phospho-mimetic mutant, transfect the plasmids into IRE1α$^{-/-}$ MEFs and perform Phos-tag based Western blot analyses of IRE1α phosphorylation. Additional markers of IRE1α activation and signaling will also be examined. These include molecular and biochemical studies of canonical UPR and ER stress markers such as IRE1α foci formation, *Xbp1* mRNA splicing, XBP1s protein production, Q-PCR analysis of UPR target genes including chaperones and degradation components, and IRE1α-mediated mRNA decay. We predict that the AAPA triple loss-of-function mutant will display defective IRE1α phosphorylation and that the DDPD phospho-mimetic mutant will exhibit an increase in basal IRE1α phosphorylation. However, if basal phosphorylation does not occur in the DDPD mutant, then additional ER stress signals are required for IRE1α activation.

Next, we will also determine the effect of the SSPS motif of IRE1α on its biological and physiological parameters including cell fate determination (survival, proliferation, apoptosis) and ER stress-dependent ER expansion.

Furthermore, generation of single and combinatorial double mutants is required to precisely characterize the requirement and importance of each serine residue to IRE1α signaling. In addition to identification of peptides with tri-phosphorylation of SSPS, peptides containing mono- or di-phosphorylation were also present (Fig. B.2). Therefore, studies using single and double phosphorylation mutants will be essential in delineating the individual as well as collective contribution of each residue to IRE1α regulation. To truly understand the physiological significance of this motif, a knock-in mouse model using the AAPA motif can be generated and used for metabolic and ER stress studies. Overall, these studies will provide a comprehensive and thorough examination of the physiological importance of the SSPS motif on IRE1α phosphorylation and signaling.

B.6 ACKNOWLEDGEMENTS

I would like to thank Xuemei Han in the Yates lab for performing and analyzing the tandem mass spectrometry data, which identified post-translational modification sites on the human IRE1α protein.

APPENDIX C*

PUTATIVE IRE1α-INTERACTING PROTEINS IDENTIFIED BY MASS SPECTROMETRY

C.1 INTRODUCTION

As previously discussed in Chapter 3, a proteomic screen on IRE1α was performed in collaboration with Xuemei Han in the Yates Lab (Scripps Research Institute) to identify potentially new IRE1α-interacting partners that may play a functional role in its activation, regulation and signaling. The mechanistic, functional and physiological role of one of the interactors, non-muscle myosin IIB (NMIIB), was characterized in response to ER stress (Chapter 3). However, other putative interacting partners were also extracted from the study. Listed in Table C.1 are five additional factors that are putative binding partners of IRE1α identified by tandem mass spectrometry (MS/MS).

C.2 RESULTS AND DISCUSSION

Briefly, IRE1α$^{-/-}$ MEFs stably expressing human pMSCV-IRE1α-HA were non-treated or treated with 300 nM Tg for 2 hr. Cells were harvested, lysed and immunoprecipitated with HA-agarose beads. Lysates were processed by Western blot and gel was stained with Coomassie Brilliant Blue. The IRE1α-HA bands from both non-treated and ER stress conditions were excised and

* This appendix is associated with Chapter 3 on uncovering novel IRE1α-interacting factors by using tandem mass spectrometry.

submitted for tandem mass spectrometry (see Chapter 3 for a detailed protocol). MS/MS identified peptides that were then mapped to proteins, representing potential IRE1α-interacting factors that may regulate its activation and signaling. These factors, along with their putative functions as characterized on UniProt, are listed in decreasing order of number of peptides recovered (Table C.1).

Interestingly, although most of these proteins are not very well characterized, their putative functions span several different biological processes including mRNA splicing, nucleosome remodeling, helicase activity, and nonsense-mediated decay. As our goal is to identify regulators of IRE1α, we further examined the number of peptides recovered from non-treated cells compared to cells exposed to ER stress (Table C.2). Surprisingly, the majority of the potential interacting factors segregated and were either enriched in control (CON) or ER stress (Tg) conditions. For example, the top hit, SF3B3 was highly enriched for control non-stress conditions whereas the next hit, FARP1, was enriched for ER stress conditions. These results indicated that our screen may have identified both negative and positive regulators of IRE1α. Recent insight into the IRE1α interactome (see Chapter 1) show that negative regulators bind to IRE1α to maintain it in an inactive conformation and dampen its signaling whereas activators bind to IRE1α under ER stress to promote and enhance its signaling. Hence, further analysis of these putative regulators are required to understand their functional and physiological roles in ER stress and UPR signaling.

Table C.1. Putative IRE1α-interacting factors.

Candidate binding partners of IRE1α and their putative functions are listed. Please refer to text for discussion regarding how these factors may potentially regulate IRE1α activation and signaling.

UniProt ID	Identification	Putative function
Q15393	SF3B3 (Splicing factor 3B subunit 3)	mRNA splicing/processing
Q9Y4F1	FARP1 (FERM, RhoGEF and pleckstrin domain-containing protein 1)	Rho-guanine nucleotide exchange factor
Q9P2R3	ANKFY1 (Ankyrin repeat and FYVE domain-containing protein 1)	Metal ion binding
O60264	SMARCA5 (SWI/SNF-related matrix-associated actin-dependent regulator of chromatin subfamily A member 5)	Helicase with ATP-dependent nucleosome-remodeling activity
Q92900	UPF1 (Regulator of nonsense transcripts 1)	RNA-dependent helicase and ATPase required for nonsense-mediated decay

Table C.2. MS/MS peptide recovery for potential IRE1α-binding partners.
MS/MS data for these factors were analyzed for the number of peptides recovered under basal non-stress conditions (CON) or when treated with a drug to induce ER stress (Tg).

Identification	# CON peptides	# Tg peptides
SF3B3	8	1
FARP1	0	8
ANKFY1	3	2
SMARCA5	1	3
UPF1	0	2

In light of the role of IRE1α in splicing *Xbp1* and other mRNAs and even potentially microRNAs under ER stress, SF3B3 and its association with the spliceosome machinery is an intriguing discovery. Even more surprising is that the interaction between IRE1α and SF3B3 appears to be enriched under basal conditions, suggesting that SF3B3 may be functioning to suppress IRE1α activation or maintaining IRE1α in an inactive monomeric conformation. An alternative possibility could be that SF3B3 is acting as an adaptor or scaffolding protein to facilitate the recruitment of other IRE1α-binding factors. FARP1 is a putative Rho-guanine nucleotide exchange factor (GEF) that activates small GTPases, which integrate into various cellular signaling pathways. It is interesting to note that one of the primary downstream targets of PERK activation, phosphorylation of eIF2α, regulates the GEF eIF2B. eIF2α phosphorylation prevents eIF2B GEF activity, resulting in attenuated protein synthesis. Understanding how FARP1 may integrate into IRE1α signaling may identify new cellular pathways that are responsive to ER stress and communicate with UPR. SMARCA5 is a nucleosome-remodeling factor with helicase and ATPase activity, and enriched for complexing with IRE1α upon ER stress. Nucleosome-remodeling factors typically act in concert with transcription factors to remodel the chromatin in preparation for transcription. XBP1s is one of the primary downstream targets of IRE1α signaling and an essential UPR transcription factor. The interaction between IRE1α and SMARCA5 may shed light on a new role for IRE1α in direct modulation of the chromatin landscape in response to ER stress to induce UPR genes. In addition to promoting *Xbp1*

splicing and generating XBP1s, IRE1α may participate in transcriptional regulation through the action of SMARCA5. Lastly, UPF1 is part of a multimeric protein complex involved in mRNA surveillance and non-sense mediated decay (NMD) that targets mRNAs containing premature stop codons for degradation. This role is reminiscent of IRE1α-mediated mRNA decay (RIDD) that functions to alleviate an elevated burden on the ER during ER stress by cleaving target mRNAs. Even though only two peptides were recovered that mapped to UPF1, both were specific to Tg-induced ER stress. Hence, this may suggest a potential role for UPF1 in RIDD. As the mechanistic details of RIDD remain elusive, elucidating how UPF1 incorporates into IRE1α signaling and function could provide key insight into RIDD. Notably, ATF4, a downstream transcription factor of PERK pathway, has been reported to be a target of NMD, further reinforcing the notion that cross-talk could occur between UPR and NMD regarding ER capacity and status, and to coordinate incoming ER load. In conclusion, this proteomic screen on IRE1α-interacting factors has yielded several exciting and promising candidates whose functions span from mRNA processing and surveillance to chromatin remodeling. Future investigations into how these factors modulate and integrate into IRE1α signaling will greatly enhance our understanding of IRE1α function.

C.3 FUTURE DIRECTIONS

The preliminary data presented here on putative IRE1α-interacting partners, though exciting and encouraging, requires further validations. First,

biochemical verification of a bona fide interaction between IRE1α and these factors are required. Along these lines, it would be interesting to note whether the interaction is indeed dependent on ER stress and if so, whether the interaction diminishes or increases with escalating ER stress. Of note, these experiments can also help us to assess the accuracy and sensitivity of our MS/MS experiment. The next step after validating the interaction would be to determine whether these factors exert a functional influence on IRE1α signaling, either positive or negative, by employing both gain- and loss-of-function approaches (see Chapter 3). Given the high concentration of factors in the cellular milieu, many proteins can appear to "interact" but lack functional significance. Finally, the in vivo physiological significance of these factors will be assessed by using mouse models. All together, investigating and establishing the functional and biological role of these factors in IRE1α signaling and UPR will be essential in obtaining a comprehensive and mechanistic view of mammalian IRE1α activation, regulation and signaling, and may identify novel targets for therapeutic development in the treatment of conformational diseases.

C.4 ACKNOWLEDGEMENTS

I thank Xuemei Han in the Yates Lab (Scripps Research Institute) who collaborated with us on the tandem mass spectrometry to identify IRE1α-interacting factors.

REFERENCES

Acosta-Alvear, D., Zhou, Y., Blais, A., Tsikitis, M., Lents, N.H., Arias, C., Lennon, C.J., Kluger, Y., and Dynlacht, B.D. (2007). XBP1 controls diverse cell type- and condition-specific transcriptional regulatory networks. *Mol Cell* **27**, 53–66.

Adelstein, R.S., and Conti, M.A. (1975). Phosphorylation of platelet myosin increases actin-activated myosin ATPase activity. *Nature* **256**, 597–598.

Aguilar, H.N., Tracey, C.N., Tsang, S.C.F., McGinnis, J.M., and Mitchell, B.F. (2011). Phos-tag-based analysis of myosin regulatory light chain phosphorylation in human uterine myocytes. *PLoS ONE* **6**, e20903.

Angel, P., Szabowski, A., and Schorpp-Kistner, M. (2001). Function and regulation of AP-1 subunits in skin physiology and pathology. *Oncogene* **20**, 2413–2423.

Arii, J., Goto, H., Suenaga, T., Oyama, M., Kozuka-Hata, H., Imai, T., Minowa, A., Akashi, H., Arase, H., Kawaoka, Y., et al. (2010). Non-muscle myosin IIA is a functional entry receptor for herpes simplex virus-1. *Nature* **467**, 859–862.

Armant, M.A., and Fenton, M.J. (2002). Toll-like receptors: a family of pattern-recognition receptors in mammals. *Genome Biol* **3**, REVIEWS3011.

Balch, W.E., Morimoto, R.I., Dillin, A., and Kelly, J.W. (2008). Adapting proteostasis for disease intervention. *Science* **319**, 916–919.

Barmada, M.M., Brant, S.R., Nicolae, D.L., Achkar, J.-P., Panhuysen, C.I., Bayless, T.M., Cho, J.H., and Duerr, R.H. (2004). A genome scan in 260 inflammatory bowel disease-affected relative pairs. *Inflamm Bowel Dis* **10**, 513–520.

Bertolotti, A., Wang, X., Novoa, I., Jungreis, R., Schlessinger, K., Cho, J.H., West, A.B., and Ron, D. (2001). Increased sensitivity to dextran sodium sulfate colitis in IRE1beta-deficient mice. *J Clin Invest* **107**, 585–593.

Bertolotti, A., Zhang, Y., Hendershot, L.M., Harding, H.P., and Ron, D. (2000). Dynamic interaction of BiP and ER stress transducers in the unfolded-protein response. *Nat Cell Biol* **2**, 326–332.

Blais, A., Tsikitis, M., Acosta-Alvear, D., Sharan, R., Kluger, Y., and Dynlacht, B.D. (2005). An initial blueprint for myogenic differentiation. *Genes Dev* **19**, 553–569.

Bonizzi, G., and Karin, M. (2004). The two NF-kappaB activation pathways and their role in innate and adaptive immunity. *Trends Immunol* **25**, 280–288.

Brant, S.R., Fu, Y., Fields, C.T., Baltazar, R., Ravenhill, G., Pickles, M.R., Rohal, P.M., Mann, J., Kirschner, B.S., Jabs, E.W., et al. (1998). American families with Crohn's disease have strong evidence for linkage to chromosome 16 but not chromosome 12. *Gastroenterology* **115**, 1056–1061.

Brenner, S. (1974). The genetics of Caenorhabditis elegans. *Genetics* **77**, 71–94.

Calfon, M., Zeng, H., Urano, F., Till, J.H., Hubbard, S.R., Harding, H.P., Clark, S.G., and Ron, D. (2002). IRE1 couples endoplasmic reticulum load to secretory capacity by processing the XBP-1 mRNA. *Nature* **415**, 92–96.

Cao, Z., Umek, R.M., and McKnight, S.L. (1991). Regulated expression of three C/EBP isoforms during adipose conversion of 3T3-L1 cells. *Genes Dev* **5**, 1538–1552.

Carbon, S., Ireland, A., Mungall, C.J., Shu, S., Marshall, B., Lewis, S., AmiGO Hub, Web Presence Working Group (2009). AmiGO: online access to ontology and annotation data. *Bioinformatics* **25**, 288–289.

Carrasco, D.R., Sukhdeo, K., Protopopova, M., Sinha, R., Enos, M., Carrasco, D.E., Zheng, M., Mani, M., Henderson, J., Pinkus, G.S., et al. (2007). The differentiation and stress response factor XBP-1 drives multiple myeloma pathogenesis. *Cancer Cell* **11**, 349–360.

Carrell, R.W., and Lomas, D.A. (1997). Conformational disease. *Lancet* **350,** 134–138.

Chen, D., Thomas, E.L., and Kapahi, P. (2009). HIF-1 modulates dietary restriction-mediated lifespan extension via IRE-1 in Caenorhabditis elegans. *PLoS Genet* **5**, e1000486.

Chen, H., and Qi, L. (2010). SUMO modification regulates the transcriptional activity of XBP1. *Biochem J* **429**, 95–102.

Chen, X., Shen, J., and Prywes, R. (2002). The luminal domain of ATF6 senses endoplasmic reticulum (ER) stress and causes translocation of ATF6 from the ER to the Golgi. *J Biol Chem* **277**, 13045–13052.

Clauss, I.M., Chu, M., Zhao, J.L., and Glimcher, L.H. (1996). The basic domain/leucine zipper protein hXBP-1 preferentially binds to and transactivates CRE-like sequences containing an ACGT core. *Nucleic Acids Res* **24**, 1855–1864.

Clauss, I.M., Gravallese, E.M., Darling, J.M., Shapiro, F., Glimcher, M.J., and Glimcher, L.H. (1993). In situ hybridization studies suggest a role for the basic region-leucine zipper protein hXBP-1 in exocrine gland and skeletal development during mouse embryogenesis. *Dev Dyn* **197**, 146–156.

Conn, P.M., Ulloa-Aguirre, A., Ito, J., and Janovick, J.A. (2007). G protein-coupled receptor trafficking in health and disease: lessons learned to prepare for therapeutic mutant rescue in vivo. *Pharmacol Rev* **59**, 225–250.

Conrad, A.H., Clark, W.A., and Conrad, G.W. (1991). Subcellular compartmentalization of myosin isoforms in embryonic chick heart ventricle myocytes during cytokinesis. *Cell Motil. Cytoskeleton* **19**, 189–206.

Copps, K.D., Hancer, N.J., Opare-Ado, L., Qiu, W., Walsh, C., and White, M.F. (2010). Irs1 serine 307 promotes insulin sensitivity in mice. *Cell Metab* **11**, 84–92.

Cox, J.S., and Walter, P. (1996). A novel mechanism for regulating activity of a transcription factor that controls the unfolded protein response. *Cell* **87**, 391–404.

Cox, J.S., Shamu, C.E., and Walter, P. (1993). Transcriptional induction of genes encoding endoplasmic reticulum resident proteins requires a transmembrane protein kinase. *Cell* **73**, 1197–1206.

Credle, J.J., Finer-Moore, J.S., Papa, F.R., Stroud, R.M., and Walter, P. (2005). On the mechanism of sensing unfolded protein in the endoplasmic reticulum. *Proc Natl Acad Sci USA* **102**, 18773–18784.

Davies, F.E., Dring, A.M., Li, C., Rawstron, A.C., Shammas, M.A., O'Connor, S.M., Fenton, J.A.L., Hideshima, T., Chauhan, D., Tai, I.T., et al. (2003). Insights into the multistep transformation of MGUS to myeloma using microarray expression analysis. *Blood* **102**, 4504–4511.

Doane, A.S., Danso, M., Lal, P., Donaton, M., Zhang, L., Hudis, C., and Gerald, W.L. (2006). An estrogen receptor-negative breast cancer subset characterized by a hormonally regulated transcriptional program and response to androgen. *Oncogene* **25**, 3994–4008.

DuRose, J.B., Tam, A.B., and Niwa, M. (2006). Intrinsic capacities of molecular sensors of the unfolded protein response to sense alternate forms of endoplasmic reticulum stress. *Mol Biol Cell* **17**, 3095–3107.

Eferl, R., and Wagner, E.F. (2003). AP-1: a double-edged sword in tumorigenesis. *Nat Rev Cancer* **3**, 859–868.

Fan, J.Q., Ishii, S., Asano, N., and Suzuki, Y. (1999). Accelerated transport and maturation of lysosomal alpha-galactosidase A in Fabry lymphoblasts by an enzyme inhibitor. *Nat Med* **5**, 112–115.

Farmer, S.R. (2006). Transcriptional control of adipocyte formation. *Cell Metab* **4**, 263–273.

Flynn, P.G., and Helfman, D.M. (2010). Non-muscle myosin IIB helps mediate TNF cell death signaling independent of actomyosin contractility (AMC). *J Cell Biochem* **110**, 1365–1375.

Gardner, B.M., and Walter, P. (2011). Unfolded Proteins Are Ire1-Activating Ligands That Directly Induce the Unfolded Protein Response. *Science* **333**, 1891–1894.

Garg, A.D., Kaczmarek, A., Krysko, O., Vandenabeele, P., Krysko, D.V., and Agostinis, P. (2012). ER stress-induced inflammation: does it aid or impede disease progression? *Trends Mol Med* **18**, 589–598.

Gass, J.N., Gifford, N.M., and Brewer, J.W. (2002). Activation of an unfolded protein response during differentiation of antibody-secreting B cells. *J Biol Chem* **277**, 49047–49054.

Gass, J.N., Jiang, H.-Y., Wek, R.C., and Brewer, J.W. (2008). The unfolded protein response of B-lymphocytes: PERK-independent development of antibody-secreting cells. *Mol Immunol* **45**, 1035–1043.

Gilchrist, M., Thorsson, V., Li, B., Rust, A.G., Korb, M., Roach, J.C., Kennedy, K., Hai, T., Bolouri, H., and Aderem, A. (2006). Systems biology approaches identify ATF3 as a negative regulator of Toll-like receptor 4. *Nature* **441**, 173–178.

Gomez, B.P., Riggins, R.B., Shajahan, A.N., Klimach, U., Wang, A., Crawford, A.C., Zhu, Y., Zwart, A., Wang, M., and Clarke, R. (2007). Human X-box binding protein-1 confers both estrogen independence and antiestrogen resistance in breast cancer cell lines. *FASEB J* **21**, 4013–4027.

Gordon, S. (2002). Pattern recognition receptors: doubling up for the innate immune response. *Cell* **111**, 927–930.

Gregor, M.F., and Hotamisligil, G.S. (2007). Thematic review series: Adipocyte Biology. Adipocyte stress: the endoplasmic reticulum and metabolic disease. *J Lipid Res* **48**, 1905–1914.

Gu, F., Nguyên, D.T., Stuible, M., Dubé, N., Tremblay, M.L., and Chevet, E. (2004). Protein-tyrosine phosphatase 1B potentiates IRE1 signaling during endoplasmic reticulum stress. *J Biol Chem* **279**, 49689–49693.

Guo, S., and Kemphues, K.J. (1996). A non-muscle myosin required for embryonic polarity in Caenorhabditis elegans. *Nature* **382**, 455–458.

Hai, T., and Hartman, M.G. (2001). The molecular biology and nomenclature of the activating transcription factor/cAMP responsive element binding family of transcription factors: activating transcription factor proteins and homeostasis. *Gene* **273**, 1–11.

Hai, T.W., Liu, F., Coukos, W.J., and Green, M.R. (1989). Transcription factor ATF cDNA clones: an extensive family of leucine zipper proteins able to selectively form DNA-binding heterodimers. *Genes Dev* **3**, 2083–2090.

Hai, T., Wolfgang, C.D., Marsee, D.K., Allen, A.E., and Sivaprasad, U. (1999). ATF3 and stress responses. *Gene Expr* **7**, 321–335.

Hai, T., Wolford, C.C., and Chang, Y.-S. (2010). ATF3, a hub of the cellular adaptive-response network, in the pathogenesis of diseases: is modulation of inflammation a unifying component? *Gene Expr* **15**, 1–11.

Hammarström, P., Wiseman, R.L., Powers, E.T., and Kelly, J.W. (2003). Prevention of transthyretin amyloid disease by changing protein misfolding energetics. *Science* **299**, 713–716.

Hampe, J., Schreiber, S., Shaw, S.H., Lau, K.F., Bridger, S., Macpherson, A.J., Cardon, L.R., Sakul, H., Harris, T.J., Buckler, A., et al. (1999). A genomewide analysis provides evidence for novel linkages in inflammatory bowel disease in a large European cohort. *Am J Hum Genet* **64**, 808–816.

Han, D., Lerner, A.G., Vande Walle, L., Upton, J.-P., Xu, W., Hagen, A., Backes, B.J., Oakes, S.A., and Papa, F.R. (2009). IRE1α Kinase Activation Modes Control Alternate Endoribonuclease Outputs to Determine Divergent Cell Fates. *Cell* **138**, 562–575.

Harding, H.P., Zeng, H., Zhang, Y., Jungries, R., Chung, P., Plesken, H., Sabatini, D.D., and Ron, D. (2001). Diabetes mellitus and exocrine pancreatic dysfunction in $Perk^{-/-}$ mice reveals a role for translational control in secretory cell survival. *Mol Cell* **7**, 1153–1163.

Harding, H.P., Zhang, Y., and Ron, D. (1999). Protein translation and folding are coupled by an endoplasmic-reticulum-resident kinase. *Nature* **397**, 271–274.

Harding, H.P., Zhang, Y., Zeng, H., Novoa, I., Lu, P.D., Calfon, M., Sadri, N., Yun, C., Popko, B., Paules, R., et al. (2003). An integrated stress response regulates amino acid metabolism and resistance to oxidative stress. *Mol Cell* **11**, 619–633.

Haze, K., Okada, T., Yoshida, H., Yanagi, H., Yura, T., Negishi, M., and Mori, K. (2001). Identification of the G13 (cAMP-response-element-binding protein-related protein) gene product related to activating transcription factor 6 as a transcriptional activator of the mammalian unfolded protein response. *Biochem J* **355**, 19–28.

Haze, K., Yoshida, H., Yanagi, H., Yura, T., and Mori, K. (1999). Mammalian transcription factor ATF6 is synthesized as a transmembrane protein and activated by proteolysis in response to endoplasmic reticulum stress. *Mol Biol Cell* **10**, 3787–3799.

He, Y., Sun, S., Sha, H., Liu, Z., Yang, L., Xue, Z., Chen, H., and Qi, L. (2010). Emerging roles for XBP1, a sUPeR transcription factor. *Gene Expr* **15**, 13–25.

Henis-Korenblit, S., Zhang, P., Hansen, M., McCormick, M., Lee, S.-J., Cary, M., and Kenyon, C. (2010). Insulin/IGF-1 signaling mutants reprogram ER stress response regulators to promote longevity. *Proc Natl Acad Sci USA* **107**, 9730–9735.

Hetz, C., Martinon, F., Rodriguez, D., and Glimcher, L.H. (2011). The Unfolded Protein Response: Integrating Stress Signals Through the Stress Sensor IRE1. *Physiol Rev* **91**, 1219–1243.

Hetz, C. (2012). The unfolded protein response: controlling cell fate decisions under ER stress and beyond. *Nat Rev Mol Cell Biol* **13**, 89–102.

Hetz, C., and Glimcher, L.H. (2009). Fine-tuning of the unfolded protein response: Assembling the IRE1α interactome. *Mol Cell* **35**, 551–561.

Hetz, C., Bernasconi, P., Fisher, J., Lee, A.-H., Bassik, M.C., Antonsson, B., Brandt, G.S., Iwakoshi, N.N., Schinzel, A., Glimcher, L.H., et al. (2006). Proapoptotic BAX and BAK modulate the unfolded protein response by a direct interaction with IRE1α. *Science* **312**, 572–576.

Hetz, C., Lee, A.-H., Gonzalez-Romero, D., Thielen, P., Castilla, J., Soto, C., and Glimcher, L.H. (2008). Unfolded protein response transcription factor XBP-1 does not influence prion replication or pathogenesis. *Proc Natl Acad Sci USA* **105**, 757–762.

Hetz, C., Thielen, P., Matus, S., Nassif, M., Court, F., Kiffin, R., Martinez, G., Cuervo, A.M., Brown, R.H., and Glimcher, L.H. (2009). XBP-1 deficiency in the nervous system protects against amyotrophic lateral sclerosis by increasing autophagy. *Genes Dev* **23**, 2294–2306.

Hollien, J., and Weissman, J.S. (2006). Decay of endoplasmic reticulum-localized mRNAs during the unfolded protein response. *Science* **313**, 104–107.

Hollien, J., Lin, J.H., Li, H., Stevens, N., Walter, P., and Weissman, J.S. (2009). Regulated Ire1-dependent decay of messenger RNAs in mammalian cells. *J Cell Biol* **186**, 323–331.

Holtz, W.A., and O'Malley, K.L. (2003). Parkinsonian mimetics induce aspects of unfolded protein response in death of dopaminergic neurons. *J Biol Chem* **278**, 19367–19377.

Hotamisligil, G.S. (2010). Endoplasmic reticulum stress and the inflammatory basis of metabolic disease. *Cell 140*, 900–917.

Hu, C.-C.A., Dougan, S.K., McGehee, A.M., Love, J.C., and Ploegh, H.L. (2009). XBP-1 regulates signal transduction, transcription factors and bone marrow colonization in B cells. *Embo J* **28**, 1624–1636.

Hu, P., Han, Z., Couvillon, A.D., Kaufman, R.J., and Exton, J.H. (2006). Autocrine tumor necrosis factor alpha links endoplasmic reticulum stress to the membrane death receptor pathway through IRE1alpha-mediated NF-kappaB activation and down-regulation of TRAF2 expression. *Mol Cell Biol* **26**, 3071–3084.

Hu, X., Chakravarty, S.D., and Ivashkiv, L.B. (2008). Regulation of interferon and Toll-like receptor signaling during macrophage activation by opposing feedforward and feedback inhibition mechanisms. *Immunol Rev* **226**, 41–56.

Hugot, J.P., Laurent-Puig, P., Gower-Rousseau, C., Olson, J.M., Lee, J.C., Beaugerie, L., Naom, I., Dupas, J.L., Van Gossum, A., Orholm, M., et al. (1996). Mapping of a susceptibility locus for Crohn's disease on chromosome 16. *Nature* **379**, 821–823.

Hurt, E.M., Thomas, S.B., Peng, B., and Farrar, W.L. (2007). Integrated molecular profiling of SOD2 expression in multiple myeloma. *Blood* **109**, 3953–3962.

Ilani, T., Vasiliver-Shamis, G., Vardhana, S., Bretscher, A., and Dustin, M.L. (2009). T cell antigen receptor signaling and immunological synapse stability require myosin IIA. *Nat Immunol* **10**, 531–539.

Iwakoshi, N.N., Lee, A.-H., Vallabhajosyula, P., Otipoby, K.L., Rajewsky, K., and Glimcher, L.H. (2003). Plasma cell differentiation and the unfolded protein response intersect at the transcription factor XBP-1. *Nat Immunol* **4**, 321–329.

Iwakoshi, N.N., Pypaert, M., and Glimcher, L.H. (2007). The transcription factor XBP-1 is essential for the development and survival of dendritic cells. *J Exp Med* **204**, 2267–2275.

Iwawaki, T., Akai, R., Kohno, K., and Miura, M. (2004). A transgenic mouse model for monitoring endoplasmic reticulum stress. *Nat Med* **10**, 98–102.

Jiang, H.-Y., Wek, S.A., McGrath, B.C., Lu, D., Hai, T., Harding, H.P., Wang, X., Ron, D., Cavener, D.R., and Wek, R.C. (2004). Activating transcription factor 3 is integral to the eukaryotic initiation factor 2 kinase stress response. *Mol Cell Biol* **24**, 1365–1377.

Juric, D., Lacayo, N.J., Ramsey, M.C., Racevskis, J., Wiernik, P.H., Rowe, J.M., Goldstone, A.H., O'Dwyer, P.J., Paietta, E., and Sikic, B.I. (2007). Differential gene expression patterns and interaction networks in BCR-ABL-positive and -negative adult acute lymphoblastic leukemias. *J Clin Oncol* **25**, 1341–1349.

Kajimura, S., Seale, P., Tomaru, T., Erdjument-Bromage, H., Cooper, M.P., Ruas, J.L., Chin, S., Tempst, P., Lazar, M.A., and Spiegelman, B.M. (2008). Regulation of the brown and white fat gene programs through a PRDM16/CtBP transcriptional complex. *Genes Dev* **22**, 1397–1409.

Kakiuchi, C., Iwamoto, K., Ishiwata, M., Bundo, M., Kasahara, T., Kusumi, I., Tsujita, T., Okazaki, Y., Nanko, S., Kunugi, H., et al. (2003). Impaired feedback regulation of XBP1 as a genetic risk factor for bipolar disorder. *Nat Genet* **35**, 171–175.

Kamimura, D., and Bevan, M.J. (2008). Endoplasmic reticulum stress regulator XBP-1 contributes to effector CD8+ T cell differentiation during acute infection. *J Immunol* **181**, 5433–5441.

Kanda, H., and Miura, M. (2004). Regulatory roles of JNK in programmed cell death. *J Biochem* **136**, 1–6.

Kaser, A., Lee, A.-H., Franke, A., Glickman, J.N., Zeissig, S., Tilg, H., Nieuwenhuis, E.E.S., Higgins, D.E., Schreiber, S., Glimcher, L.H., et al. (2008). XBP1 links ER stress to intestinal inflammation and confers genetic risk for human inflammatory bowel disease. *Cell* **134**, 743–756.

Kaufman, R.J., Scheuner, D., Schröder, M., Shen, X., Lee, K., Liu, C.Y., and Arnold, S.M. (2002). The unfolded protein response in nutrient sensing and differentiation. *Nat Rev Mol Cell Biol* **3**, 411–421.

Kebache, S., Cardin, E., Nguyên, D.T., Chevet, E., and Larose, L. (2004). Nck-1 antagonizes the endoplasmic reticulum stress-induced inhibition of translation. *J Biol Chem* **279**, 9662–9671.

Khanna, A., and Campbell, R.D. (1996). The gene G13 in the class III region of the human MHC encodes a potential DNA-binding protein. *Biochem J* **319** *(Pt 1)*, 81–89.

Kim, K.Y. (2005). Disease-associated Mutations and Alternative Splicing Alter the Enzymatic and Motile Activity of Nonmuscle Myosins II-B and II-C. *J Biol Chem* **280**, 22769–22775.

Kimata, Y., Ishiwata-Kimata, Y., Ito, T., Hirata, A., Suzuki, T., Oikawa, D., Takeuchi, M., and Kohno, K. (2007). Two regulatory steps of ER-stress sensor Ire1 involving its cluster formation and interaction with unfolded proteins. *J Cell Biol* **179**, 75–86.

Kimata, Y., Kimata, Y.I., Shimizu, Y., Abe, H., Farcasanu, I.C., Takeuchi, M., Rose, M.D., and Kohno, K. (2003). Genetic evidence for a role of BiP/Kar2 that regulates Ire1 in response to accumulation of unfolded proteins. *Mol Biol Cell* **14**, 2559–2569.

Kinoshita, E., Kinoshita-Kikuta, E., Takiyama, K., and Koike, T. (2006). Phosphate-binding tag, a new tool to visualize phosphorylated proteins. *Mol Cell Proteomics* **5**, 749–757.

Klee, M., Pallauf, K., Alcalá, S., Fleischer, A., and Pimentel-Muiños, F.X. (2009). Mitochondrial apoptosis induced by BH3-only molecules in the exclusive presence of endoplasmic reticular Bak. *Embo J* **28**, 1757–1768.

Klein, U., Casola, S., Cattoretti, G., Shen, Q., Lia, M., Mo, T., Ludwig, T., Rajewsky, K., and Dalla-Favera, R. (2006). Transcription factor IRF4 controls plasma cell differentiation and class-switch recombination. *Nat Immunol* **7**, 773–782.

Kokame, K., Kato, H., and Miyata, T. (2001). Identification of ERSE-II, a new cis-acting element responsible for the ATF6-dependent mammalian unfolded protein response. *J Biol Chem* **276**, 9199–9205.

Korennykh, A.V., Egea, P.F., Korostelev, A.A., Finer-Moore, J., Zhang, C., Shokat, K.M., Stroud, R.M., and Walter, P. (2009). The unfolded protein response signals through high-order assembly of Ire1. *Nature* **457**, 687–693.

Kozutsumi, Y., Segal, M., Normington, K., Gething, M.J., and Sambrook, J. (1988). The presence of malfolded proteins in the endoplasmic reticulum signals the induction of glucose-regulated proteins. *Nature* **332**, 462–464.

Lacroix, M., and Leclercq, G. (2004). About GATA3, HNF3A, and XBP1, three genes co-expressed with the oestrogen receptor-alpha gene (ESR1) in breast cancer. *Mol Cell Endocrinol* **219**, 1–7.

Leber, J.H., Bernales, S., and Walter, P. (2004). IRE1-independent gain control of the unfolded protein response. *PLoS Biol* **2**, E235.

Lee, A.-H., Scapa, E.F., Cohen, D.E., and Glimcher, L.H. (2008a). Regulation of Hepatic Lipogenesis by the Transcription Factor XBP1. *Science* **320**, 1492–1496.

Lee, A.-H., Chu, G.C., Iwakoshi, N.N., and Glimcher, L.H. (2005). XBP-1 is required for biogenesis of cellular secretory machinery of exocrine glands. *Embo J* **24**, 4368–4380.

Lee, A.-H., Iwakoshi, N.N., and Glimcher, L.H. (2003a). XBP-1 regulates a subset of endoplasmic reticulum resident chaperone genes in the unfolded protein response. *Mol Cell Biol* **23**, 7448–7459.

Lee, A.-H., Iwakoshi, N.N., Anderson, K.C., and Glimcher, L.H. (2003b). Proteasome inhibitors disrupt the unfolded protein response in myeloma cells. *Proc Natl Acad Sci USA* **100**, 9946–9951.

Lee, K.P.K., Dey, M., Neculai, D., Cao, C., Dever, T.E., and Sicheri, F. (2008b). Structure of the dual enzyme Ire1 reveals the basis for catalysis and regulation in nonconventional RNA splicing. *Cell* **132**, 89–100.

Lee, K., Tirasophon, W., Shen, X., Michalak, M., Prywes, R., Okada, T., Yoshida, H., Mori, K., and Kaufman, R.J. (2002). IRE1-mediated unconventional mRNA splicing and S2P-mediated ATF6 cleavage merge to regulate XBP1 in signaling the unfolded protein response. *Genes Dev* **16**, 452–466.

Lefterova, M.I., Zhang, Y., Steger, D.J., Schupp, M., Schug, J., Cristancho, A., Feng, D., Zhuo, D., Stoeckert, C.J., Liu, X.S., et al. (2008). PPAR{gamma} and C/EBP factors orchestrate adipocyte biology via adjacent binding on a genome-wide scale. *Genes Dev* **22**, 2941–2952.

Leleu, X., Hunter, Z.R., Xu, L., Roccaro, A.M., Moreau, A.-S., Santos, D.D., Hatjiharissi, E., Bakthavachalam, V., Adamia, S., Ho, A.W., et al. (2009). Expression of regulatory genes for lymphoplasmacytic cell differentiation in Waldenstrom Macroglobulinemia. *British Journal of Haematology* **145**, 59–63.

Li, H., Korennykh, A.V., Behrman, S.L., and Walter, P. (2010). Mammalian endoplasmic reticulum stress sensor IRE1 signals by dynamic clustering. P*roc Natl Acad Sci USA* **107**, 16113–16118.

Lin, J.H., Li, H., Zhang, Y., Ron, D., and Walter, P. (2009). Divergent effects of PERK and IRE1 signaling on cell viability. *PLoS ONE* **4**, e4170.

Lindholm, D., Wootz, H., and Korhonen, L. (2006). ER stress and neurodegenerative diseases. *Cell Death Differ* **13**, 385–392.

Liou, H.C., Boothby, M.R., Finn, P.W., Davidon, R., Nabavi, N., Zeleznik-Le, N.J., Ting, J.P., and Glimcher, L.H. (1990). A new member of the leucine zipper class of proteins that binds to the HLA DR alpha promoter. *Science* **247**, 1581–1584.

Lisbona, F., Rojas-Rivera, D., Thielen, P., Zamorano, S., Todd, D., Martinon, F., Glavic, A., Kress, C., Lin, J.H., Walter, P., et al. (2009). BAX inhibitor-1 is a negative regulator of the ER stress sensor IRE1alpha. *Mol Cell* **33**, 679–691.

Liu, J., Maduzia, L.L., Shirayama, M., and Mello, C.C. (2010). NMY-2 maintains cellular asymmetry and cell boundaries, and promotes a SRC-dependent asymmetric cell division. *Dev Biol* **339**, 366–373.

Loo, T.W., Bartlett, M.C., and Clarke, D.M. (2008). Correctors promote folding of the CFTR in the endoplasmic reticulum. *Biochem J* **413**, 29–36.

Luo, D., He, Y., Zhang, H., Yu, L., Chen, H., Xu, Z., Tang, S., Urano, F., and Min, W. (2008). AIP1 is critical in transducing IRE1-mediated endoplasmic reticulum stress response. *J Biol Chem* **283**, 11905–11912.

Ma, X., and Adelstein, R.S. (2012). In vivo studies on nonmuscle myosin II expression and function in heart development. *Front Biosci* **17**, 545–555.

Marcu, M.G., Doyle, M., Bertolotti, A., Ron, D., Hendershot, L., and Neckers, L. (2002). Heat shock protein 90 modulates the unfolded protein response by stabilizing IRE1alpha. *Mol Cell Biol* **22**, 8506–8513.

Martinon, F., Chen, X., Lee, A.-H., and Glimcher, L.H. (2010). TLR activation of the transcription factor XBP1 regulates innate immune responses in macrophages. *Nat Immunol* **11**, 411-418.

Masaki, T., Yoshida, M., and Noguchi, S. (1999). Targeted disruption of CRE-binding factor TREB5 gene leads to cellular necrosis in cardiac myocytes at the embryonic stage. *Biochem Biophys Res Commun* **261**, 350–356.

Mauro, C., Crescenzi, E., De Mattia, R., Pacifico, F., Mellone, S., Salzano, S., de Luca, C., D'Adamio, L., Palumbo, G., Formisano, S., et al. (2006). Central role of the scaffold protein tumor necrosis factor receptor-associated factor 2 in regulating endoplasmic reticulum stress-induced apoptosis. *J Biol Chem* **281**, 2631–2638.

McCullough, K.D., Martindale, J.L., Klotz, L.O., Aw, T.Y., and Holbrook, N.J. (2001). Gadd153 sensitizes cells to endoplasmic reticulum stress by down-regulating Bcl2 and perturbing the cellular redox state. *Mol Cell Biol* **21**, 1249–1259.

McDonald, W.H., Tabb, D.L., Sadygov, R.G., MacCoss, M.J., Venable, J., Graumann, J., Johnson, J.R., Cociorva, D., and Yates, J.R. (2004). MS1, MS2, and SQT-three unified, compact, and easily parsed file formats for the storage of shotgun proteomic spectra and identifications. *Rapid Commun Mass Spectrom* **18**, 2162–2168.

Medzhitov, R., and Horng, T. (2009). Transcriptional control of the inflammatory response. *Nat Rev Immunol* **9**, 692–703.

Meshel, A.S., Wei, Q., Adelstein, R.S., and Sheetz, M.P. (2005). Basic mechanism of three-dimensional collagen fibre transport by fibroblasts. *Nat Cell Biol* **7**, 157–164.

Millar, N.S., and Harkness, P.C. (2008). Assembly and trafficking of nicotinic acetylcholine receptors (Review). *Mol Membr Biol* **25**, 279–292.

Min, J., Shukla, H., Kozono, H., Bronson, S.K., Weissman, S.M., and Chaplin, D.D. (1995). A novel Creb family gene telomeric of HLA-DRA in the HLA complex. *Genomics* **30**, 149–156.

Mori, K., Ma, W., Gething, M.J., and Sambrook, J. (1993). A transmembrane protein with a cdc2+/CDC28-related kinase activity is required for signaling from the ER to the nucleus. *Cell* **74**, 743–756.

Moynagh, P.N. (2005). TLR signalling and activation of IRFs: revisiting old friends from the NF-kappaB pathway. *Trends Immunol* **26**, 469–476.

Munshi, N.C., Hideshima, T., Carrasco, D., Shammas, M., Auclair, D., Davies, F., Mitsiades, N., Mitsiades, C., Kim, R.S., Li, C., et al. (2004). Identification of genes modulated in multiple myeloma using genetically identical twin samples. *Blood* **103**, 1799–1806.

Nagai, A., Kadowaki, H., Maruyama, T., Takeda, K., Nishitoh, H., and Ichijo, H. (2009). USP14 inhibits ER-associated degradation via interaction with IRE1alpha. *Biochem Biophys Res Commun* **379**, 995–1000.

Nekrutenko, A., and He, J. (2006). Functionality of unspliced XBP1 is required to explain evolution of overlapping reading frames. *Trends Genet* **22**, 645–648.

Nguyên, D.T., Kebache, S., Fazel, A., Wong, H.N., Jenna, S., Emadali, A., Lee, E.-H., Bergeron, J.J.M., Kaufman, R.J., Larose, L., et al. (2004). Nck-dependent activation of extracellular signal-regulated kinase-1 and regulation of cell survival during endoplasmic reticulum stress. *Mol Biol Cell* **15**, 4248–4260.

Nishitoh, H., Kadowaki, H., Nagai, A., Maruyama, T., Yokota, T., Fukutomi, H., Noguchi, T., Matsuzawa, A., Takeda, K., and Ichijo, H. (2008). ALS-linked mutant SOD1 induces ER stress- and ASK1-dependent motor neuron death by targeting Derlin-1. *Genes Dev* **22**, 1451–1464.

Nishitoh, H., Matsuzawa, A., Tobiume, K., Saegusa, K., Takeda, K., Inoue, K., Hori, S., Kakizuka, A., and Ichijo, H. (2002). ASK1 is essential for endoplasmic reticulum stress-induced neuronal cell death triggered by expanded polyglutamine repeats. *Genes Dev* **16**, 1345–1355.

Novikoff, A.B., Novikoff, P.M., Rosen, O.M., and Rubin, C.S. (1980). Organelle relationships in cultured 3T3-L1 preadipocytes. *J Cell Biol* **87**, 180–196.

Novoa, I., Zeng, H., Harding, H.P., and Ron, D. (2001). Feedback inhibition of the unfolded protein response by GADD34-mediated dephosphorylation of eIF2alpha. *J Cell Biol* **153**, 1011–1022.

Novoa, I., Zhang, Y., Zeng, H., Jungreis, R., Harding, H.P., and Ron, D. (2003). Stress-induced gene expression requires programmed recovery from translational repression. *Embo J* **22**, 1180–1187.

Oikawa, D., Kimata, Y., Kohno, K., and Iwawaki, T. (2009). Activation of mammalian IRE1alpha upon ER stress depends on dissociation of BiP rather than on direct interaction with unfolded proteins. *Exp Cell Res* **315**, 2496–2504.

Ono, S.J., Liou, H.C., Davidon, R., Strominger, J.L., and Glimcher, L.H. (1991). Human X-box-binding protein 1 is required for the transcription of a subset of human class II major histocompatibility genes and forms a heterodimer with c-fos. *Proc Natl Acad Sci USA* **88**, 4309–4312.

Osada, S., Yamamoto, H., Nishihara, T., and Imagawa, M. (1996). DNA binding specificity of the CCAAT/enhancer-binding protein transcription factor family. *J Biol Chem* **271**, 3891–3896.

Ozcan, L., Ergin, A.S., Lu, A., Chung, J., Sarkar, S., Nie, D., Myers, M.G., and Ozcan, U. (2009). Endoplasmic reticulum stress plays a central role in development of leptin resistance. *Cell Metab* **9**, 35–51.

Ozcan, U., Cao, Q., Yilmaz, E., Lee, A.-H., Iwakoshi, N.N., Ozdelen, E., Tuncman, G., Görgün, C., Glimcher, L.H., and Hotamisligil, G.S. (2004). Endoplasmic reticulum stress links obesity, insulin action, and type 2 diabetes. *Science* **306**, 457–461.

Ozcan, U., Yilmaz, E., Ozcan, L., Furuhashi, M., Vaillancourt, E., Smith, R.O., Görgün, C.Z., and Hotamisligil, G.S. (2006). Chemical chaperones reduce ER stress and restore glucose homeostasis in a mouse model of type 2 diabetes. *Science* **313**, 1137–1140.

Papa, F.R., Zhang, C., Shokat, K., and Walter, P. (2003). Bypassing a kinase activity with an ATP-competitive drug. *Science* **302**, 1533–1537.

Park, S.W., Zhou, Y., Lee, J., Lu, A., Sun, C., Chung, J., Ueki, K., and Ozcan, U. (2010). The regulatory subunits of PI3K, p85alpha and p85beta, interact with XBP-1 and increase its nuclear translocation. *Nat Med* **16**, 429–437.

Peng, J., Elias, J.E., Thoreen, C.C., Licklider, L.J., and Gygi, S.P. (2003). Evaluation of multidimensional chromatography coupled with tandem mass spectrometry (LC/LC-MS/MS) for large-scale protein analysis: the yeast proteome. *J Proteome Res* **2**, 43–50.

Pfaffenbach, K.T., Nivala, A.M., Reese, L., Ellis, F., Wang, D., Wei, Y., and Pagliassotti, M.J. (2010). Rapamycin inhibits postprandial-mediated X-box-binding protein-1 splicing in rat liver. *J Nutr* **140**, 879–884.

Ponath, P.D., Fass, D., Liou, H.C., Glimcher, L.H., and Strominger, J.L. (1993). The regulatory gene, hXBP-1, and its target, HLA-DRA, utilize both common and distinct regulatory elements and protein complexes. *J Biol Chem* **268**, 17074–17082.

P**owers, E.T., Morimoto, R.I., Dillin, A., Kelly, J.W., and Balch, W.E.** (2009). Biological and chemical approaches to diseases of proteostasis deficiency. *Annu Rev Biochem* **78**, 959–991.

Qi, L., Saberi, M., Zmuda, E., Wang, Y., Altarejos, J., Zhang, X., Dentin, R., Hedrick, S., Bandyopadhyay, G., Hai, T., et al. (2009). Adipocyte CREB promotes insulin resistance in obesity. *Cell Metab* **9**, 277–286.

Qi, L., Yang, L., and Chen, H. (2011). Detecting and quantitating physiological endoplasmic reticulum stress. *Meth Enzymol* **490**, 137–146.

Qiu, Y., Mao, T., Zhang, Y., Shao, M., You, J., Ding, Q., Chen, Y., Wu, D., Xie, D., Lin, X., et al. (2010). A crucial role for RACK1 in the regulation of glucose-stimulated IRE1 activation in pancreatic cells. *Sci Signal* **3**, ra7–ra7.

Raven, J.F., and Koromilas, A.E. (2008). PERK and PKR: old kinases learn new tricks. *Cell Cycle* **7**, 1146–1150.

Reimold, A.M., Etkin, A., Clauss, I., Perkins, A., Friend, D.S., Zhang, J., Horton, H.F., Scott, A., Orkin, S.H., Byrne, M.C., et al. (2000). An essential role in liver development for transcription factor XBP-1. *Genes Dev* **14**, 152–157.

Reimold, A.M., Iwakoshi, N.N., Manis, J., Vallabhajosyula, P., Szomolanyi-Tsuda, E., Gravallese, E.M., Friend, D., Grusby, M.J., Alt, F., and Glimcher, L.H. (2001). Plasma cell differentiation requires the transcription factor XBP-1. *Nature* **412**, 300–307.

Reimold, A.M., Ponath, P.D., Li, Y.S., Hardy, R.R., David, C.S., Strominger, J.L., and Glimcher, L.H. (1996). Transcription factor B cell lineage-specific activator protein regulates the gene for human X-box binding protein 1. *J Exp Med* **183**, 393–401.

Richardson, C.E., Kooistra, T., and Kim, D.H. (2010). An essential role for XBP-1 in host protection against immune activation in C. elegans. *Nature* **463**, 1092–1095.

Roach, J.C., Smith, K.D., Strobe, K.L., Nissen, S.M., Haudenschild, C.D., Zhou, D., Vasicek, T.J., Held, G.A., Stolovitzky, G.A., Hood, L.E., et al. (2007). Transcription factor expression in lipopolysaccharide-activated peripheral-blood-derived mononuclear cells. *Proc Natl Acad Sci USA* **104**, 16245–16250.

Romero-Ramirez, L., Cao, H., Nelson, D., Hammond, E., Lee, A.-H., Yoshida, H., Mori, K., Glimcher, L.H., Denko, N.C., Giaccia, A.J., et al. (2004). XBP1 is essential for survival under hypoxic conditions and is required for tumor growth. *Cancer Res* **64**, 5943–5947.

Ron, D., and Habener, J.F. (1992). CHOP, a novel developmentally regulated nuclear protein that dimerizes with transcription factors C/EBP and LAP and functions as a dominant-negative inhibitor of gene transcription. *Genes Dev* **6**, 439–453.

Ron, D., and Hubbard, S.R. (2008). How IRE1 reacts to ER stress. *Cell* **132**, 24–26.

Ron, D., and Walter, P. (2007). Signal integration in the endoplasmic reticulum unfolded protein response. *Nat Rev Mol Cell Biol* **8**, 519–529.

Rubio, C., Pincus, D., Korennykh, A., Schuck, S., El-Samad, H., and Walter, P. (2011). Homeostatic adaptation to endoplasmic reticulum stress depends on Ire1 kinase activity. *J Cell Biol* **193**, 171–184.

Sado, M., Yamasaki, Y., Iwanaga, T., Onaka, Y., Ibuki, T., Nishihara, S., Mizuguchi, H., Momota, H., Kishibuchi, R., Hashimoto, T., et al. (2009). Protective effect against Parkinson's disease-related insults through the activation of XBP1. *Brain Res* **1257**, 16–24.

Saitoh, M., Ishikawa, T., Matsushima, S., Naka, M., and Hidaka, H. (1987). Selective inhibition of catalytic activity of smooth muscle myosin light chain kinase. *J Biol Chem* **262**, 7796–7801.

Schardt, J.A., Weber, D., Eyholzer, M., Mueller, B.U., and Pabst, T. (2009). Activation of the unfolded protein response is associated with favorable prognosis in acute myeloid leukemia. *Clin Cancer Res* **15**, 3834–3841.

Schröder, M., and Kaufman, R.J. (2005). The mammalian unfolded protein response. *Annu Rev Biochem* **74**, 739–789.

S**eale, P., Bjork, B., Yang, W., Kajimura, S., Chin, S., Kuang, S., Scimè, A., Devarakonda, S., Conroe, H.M., Erdjument-Bromage, H., et al.** (2008). PRDM16 controls a brown fat/skeletal muscle switch. *Nature* **454**, 961–967.

Sha, H., He, Y., Chen, H., Wang, C., Zenno, A., Shi, H., Yang, X., Zhang, X., and Qi, L. (2009). The IRE1alpha-XBP1 pathway of the unfolded protein response is required for adipogenesis. *Cell Metab* **9**, 556–564.

Sha, H., He, Y., Yang, L., and Qi, L. (2011). Stressed out about obesity: IRE1α-XBP1 in metabolic disorders. *Trends Endocrinol Metab* **22**, 374–381.

Shaffer, A.L., Lin, K.I., Kuo, T.C., Yu, X., Hurt, E.M., Rosenwald, A., Giltnane, J.M., Yang, L., Zhao, H., Calame, K., et al. (2002). Blimp-1 orchestrates plasma cell differentiation by extinguishing the mature B cell gene expression program. *Immunity* **17**, 51–62.

Shaffer, A.L., Shapiro-Shelef, M., Iwakoshi, N.N., Lee, A.-H., Qian, S.-B., Zhao, H., Yu, X., Yang, L., Tan, B.K., Rosenwald, A., et al. (2004). XBP1, downstream of Blimp-1, expands the secretory apparatus and other organelles, and increases protein synthesis in plasma cell differentiation. *Immunity* **21**, 81–93.

Shen, J., and Prywes, R. (2004). Dependence of site-2 protease cleavage of ATF6 on prior site-1 protease digestion is determined by the size of the luminal domain of ATF6. *J Biol Chem* **279**, 43046–43051.

Shen, J., Chen, X., Hendershot, L., and Prywes, R. (2002). ER stress regulation of ATF6 localization by dissociation of BiP/GRP78 binding and unmasking of Golgi localization signals. *Dev Cell* **3**, 99–111.

Shen, X., Ellis, R.E., Sakaki, K., and Kaufman, R.J. (2005). Genetic interactions due to constitutive and inducible gene regulation mediated by the unfolded protein response in C. elegans. *PLoS Genet* **1**, e37.

Shi, Y., An, J., Liang, J., Hayes, S.E., Sandusky, G.E., Stramm, L.E., and Yang, N.N. (1999). Characterization of a mutant pancreatic eIF-2alpha kinase, PEK, and co-localization with somatostatin in islet delta cells. *J Biol Chem* **274**, 5723–5730.

Shi, Y., Vattem, K.M., Sood, R., An, J., Liang, J., Stramm, L., and Wek, R.C. (1998). Identification and characterization of pancreatic eukaryotic initiation factor 2 alpha-subunit kinase, PEK, involved in translational control. *Mol Cell Biol* **18**, 7499–7509.

Sicheri, F., and Silverman, R.H. (2011). Putting the brakes on the unfolded protein response. *J Cell Biol* **193**, 17–19.

Sidrauski, C., and Walter, P. (1997). The transmembrane kinase Ire1p is a site-specific endonuclease that initiates mRNA splicing in the unfolded protein response. *Cell* **90**, 1031–1039.

So, J.-S., Hur, K.Y., Tarrio, M., Ruda, V., Frank-Kamenetsky, M., Fitzgerald, K., Koteliansky, V., Lichtman, A.H., Iwawaki, T., Glimcher, L.H., et al. (2012). Silencing of lipid metabolism genes through IRE1α-mediated mRNA decay lowers plasma lipids in mice. *Cell Metab* **16**, 487–499.

Spiotto, M.T., Banh, A., Papandreou, I., Cao, H., Galvez, M.G., Gurtner, G.C., Denko, N.C., Le, Q.T., and Koong, A.C. (2010). Imaging the Unfolded Protein Response in Primary Tumors Reveals Microenvironments with Metabolic Variations that Predict Tumor Growth. *Cancer Res* **70**, 78–88.

Sriburi, R., Jackowski, S., Mori, K., and Brewer, J.W. (2004). XBP1: a link between the unfolded protein response, lipid biosynthesis, and biogenesis of the endoplasmic reticulum. *J Cell Biol* **167**, 35–41.

Stark, G.R., Kerr, I.M., Williams, B.R., Silverman, R.H., and Schreiber, R.D. (1998). How cells respond to interferons. *Annu Rev Biochem* **67**, 227–264.

Straight, A.F., Cheung, A., Limouze, J., Chen, I., Westwood, N.J., Sellers, J.R., and Mitchison, T.J. (2003). Dissecting temporal and spatial control of cytokinesis with a myosin II Inhibitor. *Science* **299**, 1743–1747.

Suganami, T., Yuan, X., Shimoda, Y., Uchio-Yamada, K., Nakagawa, N., Shirakawa, I., Usami, T., Tsukahara, T., Nakayama, K., Miyamoto, Y., et al. (2009). Activating transcription factor 3 constitutes a negative feedback mechanism that attenuates saturated Fatty acid/toll-like receptor 4 signaling and macrophage activation in obese adipose tissue. *Circ Res* **105**, 25–32.

Tabb, D.L., McDonald, W.H., and Yates, J.R. (2002). DTASelect and Contrast: tools for assembling and comparing protein identifications from shotgun proteomics. *J Proteome Res* **1**, 21–26.

Takeda, K., Kishi, H., Ma, X., Yu, Z.-X., and Adelstein, R.S. (2003). Ablation and mutation of nonmuscle myosin heavy chain II-B results in a defect in cardiac myocyte cytokinesis. *Circ Res* **93**, 330–337.

Taniguchi, C.M., Aleman, J.O., Ueki, K., Luo, J., Asano, T., Kaneto, H., Stephanopoulos, G., Cantley, L.C., and Kahn, C.R. (2007). The p85alpha regulatory subunit of phosphoinositide 3-kinase potentiates c-Jun N-terminal kinase-mediated insulin resistance. *Mol Cell Biol* **27**, 2830–2840.

Taniguchi, C.M., Tran, T.T., Kondo, T., Luo, J., Ueki, K., Cantley, L.C., and Kahn, C.R. (2006). Phosphoinositide 3-kinase regulatory subunit p85alpha suppresses insulin action via positive regulation of PTEN. *Proc Natl Acad Sci USA* **103**, 12093–12097.

Tirasophon, W., Lee, K., Callaghan, B., Welihinda, A., and Kaufman, R.J. (2000). The endoribonuclease activity of mammalian IRE1 autoregulates its mRNA and is required for the unfolded protein response. *Genes Dev* **14**, 2725–2736.

Tirasophon, W., Welihinda, A.A., and Kaufman, R.J. (1998). A stress response pathway from the endoplasmic reticulum to the nucleus requires a novel bifunctional protein kinase/endoribonuclease (Ire1p) in mammalian cells. *Genes Dev* **12**, 1812–1824.

Tirosh, B., Iwakoshi, N.N., Glimcher, L.H., and Ploegh, H.L. (2005). XBP-1 specifically promotes IgM synthesis and secretion, but is dispensable for degradation of glycoproteins in primary B cells. *J Exp Med* **202**, 505–516.

Tirosh, B., Iwakoshi, N.N., Glimcher, L.H., and Ploegh, H.L. (2006). Rapid turnover of unspliced Xbp-1 as a factor that modulates the unfolded protein response. *J Biol Chem* **281**, 5852–5860.

Todd, D., Lee, A., and Glimcher, L. (2008). The endoplasmic reticulum stress response in immunity and autoimmunity. *Nat Rev Immunol* **8**, 663–674.

Todd, D.J., McHeyzer-Williams, L.J., Kowal, C., Lee, A.-H., Volpe, B.T., Diamond, B., McHeyzer-Williams, M.G., and Glimcher, L.H. (2009). XBP1 governs late events in plasma cell differentiation and is not required for antigen-specific memory B cell development. *J Exp Med* **206**, 2151–2159.

Tontonoz, P., and Spiegelman, B.M. (2008). Fat and beyond: the diverse biology of PPARgamma. *Annu Rev Biochem* **77**, 289–312.

Travers, K.J., Patil, C.K., Wodicka, L., Lockhart, D.J., Weissman, J.S., and Walter, P. (2000). Functional and genomic analyses reveal an essential coordination between the unfolded protein response and ER-associated degradation. *Cell* **101**, 249–258.

Upton, J.-P., Wang, L., Han, D., Wang, E.S., Huskey, N.E., Lim, L., Truitt, M., McManus, M.T., Ruggero, D., Goga, A., et al. (2012). IRE1α cleaves select microRNAs during ER stress to derepress translation of proapoptotic Caspase-2. *Science* **338**, 818–822.

Urano, F., Wang, X., Bertolotti, A., Zhang, Y., Chung, P., Harding, H.P., and Ron, D. (2000). Coupling of stress in the ER to activation of JNK protein kinases by transmembrane protein kinase IRE1. *Science* **287**, 664–666.

Vecchi, C., Montosi, G., Zhang, K., Lamberti, I., Duncan, S.A., Kaufman, R.J., and Pietrangelo, A. (2009). ER stress controls iron metabolism through induction of hepcidin. *Science* **325**, 877–880.

Vermeire, S., Rutgeerts, P., Van Steen, K., Joossens, S., Claessens, G., Pierik, M., Peeters, M., and Vlietinck, R. (2004). Genome wide scan in a Flemish inflammatory bowel disease population: support for the IBD4 locus, population heterogeneity, and epistasis. *Gut* **53**, 980–986.

Vicente-Manzanares, M., Ma, X., Adelstein, R.S., and Horwitz, A.R. (2009). Non-muscle myosin II takes centre stage in cell adhesion and migration. *Nat Rev Mol Cell Biol* **10**, 778–790.

Walter, P., and Ron, D. (2011). The Unfolded Protein Response: From Stress Pathway to Homeostatic Regulation. *Science* **334**, 1081–1086.

Wang, Q., Mora-Jensen, H., Weniger, M.A., Perez-Galan, P., Wolford, C., Hai, T., Ron, D., Chen, W., Trenkle, W., Wiestner, A., et al. (2009a). ERAD inhibitors integrate ER stress with an epigenetic mechanism to activate BH3-only protein NOXA in cancer cells. *Proc Natl Acad Sci USA* **106**, 2200–2205.

Wang, Y., Shen, J., Arenzana, N., Tirasophon, W., Kaufman, R.J., and Prywes, R. (2000). Activation of ATF6 and an ATF6 DNA binding site by the endoplasmic reticulum stress response. *J Biol Chem* **275**, 27013–27020.

Wang, Y., Vera, L., Fischer, W., and Montminy, M. (2009b). The CREB coactivator CRTC2 links hepatic ER stress and fasting gluconeogenesis. *Nature* **460**, 534-537.

Wen, X.Y., Stewart, A.K., Sooknanan, R.R., Henderson, G., Hawley, T.S., Reimold, A.M., Glimcher, L.H., Baumann, H., Malek, L.T., and Hawley, R.G. (1999). Identification of c-myc promoter-binding protein and X-box binding protein 1 as interleukin-6 target genes in human multiple myeloma cells. *Int J Oncol* **15**, 173–178.

Whitmore, M.M., Iparraguirre, A., Kubelka, L., Weninger, W., Hai, T., and Williams, B.R.G. (2007). Negative regulation of TLR-signaling pathways by activating transcription factor-3. *J Immunol* **179**, 3622–3630.

Wiseman, R.L., Zhang, Y., Lee, K.P.K., Harding, H.P., Haynes, C.M., Price, J., Sicheri, F., and Ron, D. (2010). Flavonol activation defines an unanticipated ligand-binding site in the kinase-RNase domain of IRE1. *Mol Cell* **38**, 291–304.

Woehlbier, U., and Hetz, C. (2011). Modulating stress responses by the UPRosome: a matter of life and death. *Trends Biochem Sci* **36**, 329–337.

Wolfgang, C.D., Liang, G., Okamoto, Y., Allen, A.E., and Hai, T. (2000). Transcriptional autorepression of the stress-inducible gene ATF3. *J Biol Chem* **275**, 16865–16870.

Xue, Z., He, Y., Ye, K., Gu, Z., Mao, Y., and Qi, L. (2011). A conserved structural determinant located at the interdomain region of mammalian inositol-requiring enzyme 1alpha. *J Biol Chem* **286**, 30859–30866.

Yamamoto, K., Sato, T., Matsui, T., Sato, M., Okada, T., Yoshida, H., Harada, A., and Mori, K. (2007). Transcriptional induction of mammalian ER quality control proteins is mediated by single or combined action of ATF6alpha and XBP1. *Dev Cell* **13**, 365–376.

Yanagitani, K., Imagawa, Y., Iwawaki, T., Hosoda, A., Saito, M., Kimata, Y., and Kohno, K. (2009). Cotranslational Targeting of XBP1 Protein to the Membrane Promotes Cytoplasmic Splicing of Its Own mRNA. *Mol Cell* **34**, 191–200.

Yang, L., Xue, Z., He, Y., Sun, S., Chen, H., and Qi, L. (2010). A Phos-tag-based approach reveals the extent of physiological endoplasmic reticulum stress. *PLoS ONE* **5**, e11621.

Ye, J., Rawson, R.B., Komuro, R., Chen, X., Davé, U.P., Prywes, R., Brown, M.S., and Goldstein, J.L. (2000). ER stress induces cleavage of membrane-bound ATF6 by the same proteases that process SREBPs. *Mol Cell* **6**, 1355–1364.

Yoneda, T., Imaizumi, K., Oono, K., Yui, D., Gomi, F., Katayama, T., and Tohyama, M. (2001). Activation of caspase-12, an endoplastic reticulum (ER) resident caspase, through tumor necrosis factor receptor-associated factor 2-dependent mechanism in response to the ER stress. *J Biol Chem* **276**, 13935–13940.

Yoo, C.L., Yu, G.J., Yang, B., Robins, L.I., Verkman, A.S., and Kurth, M.J. (2008). 4"-Methyl-4,5-"bithiazole-based correctors of defective delta F508-CFTR cellular processing. *Bioorg Med Chem Lett* **18**, 2610–2614.

Yoshida, H., Haze, K., Yanagi, H., Yura, T., and Mori, K. (1998). Identification of the cis-acting endoplasmic reticulum stress response element responsible for transcriptional induction of mammalian glucose-regulated proteins. Involvement of basic leucine zipper transcription factors. *J Biol Chem* **273**, 33741–33749.

Yoshida, H., Matsui, T., Yamamoto, A., Okada, T., and Mori, K. (2001). XBP1 mRNA is induced by ATF6 and spliced by IRE1 in response to ER stress to produce a highly active transcription factor. *Cell* **107**, 881–891.

Yoshida, H., Okada, T., Haze, K., Yanagi, H., Yura, T., Negishi, M., and Mori, K. (2000). ATF6 activated by proteolysis binds in the presence of NF-Y (CBF) directly to the cis-acting element responsible for the mammalian unfolded protein response. *Mol Cell Biol* **20**, 6755–6767.

Yoshida, H., Matsui, T., Hosokawa, N., Kaufman, R.J., Nagata, K., and Mori, K. (2003). A time-dependent phase shift in the mammalian unfolded protein response. *Dev Cell* **4**, 265–271.

Yoshida, H., Oku, M., Suzuki, M., and Mori, K. (2006). pXBP1(U) encoded in XBP1 pre-mRNA negatively regulates unfolded protein response activator pXBP1(S) in mammalian ER stress response. *J Cell Biol* **172**, 565–575.

Yoshiuchi, K., Kaneto, H., Matsuoka, T.-A., Kohno, K., Iwawaki, T., Nakatani, Y., Yamasaki, Y., Hori, M., and Matsuhisa, M. (2008). Direct monitoring of in vivo ER stress during the development of insulin resistance with ER stress-activated indicator transgenic mice. *Biochem Biophys Res Commun* **366**, 545–550.

Zambelli, A., Mongiardini, E., Villegas, S.N., Carri, N.G., Boot-Handford, R.P., and Wallis, G.A. (2005). Transcription factor XBP-1 is expressed during osteoblast differentiation and is transcriptionally regulated by parathyroid hormone (PTH). *Cell Biol Int* **29**, 647–653.

Zhang, C., Kawauchi, J., Adachi, M.T., Hashimoto, Y., Oshiro, S., Aso, T., and Kitajima, S. (2001). Activation of JNK and transcriptional repressor ATF3/LRF1 through the IRE1/TRAF2 pathway is implicated in human vascular endothelial cell death by homocysteine. *Biochem Biophys Res Commun* **289**, 718–724.

Zhang, K., Shen, X., Wu, J., Sakaki, K., Saunders, T., Rutkowski, D.T., Back, S.H., and Kaufman, R.J. (2006). Endoplasmic reticulum stress activates cleavage of CREBH to induce a systemic inflammatory response. *Cell* **124**, 587–599.

Zhang, K., Wong, H.N., Song, B., Miller, C.N., Scheuner, D., and Kaufman, R.J. (2005). The unfolded protein response sensor IRE1alpha is required at 2 distinct steps in B cell lymphopoiesis. *J Clin Invest* **115**, 268–281.

Zhang, X., Zhang, G., Zhang, H., Karin, M., Bai, H., and Cai, D. (2008). Hypothalamic IKKbeta/NF-kappaB and ER stress link overnutrition to energy imbalance and obesity. *Cell* **135**, 61–73.

Zhou, J., Liu, C.Y., Back, S.H., Clark, R.L., Peisach, D., Xu, Z., and Kaufman, R.J. (2006). The crystal structure of human IRE1 luminal domain reveals a conserved dimerization interface required for activation of the unfolded protein response. *Proc Natl Acad Sci USA* **103**, 14343–14348.

Zmuda, E.J., Viapiano, M., Grey, S.T., Hadley, G., Garcia-Ocaña, A., and Hai, T. (2010). Deficiency of Atf3, an adaptive-response gene, protects islets and ameliorates inflammation in a syngeneic mouse transplantation model. *Diabetologia* **53**, 1438–1450.